

**DEVELOPMENT OF AN AUTOMATED HALL EFFECT EXPERIMENTATION
METHOD FOR THE ELECTRICAL CHARACTERIZATION OF THIN FILMS**

OWEN ALFREDS OREGA

**A Thesis Submitted to the Institute of Postgraduate Studies of Kabarak University in
Partial Fulfillment of the Requirements for the Award of the Master of Science Degree
in Physics**

KABARAK UNIVERSITY

NOVEMBER, 2023

DECLARATION

I. I do declare that:

- i. This thesis is my original work prepared with no other than the indicated sources and to the best of my knowledge, it has not been presented for the award of a degree in any university or college.
- ii. The work has not incorporated material from other works or a paraphrase of such material without due and appropriate acknowledgement.
- iii. The work has been subjected to processes of anti-plagiarism and has met Kabarak University's 15% similarity index threshold.

2. I do understand that issues of academic integrity are paramount and therefore I may be suspended or expelled from the University or my degree may be recalled for academic dishonesty or any other related academic malpractices.

Signature.....

Date.....

Owen Alfreds

GMP/M/0286/04/18

RECOMMENDATION

To the Institute of Postgraduate Studies:

The research thesis entitled "**Development of an Automated Hall Effect Experimentation Method for Electrical Characterization of Thin Films**" written by **Owen Alfreds** is presented to the Institute of Postgraduate Studies of Kabarak University. We have reviewed the research thesis and recommend it to be accepted in partial fulfilment of the requirements for the award of the degree of Master of Science in Physics.

Signed.....

Date.....

Prof. Mghendi Mwamburi

Department of Physics

University of Eldoret

Signed.....

Date.....

Prof. Christopher Maghanga

Department of Biological and Physical Sciences

Kabarak University

COPYRIGHT

© 2023

Owen Alfreds

All rights reserved. No part of this Thesis may be reproduced or transmitted in any form using either mechanical, including recording, photocopying or any other information retrieval or storage system without permission in writing from the author or Kabarak University.

ACKNOWLEDGEMENT

First and foremost, I give thanks to God for my excellent health and the chance to complete my studies despite all obstacles. Thanks to Kabarak University for the opportunity to enrol and study there. I want to express my profound gratitude to Prof. Mghendi Mwamburi and Prof. Christopher Maghanga, who served as my supervisors throughout this research, for their insightful criticisms, recommendations, and remarks. A special thanks to the Department of Physics at the University of Eldoret, which made it possible for me to use their laboratory and equipment to complete my research.

DEDICATION

I dedicate this work to my family.

ABSTRACT

There has been drastic growth in the microelectronics industry in the recent past. These industries utilize different materials, the main being thin-film semiconductors. The performance of these materials is influenced by their structural, electrical, and optical properties among others, depending on their applications. Therefore, the need to electrically characterize semiconductors precisely, quickly, and conveniently cannot be overstated. Some of the desirable features of measurements include usability, accuracy, resolution, repeatability, and consistency which cannot be assured with manually operated systems. This study strived to design, build, interface and assemble an automated computer-aided four-point probe test equipment that can characterize materials to determine their electrical properties such as resistivity, charge carrier type, charge density, and carrier mobility. A four-point probe head, two magnets, NI Keithley model 6220 Precision current source, model 7001 switch, model 2182A Nanovoltmeter, and model 7065 Hall Effect card instruments were interfaced with the NI LabVIEW program running in a computer through a GPIB hub to a PC USB for its full control. The four-probe head was utilized to probe the samples with a square symmetry that was adopted for the measurement of the semiconductor properties. Reliability tests were then used to measure a semiconductor sample's electrical properties compared with the expected results. This work forms a basis for automating similar systems that were inherently designed to be operated manually. The electrical properties of a P-type Germanium thin film sample 1.00 cm wide, 2.00 cm long, and 1.00 mm thick were obtained to validate the Hall Effect measurement system. When the sample was placed perpendicularly across a magnetic field strength of 258.125mT at a room temperature of 292.45K, a resistance of 1.97711 Ω , a conductivity of 252.8946 Sm^{-1} , resistivity of $3.9542 \times 10^{-3} \Omega\text{m}$, a Hall Co-efficient of $7.6595 \times 10^{-3} \text{ m}^3/\text{C}$ a carrier concentration of $8.1487 \times 10^{22} \text{ m}^{-3}$, a Hall angle of 0.4637rad, carrier mobility of $1.9370 \text{ m}^2(\text{vs})^{-1}$ and a doping type of P-type was reported. These results had a deviation of 0.3% in comparison to the data collected and analyzed manually. The measurements concluded that a system offering a fast, simple, effective and reliable method for thin film Hall Effect electrical characterization can be developed and built.

Keywords: *Electrical Characterization, Thin Films, Automated Hall Effect, Manually Operated Systems, String Manipulation Routines.*

TABLE OF CONTENTS

DECLARATION	ii
RECOMMENDATION	iii
COPYRIGHT	iv
ACKNOWLEDGEMENT	v
DEDICATION	vi
ABSTRACT	vii
TABLE OF CONTENTS	viii
LIST OF TABLES	xi
LIST OF FIGURES	xii
LIST OF ABBREVIATIONS AND ACRONYMS	xvii
CHAPTER ONE	1
INTRODUCTION	1
1.1 Overview	1
1.2 Background of Study	1
1.3 Problem Statement.....	5
1.4 Objectives of the Study.....	6
1.5 Research Questions.....	7
1.6 Justification for the Study	7
1.7 Scope of the Study.....	8
1.8. Significance of the Study	8
1.9 Limitations of the Study.....	8
1.10 Assumptions of the Study	9
CHAPTER TWO	10
LITERATURE REVIEW	10

2.1 Introduction	10
2.2 Theoretical Review	10
2.3 Empirical Review	38
2.4 Research Gap.....	40
CHAPTER THREE	42
RESEARCH DESIGN AND METHODOLOGY	42
3.1 Introduction	42
3.2 Research Design	42
3.3 Location of the Study.....	42
3.4 Instruments Used in Electrical Characterization	42
3.5 Devices Set-up and Configuration.....	46
3.6 Data Input and Collection	52
3.7 Data Validation.....	55
3.8 Data Analysis	55
3.9 Ethical Considerations	55
CHAPTER FOUR.....	56
DATA ANALYSIS, RESULTS, AND INTERPRETATIONS.....	56
4.1 Introduction	56
4.2 Results and Discussions of the Study	56
4.3 Discussions of the Findings	114
CHAPTER FIVE.....	115
SUMMARY, CONCLUSIONS, AND RECOMMENDATION.....	115
5.1 Introduction	115
5.2 Summary of Major Findings	115
5.3 Conclusion	116

5.4 Recommendation.....	110
REFERENCES.....	112
APPENDIX I: IPGS INTRODUCTORY LETTER.....	121
APPENDIX II: KUREC LETTER	122
APPENDIX III: NACOSTI PERMIT	123
APPENDIX IV: KEITHLEY INSTRUMENTS	125
APPENDIX V: NATIONAL INSTRUMENTS' SOFTWARE	141
APPENDIX VI: CONFERENCE CERTIFICATE	143
APPENDIX VII: PUBLICATION	144

LIST OF TABLES

Table 1. Female IEEE 488 connector pin definitions.....	13
Table 2. Summary of previous related research and their limitations	40
Table 3. Selects and addresses	57
Table 4. The default setup for 2182A.....	76
Table 5. Sweep status model bits in model 6220	92
Table 6. Hall Effect I – V data	96
Table 7. Sweep Settings.....	100
Table 8. Trials and Percentage Errors	110
Table 9. Manually collected IV data	110
Table 10. Manually obtained VI data analysis.....	113
Table 11. Comparison between automated and manually obtained values	113

LIST OF FIGURES

Figure 1. Standard Type A and B USB male ports and pinouts	11
Figure 2. Female GPIB connector and layout.....	12
Figure 3. ATE components.....	17
Figure 4. A sample of automated test equipment	19
Figure 5. Instruments Communications Block Diagram.....	20
Figure 6. Hall Effect measurement convention	22
Figure 7. Germanium FCC structure.....	27
Figure 8. A graph of V_H against I for n - Ge	29
Figure 9. A graph of V_H against I for p - Ge.....	29
Figure 10. A graph of $(R_m - R_0)/R_0$ against (B) for n - Ge.....	30
Figure 11. A graph of $(R_m - R_0)/R_0$ against (B) p - Ge.....	31
Figure 12. A graph of $1/V_P$ against $1/T$ for n - Ge.....	32
Figure 13. A graph of $1/V_P$ against $1/T$ for p - Ge.....	32
Figure 14. A graph of V_H against B for n - Ge	33
Figure 15. A graph of V_H against B for p -Ge	33
Figure 16. A graph of V_H against T for n - Ge	34
Figure 17. A graph of V_H against T for p - Ge	36
Figure 18. Schematic diagram of the system.....	37
Figure 19. Fixed magnets used in the experiment	43
Figure 20. Probed Germanium sample.....	46
Figure 21. Keithley 7001 External Connection	48
Figure 22. Model 2107 input cable	49
Figure 23. Model 237-ALG-2 Triax connector and ground point	50

Figure 24. Model 237-ALG-2 Output configuration	51
Figure 25. Output connection and shielding	52
Figure 26. Data flow diagram for the automated test system	54
Figure 27. Block diagram for initializing model 7001 (a).....	58
Figure 28. Block diagram for initializing model 7001 (b)	58
Figure 29. Block diagram for initializing model 7001 (c).....	59
Figure 30. Block diagram for sending a message to model 7001 (a).....	59
Figure 31. Block diagram for sending a message to model 7001 (b)	60
Figure 32. Block diagram for sending a message to model 7001 (c).....	60
Figure 33. Block diagram for receiving a message from model 7001 (a).....	61
Figure 34. Block diagram for receiving a message from model 7001 (b).....	61
Figure 35. Block diagram for receiving a message from model 7001 (c).....	61
Figure 36. Block diagram for resetting model 7001	62
Figure 37. Block diagram for error querying model 7001(a)	62
Figure 38. Block diagram for error querying model 7001(b)	63
Figure 39. Block diagram for configuring 7168 scanner card in model 7001.....	63
Figure 40. Block diagram for session closure in model 7001	64
Figure 41. Block diagram for Global Error querying (a) in model 7001	65
Figure 42. Block diagram for Global Error querying (b) in model 7001	65
Figure 43. Block diagram for Global Error querying (c) in model 7001	67
Figure 44. Block diagram for Global Error querying (d) in model 7001	67
Figure 45. Block diagram for Global Error querying (e) in model 7001	68
Figure 46. Block diagram for Global Error querying (f) in model 7001.....	68
Figure 47. Block diagram for Global Error querying (g) in model 7001	69
Figure 48. Block diagram for Simple Error querying	69

Figure 49. Block diagram for scanning channels in model 7001	70
Figure 50. Block diagram for populating channel list in model 7001	70
Figure 51. Block diagram for Opening/Closing Channels in model 7001	71
Figure 52. Block diagram for Reading SCPI Error Queue in model 7001 (a)	71
Figure 53. Block diagram for Reading SCPI Error Queue in model 7001 (b)	72
Figure 54. Block diagram for Switching digital output in 7056 card	72
Figure 55. Front panel diagram for controlling model 7001	73
Figure 56. Block diagram for opening session in model 2182A	74
Figure 57. Block diagram for querying instrument ID in model 2182A.....	74
Figure 58. Block diagram for resetting model 2182A	75
Figure 59. Block diagram for restoring model 2182A to the default setting.....	75
Figure 60. Block diagram for error Session termination in model 2182A	76
Figure 61. Block diagram for Error querying and reporting in model 2182A	77
Figure 62. Block diagram for self-testing model 2182A.....	78
Figure 63. Front panel photo of model 2182A displaying a voltage reading	79
Figure 64. Block diagram of voltage and time interval measurements in model 2182A.....	80
Figure 65. Screenshot of front panel interface for model 2182A	80
Figure 66. Block diagram for opening model 6220	81
Figure 67. Block diagram for querying model 6220 ID.....	82
Figure 68. Block diagram for resetting model 6220 (a).....	82
Figure 69. Block diagram for resetting model 6220 (b).....	83
Figure 70. Block diagram for resetting model 6220 (c).....	83
Figure 71. Block diagram for error checking and terminating session in model 6220 (a).....	84
Figure 72. Block diagram for error checking and terminating session in model 6220 (b)	84
Figure 73. Block diagram for obtaining linear staircase points	85

Figure 74. Block diagram for obtaining logarithmic staircase points	86
Figure 75. Block diagram for setting the sweep type in model 6220	86
Figure 76. Block diagram for arming and initializing sweep in model 6220 (a).....	87
Figure 77. Block diagram for arming and initializing sweep in model 6220 (b)	87
Figure 78. Front panel for setting sweep parameters in model 6220	88
Figure 79. Block diagram for setting Lin Log parameters in model 6220	89
Figure 80. Block diagram for setting source delay in model 6220	89
Figure 81. Block diagram for concatenating current array.....	90
Figure 82. Block diagram for getting operation event register in model 6220.....	93
Figure 83. Block diagram for getting operation event register in model 6220.....	93
Figure 84. Block diagram for toggling the output state in model 6220	94
Figure 85. Block diagram for setting compliance in model 6220.....	95
Figure 86. Front panel for inputting sample size, compliance and the magnetic field strength	95
Figure 87. Front panel showing $V - t$ graphs	98
Figure 88. Block diagram for exporting $I-V$ data	98
Figure 89. Block diagram for exporting input and output parameters	99
Figure 90. Front panel Showing $V - I$ graphs	101
Figure 91. Block diagram for plotting $V - I$ and $V - t$ graph.....	101
Figure 92. Front panel Showing average resistance for different permutations	102
Figure 93. Front panel Showing average resistance and elapsed time.....	102
Figure 94. Block diagram for constrained linear fit VI	104
Figure 95. Block diagram for generating the Elapsed time	104
Figure 96. Block diagram for calculating the Hall parameters	105
Figure 97. Photo of the PC and Keithley Instruments.....	105

Figure 98. Front panel Showing Hall Effect experiment results 106

Figure 99. The front panel of dS - t graphs 108

Figure 100. Manually obtained vs automatically obtained VI Data Graphs 112

LIST OF ABBREVIATIONS AND ACRONYMS

API	Application Programming Interface
ATE	Automated Test Equipment
CSV	Comma Separated Value
DC	Direct Current
DIY	Do It Yourself
DUT	Device under Test
FVR	Frequency Variable Resistor
GUI	Graphical User Interface
GPIB	General Purpose Interface Bus
HP	Hewlett-Packard
IEEE	Institute of Electrical and Electronic Engineers
IDE	Integrated Development Environment
IVI	Interchangeable Virtual Instrument
LabVIEW	Laboratory Virtual Instruments Engineering Workshop
LPT	Line Print Terminal
NI	National Instrument Corporation
OS	Operating System
PC	Personal Computer
PCI	Peripheral Component Interconnect
RS	Recommended Standard
SCPI	Standard Commands for Programmable Instruments
USB	Universal Serial Bus
UUT	Unit under Test

VI	Virtual Instruments
VISA	Virtual Instruments Software Architecture
VXI	VME eXtensions for Instrumentation
VME	Virtual Machine Environment
Wi-Fi	Wireless Area Network

CHAPTER ONE

INTRODUCTION

1.1 Overview

This chapter contains the background of the study, the problem statement, the purpose of the research study, the objectives of the study, the research questions, the justification, scope, limitations, and assumptions of this study.

1.2 Background of Study

Thin-film semiconductors have received a lot of attention because of their rapid scientific and technological importance (Chen, 2021). Demand for thin-film semiconductors production is expected to rise significantly in the coming years as chips become even more deeply embedded in today's and tomorrow's critical technologies (Sarah, 2022) further extending Moore's law (Shalf, 2020). This has led to suppliers working feverishly to increase output, adding new factories, and spending billions of dollars in capital expenditures to avert shortages due to stronger demand for more advanced chips from consumer electronics and industries (Dashveenjit, 2021).

Thin-film characterization has relentlessly advanced over time to improve materials assessment quality and reliability. This comprises physical, chemical, optical, and electrical characterization. Rapid advances in the efficiency and production of materials including semiconductors have been vital factors of technological dominance (Jamal, 2017). Materials with sophisticated electrical characteristics are in high demand for the production of a wide range of information technology products (McCain, 2022). In electrical characterization, physical parameters such as resistivity, conductivity, charge carrier concentration, and mobility, as well as charge carriers' type - electrons or holes, are of significant interest and can be determined by measuring the Hall Effect (Green, 2011; Wang *et al.*, 2013), which is among

the most important semiconductor characterization techniques (Onwujiariri, 2020) used in both industries and research.

Hall Effect arises when an electric current flows perpendicular to a magnetic field through an n-type (p-type) semiconductor hence deflecting the electrons (holes). The Hall voltage is created when these charged carriers deflect, and its polarity depends on the effective charge of the carrier (Gaj, 2011). The Hall Effect has a wide range of applications in several scientific and technological domains. To accurately determine the intensity and polarity of magnetic fields, it is mostly used in their measurement and characterization (Bestwick *et al.*, 2015). Hall Effect sensors are essential parts of equipment like vehicle speedometers (Anwar *et al.*, 2015), industrial automation systems (Manojkumar *et al.*, 2022), and current sensors for power management because they are employed in electronics for location sensing, speed detection, and current measurements (Chen *et al.*, 2017; Lekdim *et al.*, 2022; Saputra *et al.*, 2020). The Hall Effect also flourishes in semiconductor and materials science research, allowing for the examination of charge carrier characteristics in solid-state materials and the creation of novel electrical and magneto-optical devices (Choi *et al.*, 2020; Karsenty, 2020; Liu *et al.*, 2020).

In electrical characterization, the four-point probe technique has evolved into an integrative characterization tool in various disciplines and fields, and it is used for both profound and application-driven studies. (Miccoli *et al.*, 2015). The four-point probe gets its name from the four probes that touch the sample on the surface. The four-point probe is a device that measures a material's electrical conductivity and resistance by passing a small current through two contacts and measuring the potential difference between two of them. This method is regarded as one of the most reliable and accurate methods for characterizing the electrical properties of materials (Li *et al.*, 2012), particularly thin films and substrates with low conductivity or resistance. The four-point probe is commonly used in the manufacturing of thin-film transistors, integrated circuits, solar cells, and other electronic materials.

The rapid development of technology and computers larger number of students (Schindler *et al.*, 2017). Similarly, technology is used as a tool to conduct laboratory research. This technology can range from a simple manual data recorder in the form of literacy among users, as well as the growing popularity of Internet connection has provided various institutions around the world with an opportunity to enhance outcomes and provide access to a spreadsheet (Hauer, 2020) to a very sophisticated experimentation system in which the computer controls the entire setup. This necessitates a laboratory experience by making simulation programs of laboratory exercises via computer programs (Liscouski, 2015), or, having a remote laboratory which is equipped with real instruments allowing for experiments to be carried out by operating the devices and, viewing real data from a distant place via the network (Coito, 2008). The demand for more advanced methods used to determine the electrical characterization of semiconductors has been an important aspect of the rapid growth in the development and manufacturing of solid-state devices.

Groover (2014) defines automation as the technology that allows a particular procedure to be done with minimal human assistance. In conducting laboratory tests and measurements, automation entails flexible, simple, and high-efficiency data acquisition, processing, and analysis in real time. Integration of automation in laboratories yields intelligent solutions with higher quality and productivity while reducing time and errors (Herrera, 2022). It entails employing various control devices, including Personal computers (PCs), various sensors and actuators, communication buses and modules, machines, human-machine interface systems, and other control equipment (Choudhary *et al.*, 2018).

For the PC to communicate with the peripheral device, it should have an interface. An interface is defined as a common boundary that allows two or more computer system components to send and receive information, facilitating the computer software, computer

hardware, peripheral devices and drivers, users, and combinations of all these can exchange information (Hookway, 2014).

The commonly available stand-alone industry-standard buses include the serial port (RS-485, RS-422, or RS-232), Line Print Terminal (LPT) port, Universal Serial Bus (USB), General Purpose Interface Bus (GPIB), Ethernet, and Firewire (Institute of Electrical and Electronic Engineers (IEEE) 1394). A bus transports data between a Central Processing Unit and the system memory via the motherboard. (Sahana, 2021). With the widespread and advent development of wireless communications, most recently manufactured measuring instruments can support Bluetooth or Wi-Fi technologies in establishing communications (Alomari *et al.*, 2011). Automation and precise computerized control of taking measurements are critical steps toward an experiment's high accuracy, precision, and reliability (Nelson, 2015). Moreover, an automated system with advanced software such as Laboratory Virtual Instruments Engineering Workshop (LabVIEW) can provide real-time control and data processing capabilities, (Khalifa *et al.*, 2021) lowering characterization time dramatically coupled with high-precision measuring instruments with low-noise cables and probes.

Automated electrical characterization is an important part of quality control in the electronic industry because it allows manufacturers to determine the electrical properties of their products quickly and efficiently, as well as detect any defects or issues early in the production process. There are numerous advantages to automated electrical characterization. It is much faster and more accurate than manual testing methods, and it reduces the possibility of human error. Additionally, automated testing ensures that the results are consistent and repeatable. This can be reported from the works of Agumba *et al.* (2011) and Garnica *et al.* (2019).

1.3 Problem Statement

The need for thin film materials is expanding due to high demand from current and future applications, a growing need for efficiency and miniaturization, technical innovation, and governmental requirements, mandates, and subsidies. ("Thin Film Material Market," 2022). It is therefore crucial to have quick, nondestructive, precise, and simple electrical characterization techniques accessible for evaluating material quality and device reliability (Deen *et al.*, 2017). This will enable the industries to cope with the demand for upgraded materials and possibly lower the cost of resulting devices as a product of balanced demand and supply.

Traditional electrical characterization of materials is often plagued with inefficiencies and inaccuracies arising from human factors owing to the immense data that must be manually acquired and analyzed. These can be minimized by automation which may provide several advantages, such as improved speed, accuracy, and error reduction as evidenced by the works of Agumba *et al.* (2011), Cervantes *et al.* (2018), Valladares *et al.* (2019) and Garnica *et al.* (2019). However, their systems were limited to obtaining thin-film sheet resistivity, conductivity, and capacitance measurements since they are based on current-voltage (I-V) and temperature measurements and did not support remote experimentation.

While fully automated commercial Hall Effect Apparatus are widely available, they frequently come at a high price and with restricted modification possibilities, making them less accessible to educational institutions and amateurs (Kelley, 2023). A Do it yourself (DIY) automated Hall Effect Apparatus is a wonderful instructional tool that fosters a deeper grasp of fundamental physics principles as well as hands-on engineering abilities. Building one's automated setup encourages not only resourcefulness but also personalized exploration, boosting ingenuity and creativity in studying the Hall Effect phenomena. Furthermore, the process of building and programming such an apparatus improves students' problem-solving

skills and technical ability, supplementing theoretical information received from commercial alternatives. A deeper and more comprehensive understanding of the Hall Effect and its applications is fostered by the DIY version, which essentially gives students the power to close the gap between theory and practice.

This thesis reports on a DIY Hall Effect system that is not limited to conducting thin-film sheet resistivity, conductivity and capacitance measurements but can additionally obtain the Hall voltage, charge carrier mobility, carrier concentration, Hall coefficient, Hall angle and the conductivity type (N or P) of thin-film sheets which cannot be obtained by ordinary four-point probe I-V measurements.

1.4 Objectives of the Study

1.4.1 General Objective of the Study

To design, build, interface and assemble a LabVIEW-based automated Hall Effect test system for electrical characterization of thin films.

1.4.2 Specific Objectives of the Study

- i. To configure the Interfaces for Keithley 2182A, 6220, and 7001 Instruments for LabVIEW remote operations
- ii. To develop LabVIEW Virtual Instruments (VIs) and Sub-VIs to remote control the Keithley instruments and derive the electrical characteristics for a semiconductor sample.
- iii. To integrate the LabVIEW VIs and Sub-VIs with the Keithley Instruments
- iv. To validate the automated Hall Effect apparatus by subjecting a Germanium semiconductor sample to tests.

1.5 Research Questions

- i. How are Keithley 2182A, 6220, and 7001 Instruments configured for LabVIEW remote operations?
- ii. How are LabVIEW VIs and sub-VIs developed for remote controlling Keithley instruments and deriving electrical characteristics of a semiconductor sample?
- iii. How are LabVIEW VIs and sub-VIs integrated with the Keithley Instruments?
- iv. How are automated Hall Effect apparatuses validated using semiconductor samples?

1.6 Justification for the Study

According to Chen (2021), thin films particularly, semiconductors are not only valuable but also in great demand, especially in microelectronics industries, which necessitates taking measurements of their properties in a simpler, more accurate, cheaper, and real-time. Most commercial devices used for electric characterization are manual, quite expensive, tedious to use, and not user-friendly. Hence, there is a need to design and develop a system that is less expensive and has ease of use. This study aims to provide an interactive and simple Graphical user interface (GUI) system that intends to generate the electrical properties of materials by utilizing the four-point probe technique, Keithley instruments, a four-point probe, and a PC by use of LabVIEW VIs which is not available.

This system can measure, display and analyze both I-V characteristics of the thin films and use these variables for the calculation of their electric properties while concurrently monitoring changes in carrier concentration and mobility in situ when the physical parameters are changed.

This research will help the end-users to carry out four-point probe measurements easily and fast with interactive data collection via LabVIEW VIs and Standard Commands for Programmable Instruments

(SCPI) commands for data transfer to and from the Keithley instruments via GPIB - USB port and also provide a user-friendly device interface for instrument interaction, control, data collection and control, analysis and presentations. Besides, it will add to the wealth of knowledge in the instrumentation field.

1.7 Scope of the Study

This study focuses on the electrical characterization of various thin-film semiconductors. Calibration of the instruments was done according to the instructional manual provided by Keithley. After the instrumentation, the system was applicable for use in thin-film semiconductors only.

1.8. Significance of the Study

This study aims at introducing a simple but effective and flexible system that can be adapted to meet changing needs. The developed system is available for use in characterizing thin film samples.

1.9 Limitations of the Study

There is a small volume of information and research done on developing automated test equipment for thin films' electrical characterization. Therefore, it is challenging to compare findings with other similar research done. This limitation, however, was solved by comparing the findings with the one that was manually done. Furthermore, resources are hardly available since there are a few thin-film samples to be used and the instruments used are to be sourced from overseas which may take some time to acquire.

1.10 Assumptions of the Study

The study made the following assumptions;

- i. The program and the ports used were able to communicate and transfer data without lagging to obtain real-time values and visualizations
- ii. The apparatus to be used in all the experimental work is readily available, in good condition, and provides accurate, precise, and reliable results.

CHAPTER TWO

LITERATURE REVIEW

2.1 Introduction

This chapter consists of a theoretical review and an empirical review.

2.2 Theoretical Review

This section discusses the background of the four-point probe, the peripheral computer interfaces, and configurations of the device, the electrical properties of thin films, the LabVIEW IDE, and the conceptual framework.

2.2.1 Interfacing and Configuration of Measuring Instruments

Hookway (2014) defines interfacing as the process of making communication between devices or systems technically compatible so that they can work together as needed. Computers are frequently used to automate measuring processes by interacting with measurement equipment (Hadley, n.d). The computer has various standard built-in ports that are used to interface devices. Ports provide external connections to a computer which facilitates interactions with peripheral devices. Teja (2021) describes a computer port as a terminal or an interface between a computer and its peripheral devices. A computer port is sometimes known as a communication port because it facilitates communication between the computer and its peripheral devices. The female end of the connection is commonly referred to as a port, and it is normally located on the motherboard. Only devices and ports intended to be used are discussed in this section.

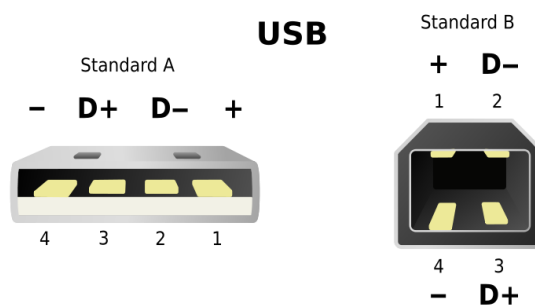
2.2.1.1 Universal Serial Bus (USB)

Techopedia (2020) describes the Universal Serial Bus (USB) as a standard interface that allows devices to communicate with a host controller, such as a PC or smartphone. It

interfaces with peripheral devices such as digital cameras, mice, keyboards, printers, scanners, media players, external hard drives, and flash drives. As of now, there is an overwhelming use of the USB interface. Almost all peripherals made in this day and age come with a USB version (Cunningham, 2014). Composite devices, which can have several configurations and interfaces, each of which is a separate entity, are where USB's actual flexibility lies. (Tian *et al.*, 2018) . Moreover, its popularity is due to its versatile and ultrafast structure that enables interconnectivity between USB-enabled devices and the computer by employing a common interfacing standard (Schilling *et al.*, 2016). In the USB ports, up to five layers of additional USB hubs may be added to accommodate up to 127 devices linked to a single host controller. It exists in various types and has gone through four generations to date, including eleven connectors of different types of which USB-C is the most recent (Hachman, 2019). Figure 1 shows two commonly found types of USB and their respective pinouts.

Figure 1.

Standard Type A and B USB male ports and pinouts



Note: Pin 1 = VBUS (+5 v), Pin 2 = Data -, Pin 3 = Data +, Pin 4 = Ground. From *Standard USB connectors, types A and B*, graphic by E. Simon, 2008.

(<https://www.pngegg.com/en/png-mlpnf>) CC BY-NC

2.2.1.2 General Purpose Interface Bus (IEEE 488)

This port is an 8-bit parallel multi-master interface bus called the IEEE 488 bus that is used for short-range communications. The bus was given the name General Purpose Interface Bus

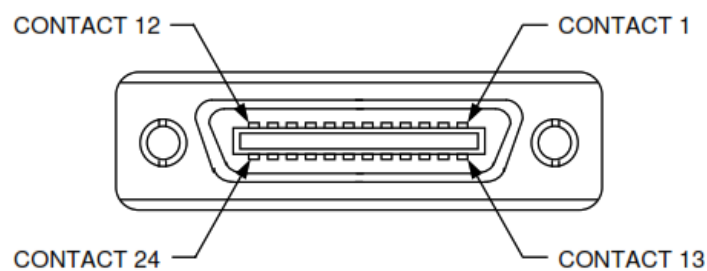
(GPIB) as it evolved into the primary interface that complied with numerous standards. Due to its adaptability, data transmission can occur between any devices on the bus that have a speed appropriate for the slowest active device. (Lott, 2022; WatElectronics, 2022)

The port was developed by Hewlett-Packard and later standardized by IEEE to ease connections between instruments and controllers, such as computers (Romanchik, 2015). It is a digital, Eight-bit parallel communication interface with a high data transfer rate of up to 8 Mbps. It can support up to 31 5-bit primary device numbers from 0 to 30. Each device on the bus must be assigned a unique address for identification and communication according to NI ("GPIB Messages," 2020). The bus provides one system controller for up to 15 instruments and cabling for up to 20 m. There is a master controller (often a computer) that manages the data transfer between transmitters and receivers so that multiple devices can "coexist" on the bus. The controller, which is typically the only one, can designate one or more devices as listeners and one or more as talkers, each of which can transmit and receive data. (Sivaranjith, 2018)

Using GPIB expanders and active extenders, this constraint may be bypassed. To decrease noise, GPIB cables and connections are normally industrially insulated. The Keithley 6220, 7001, and 2182A have this amongst other ports for sending and receiving commands. The pinouts for this port are given in Figure 2 and illustrated in Table 1

Figure 2.

Female GPIB connector and layout



Note. From *IEEE-488 GPIB Communications*.

(https://magna-power.com/assets/docs/html_ts/_images/connector-ieee488.svg) Copyright 2020, Magna-Power Electronics, Inc.

Table 1.

Female IEEE 488 connector pin definitions

Terminal	Signal	Description
1	DIO1	Data input/output bit.
2	DIO2	Data input/output bit.
3	DIO3	Data input/output bit.
4	DIO4	Data input/output bit.
5	EOI	End-or-identify.
6	DAV	Data valid.
7	NRFD	Not ready for data.
8	NDAC	No data accepted.
9	IFC	Interface clear.
10	SRQ	Service request.
11	ATN	Attention.
12	SHIELD	Shield
13	DIOS	Data input/output bit.
14	DIO6	Data input/output bit.
15	DIO7	Data input/output bit.
16	DIO8	Data input/output bit.
17	REN	Remote enable.
18	GND	(Wire twisted with DAV)
19	GND	(Wire twisted with NRFD)
20	GND	(Wire twisted with NDAC)
21	GND	(Wire twisted with IFC)
22	GND	(Wire twisted with SRQ)
23	GND	(Wire twisted with ATN)
24	Signal Ground	Logic ground

Note. Adapted from *IEEE-488 GPIB Communications*.

(https://magna-power.com/assets/docs/html_ts/index-operation_computer_programming.html)

Copyright 2020, Magna-Power Electronics, Inc.

Measuring instruments have several connection ports that can be utilized. This includes GPIB, RS-232, LAN port, and USB port. According to Keysight Technologies (2014), the most common interfaces for connecting instruments to PCs conducting tests and measurements have been the RS-232 and GPIB. RS-232 has been a cheaper alternative but is characterized by low baud rate and connection constraints (can only allow one device at a time) making it slow and inconvenient for more of today's measuring applications. On the other hand, GPIB technology has significantly provided high-performance and steady communications for more than two decades according to Agilent Technologies (2009). USB and LAN ports are nowadays incorporated into most modern PCs evolving into an acceptable option for controlling and automating test and measurement instruments. A USB/ GPIB converter is the easiest and quickest way to interface instruments to a PC allowing a direct connection from your PC's USB port to GPIB instruments. The ANSI/IEEE 488.21987 standard defined precisely the SCPI language in which the controllers and instruments should communicate. Keithley 7001, 6220, and 2182A have only RS-232, GPIB, and Local Area Network (LAN) ports. Selection has to be made in the front panel for the port (RS-232 or GPIB) and the desired language (SCPI or KI-220).

2.2.2 Programming Languages and Environment

The system software has reduced the programming in machine codes. With concerns about user interactions in the software industry, in recent years, visual programming has transmogrified the art of coding from cumbersome machine coding to dragging and dropping of icons in seamless transformation. This has been accomplished through the creation of dedicated Integrated Development Environment (IDE) platforms such as LabVIEW (Ray,

2017). Red Hat (2019) defines IDE as a software application that gives complete software development features to computer professionals. It is comprised of a source code editor, build automation tools and a debugger. Although, some also include a compiler, interpreter, or both. Implementing the VISA is done with some instruments. The plug-and-play functionality of the instruments is provided by this standard. VISA-compliant software, like LabVIEW ("Using VISA in LabVIEW - NI," 2022) or Python (PyVISA, 2022), can identify the instruments that are connected to the computer and interact with them. Sending text strings to the instrument is often how this communication happens. Standard Commands for Programmable Instruments (SCPI) is an established format (Hadley, n.d). To connect with some manufacturers' instruments since they do not adhere to these standards, drivers must be installed. LabVIEW IDE and SCPI were used in this study.

2.2.2.1 LabVIEW Integrated Development Environment

Laboratory Virtual Instrument Engineering Workbench (LabVIEW) is a graphically-based IDE developed by the National Instrument Corporation (NI) in the late 1980s. Because of its graphical character, it is appropriate for applications for conducting tests and measurements, instrument control, automation, data collection, and analysis (Bitter *et al.*, 2017). Furthermore, for design, tests, measurements, automation, and control applications, LabVIEW is widely regarded as the industry standard (Bishop, 2015). NI focuses on test and measurement products. Therefore, they have outstanding knowledge of LabVIEW design and development. Engineers, scientists, and students utilize it to create measurement, test, and control applications. Because it boasts unequally, LabVIEW is well-suited for this purpose courtesy of its integration with many hardware devices and dozens of in-built libraries for data analysis and visualization (Bress *et al.*, 2013). A LabVIEW program is called a "virtual instrument" or simply a VI while a sub-program is referred to as Sub-VI.

In LabVIEW, diagrams that perform numerous actions at the same time can be created (Boubaker, 2011). As a result, LabVIEW is a multitasking system capable of executing several execution threads and many VIs at the same time. Thus, LabVIEW accelerates development by a factor of ten when compared to traditional textual programming, and it has a lot of cool features that make it a great tool for device interface, data acquisition, data processing, and data displays (Du *et al.*, 2017) which are core areas of this study. The LabVIEW VI program was used to control the Keithley 6220 Precision current source, Keithley 7001 switching system, and Keithley 2182A Nanovoltmeter instruments both developed by NI.

2.2.2.2 Standard Commands for Programmable Instruments

Standard Commands for Programmable Instruments (SCPI) is an ASCII-based programming language that employs a tree architecture, which is a hierarchical structure (Houlihan *et al.*, 2014). Subsystems are formed when related commands are clustered under a single node or root. SCPI is a standardized instrument command language for controlling instruments by addressing a wide range of instrument functions and ensuring consistency amongst instruments of the same class and functional capacity from a remote programming position. (Balaji *et al.*, 2021). An example of SCPI code that sweeps Direct current (DC) voltage is written as;

```
SENSe:
    VOLTage:
        DC:RANGe {<range>|MIN|MAX|DEF}
        DC: RANGe? [MINimum | MAXimum | DEFault]
```

SCPI is used by the greater part of programmable bench devices (Desjardin, 2013).

2.2.3 Automation and Remote Operations

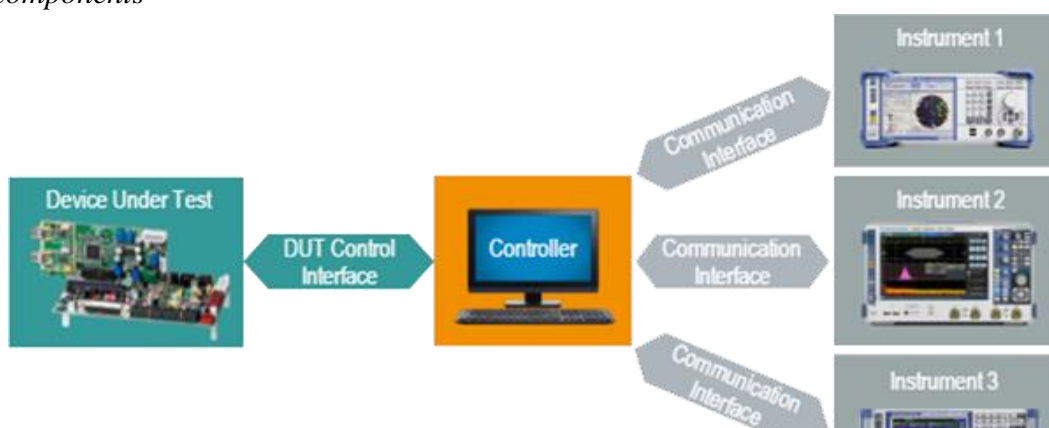
Automation is an interfacing technique that implements the control of equipment such as laboratory equipment or intelligent devices with advanced technology, to get reliable, accurate and remote operation. According to Portolan (2019), the most significant testing advancements have been made possible by automation, which has become a staple of the electronics industry. Reducing human interaction has been one of the key forces behind testing because it has led to more repeatable, dependable, and predictable outcomes as well as significant cost savings and improved inter-vendor portability. Automation has become so common in conducting tests and measurements that almost every contemporary measurement device may now be operated remotely. A control device for remotely controlling a measurement device includes a graphical user interface to process user commands, a processor to turn the commands into a signal, a transceiver to transmit the signal to the measurement device, and a receiver to receive a return signal from the measurement device.

Automated test equipment (ATE) is the terminology for the tools used to carry out automated operations. According to Rohde *et al.* (2022), An ATE includes a controller, which is typically a PC, laptop, or industrial computer, A physical communication interface between the controller and the measuring instrument(s), one or more measurement equipment that may be operated remotely, a remote control software running on your control computer, and the units under test (UUTs) or device under test (DUT). Test and measurement programs require some types of I/O library to facilitate communication with the test instrument (Zhang *et al.*, 2013).

Figure 3 shows automated test equipment components

Figure 3.

ATE components



Note. Reprinted from *Basics of Instrument Remote Control* by Rohde & Schwarz.

(https://cdn.rohde-schwarz.com/pws/service_support/driver_pagedq/ch_1_inred/CH1_ATEgeneral_16x9_w900_hX.png) Copyright 2023 Rohde & Schwarz.

The global market for automated test equipment is anticipated to develop at a compound yearly growth rate of 3.60% from 2019 to 2025, according to experts at Zion Market Research (2022). Automated test equipment is a tool that uses automation to run tests on a variety of UUTs or DUTs to do measurements and quickly evaluate the outcomes. The key factors driving the growth of the global ATE test equipment market include an increase in semiconductor device manufacturing, an increase in the complexity and required performance level of semiconductors used in consumer electronic products and the development of next-generation devices and technologies associated with these devices. Analysts believe that the rapid evolution of a 28 nm node application processor production process will increase the demand for IC testing equipment, driving the growth of the ATE. Figure 4 shows a sample ATE from Avera Technologies.

Figure 4.

A sample of automated test equipment



Note. Reprinted from *Automated Test Equipment*, Photograph by Avera 2023.

(https://www.avera.com/hubfs/Avera_April2021/Images/ate-1000-863.jpg) Copyright 2023

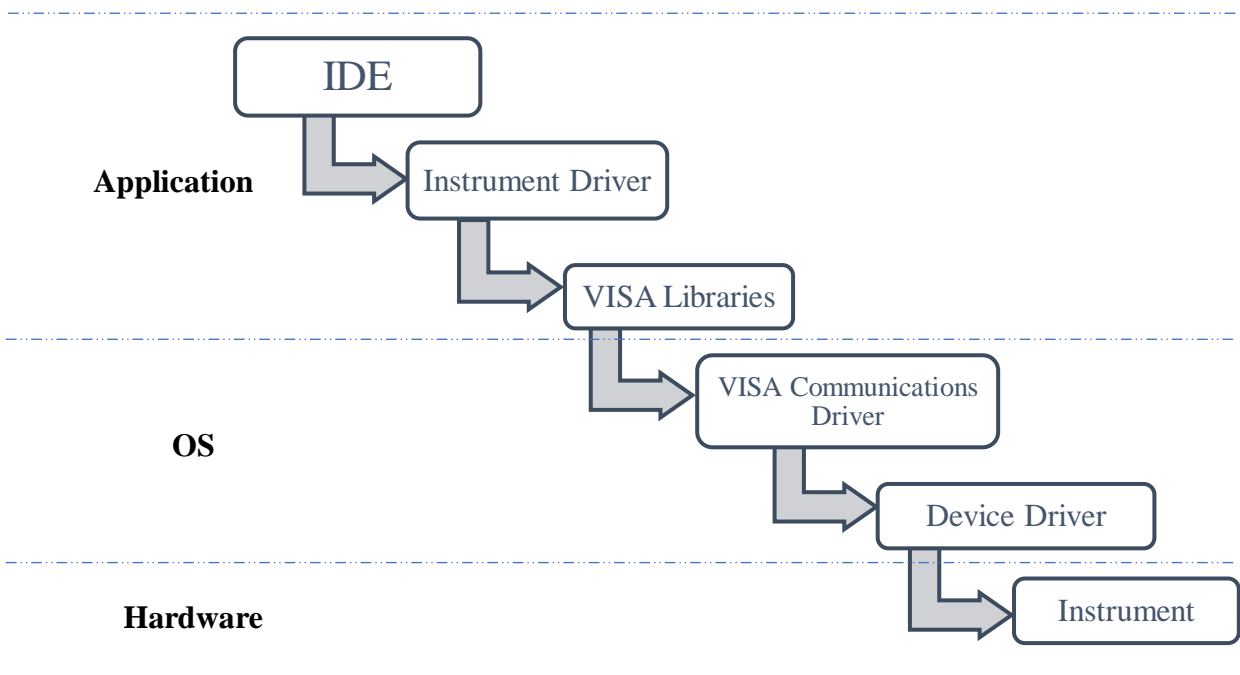
Avera

Instrument drivers provide a layer of abstraction between remote control software and the SCPI commands of a measuring instrument enabling instrument configuration and remote

control. Some instrument drivers employ an IVI driver protocol. These drivers provide enormous control and customization capabilities (Bitter *et al.*, 2017; Mary, 2022). VISA is a communication application programming interface for use with test and measurement instruments that is industry standard. It enables the creation of bus-independent programs. VISA libraries support a variety of interfaces, including GPIB, USB, RS232, and Ethernet (NI-VISA, 2015). The interaction between the application, OS, and hardware is illustrated in Figure 5.

Figure 5.

Instruments Communications Block Diagram



Note. Adapted from *What Are The Differences Between Device Drivers And Instrument Drivers?* By Tektronix, 2023. (<https://www.tek.com/en/support/faqs/what-are-differences-between-device-drivers-and-instrument-drivers>) Copyright Tektronix, 2023.

DIY measuring devices have grown in favour among hobbyists, academics, and tinkerers due to their adaptability and cost (Staron *et al.*, 2011). Utilizing easily accessible components like microcontrollers, sensors, and open-source software, these systems include building unique measuring setups. DIY enthusiasts may create measuring systems that are customized for their

requirements, whether they are for scientific research, home automation, or environmental monitoring (Munro, 2019; Tunyagi *et al.*, 2018). DIY measuring devices encourage problem-solving ingenuity while providing essential hands-on learning opportunities, even if they may not always match the accuracy of commercial equipment. Additionally, they promote a cooperative online community where creators exchange ideas, programs, and know-how, helping to democratize science and technology by making sophisticated measuring tools available to a wider audience.

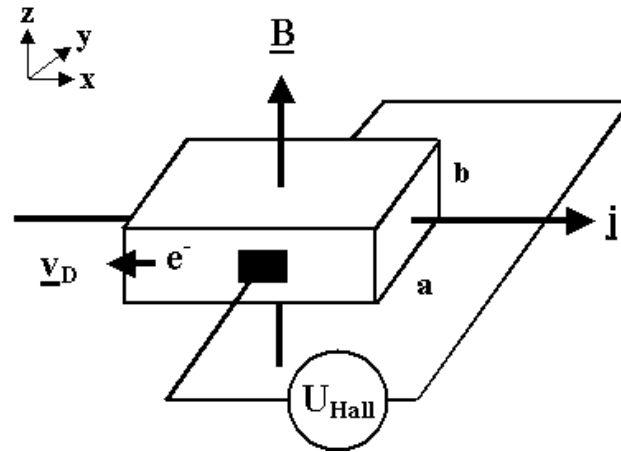
2.2.4 Electrical Characterization

This includes different techniques used to determine the electric transport properties. For any useful devices to be produced, the electric and electronic properties of semiconductors must be thoroughly understood as asserted by Lughfi (2012). There is a wide range of techniques available that examine various aspects of a material's electronic structure and exploit different effects (Jamal, 2017). The Hall Effect Measurements technique was used in this research to characterize thin films. When an electron moves perpendicular to a magnetic field, it encounters a force acting in both directions and moves in reaction to this force as well as the force influenced by the internal electric field. Leadley (2011) asserts that the Lorentz force is the fundamental physical principle vital for the Hall Effect.

Any movement of free carriers in conductors and semiconductors leads to a flowing current. This flow can be triggered by an electric field which can be due to an externally applied or induced voltage since the carriers are charged particles. Besides, carriers also flow from high to low carrier density regions. This movement varies from one material to another, in thin films, the four-point probe method has been widely used for characterizing both electrical properties over the years according to Miccoli *et al.* (2015). This section presents Hall properties that have been empirically obtained using a four-point probe method as shown in Figure 6.

Figure 6.

Hall Effect measurement convention



Note. Reprinted from “The Hall Effect” by H. Foll, n.d, Journal of *Electronic Materials* (https://www.tf.uni-kiel.de/matwis/amat/elmat_en/kap_1/illustr/hall_effect.png), copyright H. Foll, n.d

Individual properties of thin-film semiconductors that intend to be studied are as follows.

2.2.4.1 Hall Voltage (V_H)

Electric current flowing through a conductor placed in a region influenced by a magnetic field experiences a transverse force (Lorentz force) on the flowing charge carriers with a tendency to push on one side of the current-carrying conductor. This force (\vec{F}), is directly proportional to the magnitude of the particle charge, the magnitude of the magnetic field (\vec{B}) around the charged particle and the velocity (\vec{v}) of the particle. (Agarwal, 2020)

$$\vec{F}_B = -q\vec{v} \times \vec{B} \quad [2.1]$$

These pushed charges to build up at the side till the net force (\vec{F}_{net}) is balanced producing a determinate voltage between the two sides of the conductor due to the electric field ($q\vec{E}$) and the force due to the magnetic field (\vec{B}). (Agarwal, 2020)

$$\vec{F}_{Net} = q\vec{E} - q\vec{V} \times \vec{B} \quad [2.2]$$

The resultant electric potential difference formed across a given sample with a distance, w between the two sides of the sample is known as Hall voltage (V_H). It is given by, (Agarwal, 2020)

$$V_H = \Delta V = Ew \quad [2.3]$$

2.2.4.2 Material Resistivity (ρ) and Conductivity (σ)

Electrical resistivity (ρ) is a measure of how well a material conducts electrical current and is measured in ohms·centimetres. This measurement is obtained when a current flows alongside one edge of a sample under test while the voltage on the opposite edge for a sample of a given length l , thickness t , width w , and placed between a magnetic field (\vec{B}). From Ohms Law, the resistance (R) of the material is given by;

$$R = \frac{V}{I} \quad [2.4]$$

When multiple values of R are obtained and then averaged, an average resistance R_S is obtained, and the resistivity is then found by the formula;

$$\rho = R_S \cdot tw/l \quad [2.5]$$

Conductivity (σ) is the measure of how easily the electrical charges flow in a material and is given in Siemens per centimetre (S/m). It is the inverse of resistivity (Libretexts, 2021a)

$$\sigma = \frac{1}{\rho} \quad [2.6]$$

The reduction in the mean free path of the charge carriers is related to the change in sample resistance brought on by the magnetic field \vec{B} , while the measurement is being done while the current is steady. The resistance change is given by; (PHYWE, n.d)

$$\frac{R_m - R_0}{R_0} = \frac{U_m - U_0}{U_0} \quad [2.7]$$

where R_m and U_m represent the sample's resistance and voltage respectively in the presence of a magnetic field \vec{B} , and R_0 , U_0 represent the sample's resistance and voltage when $\vec{B} = 0$.

The intrinsic conductivity can be given as; (PHYWE, n.d)

$$\sigma = \sigma_0 \cdot \exp\left(-\frac{E_g}{2kT}\right) \quad [2.8]$$

where E_g = energy of bandgap, k = Boltzmann constant, and T = absolute temperature.

2.2.4.3 Hall Coefficient (R_H) and Material Doping Type

The doping type of a semiconductor is derived from an obtained value of the Hall coefficient (R_H), which is defined by, (Bhavsar, 2014)

$$R_H = \frac{V}{I} \cdot \frac{t}{B} = \rho \frac{t}{B} \quad [2.9]$$

The unit of R_H is expressed in m^3/C , as a result, The Hall Effect is an excellent tool for measuring either charge carrier density or magnetic field. Positive values of R_H imply that the majority of carriers are holes (P-Type) while negative values imply that the majority of carriers are electrons (N-Type)

2.2.4.4 Charge Carrier's Concentration (n)

When a semiconductor sample is kept across a magnetic field, its charge carrier experiences a force in the direction normal to both the magnetic field \vec{B} and the current I . Positive and negative charges flow to the opposite ends of the sample with a drift velocity until a steady state is reached. This causes a potential difference across the edges of the semiconductor. The concentration of the charge carriers (n) is given by; (Bhavsar, 2014)

$$n = -\frac{1}{eR_H} \quad [2.10]$$

2.2.4.5 Mobility (μ_m), and Hall Angle (Φ)

The Hall coefficient is also used to find the mobility of a semiconductor or a conductor sample (μ_m), and the Hall angle (Φ). Electrons or holes move with an average velocity when an electric field is applied across the semiconductor, The Hall mobility expresses the extent to which the Hall Effect takes place and is given by; ("What is Hall Effect?," 2020)

$$\mu_m = \frac{R_H}{\rho} \quad [2.11]$$

Alternatively, it can be obtained by finding the product of conductivity and the Hall constant for a conductor or semiconductor whereas the angle which exists between the resulting electric field strength and the current density i.e. Hall angle is given by; ("What is Hall Effect?," 2020)

$$\Phi = \tan^{-1}(\mu_m \vec{B}) \quad [2.12]$$

2.2.4.6 Magnetoresistance ($\Delta\rho/\rho_0$)

Depending on its nature, the resistivity (magnetoresistivity) of a sample under test might vary in the presence of the external magnetic field (\vec{B}). It is given by; (Hishiyama *et al.*, 2013)

$$\Delta\rho/\rho_0 = \frac{\rho(\vec{B}) - \rho_0}{\rho_0} = \frac{R(\vec{B}) - R_0}{R_0} \quad [2.13]$$

where ρ_0 and $\rho(\vec{B})$ are resistivities in magnetic fields of a magnitude zero and \vec{B} , respectively, and $R(\vec{B})$ and R_0 are similar electrical resistances and is proportional to; (Hishiyama *et al.*, 2013)

$$R \propto (1 + (\mu(\vec{B}))^2) \quad [2.14]$$

2.2.5 Theoretical Review of Germanium Semiconductor

Germanium (Ge), a chemical element in Group 14 (IVa) of the periodic table, is a silvery-grey metalloid with properties intermediate between metals and nonmetals ("Germanium | Encyclopedia ", 2018). Its atomic radius is 0.137 nm, and its electronic configuration is Ar 3d10 4s2 4p2. Except for a few compounds, germanium is a non-toxic element. According to Melcher *et al.* (2014), Germanium is an extremely rare element found in rocks. However, due to its siderophile, lithophile, chalcophile, and organophilic properties, it is present in trace amounts in most rock types. Most oxidic and sulfidic metalliferous deposits, such as banded iron formations, manganese nodules, shale-hosted sedimentary copper deposits, and porphyry copper deposits, contain trace amounts of germanium.

About 30% of the total amount of germanium consumed worldwide is made from recycled materials. More than 60% of the total of the germanium metal used in the production of most optical devices is regularly recycled as new scrap according to the U.S. Geological Survey (2020). The development of the germanium transistor paved the way for a wide range of solid-state electronics applications. Currently, fibre-optic communication networks (Sui *et al.*, 2017) and infrared night vision systems (Curtolo *et al.*, 2017; "Germanium Windows for Thermal Imaging and Night Vision," 2021) are some of the applications for germanium and its compounds. Additionally, single-crystal detectors made from highly purified germanium can

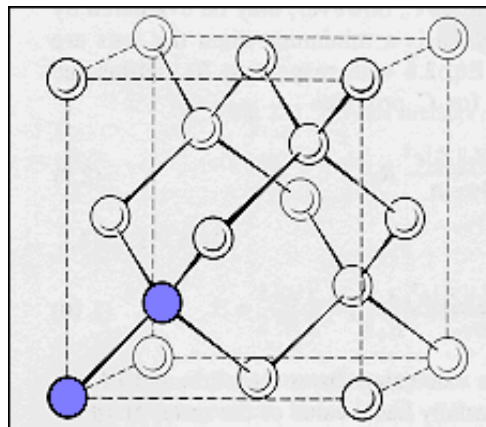
be used to locate radiation sources because germanium acts as a catalyst for some polymerization reactions

2.2.5.1 Structure of Germanium

It has the same crystal structure as a diamond and is a hard, greyish-white element with a metallic lustre. Germanium has a diamond lattice structure, with a basis of two germanium atoms at $(0,0,0)$ and $(1/4, 1/4, 1/4)$. It can be visualized as two intersecting fcc lattices of germanium atoms, with their origins displaced by $(1/4, 1/4, 1/4)$ (Royce *et al.*, 2002)

Figure 7.

Germanium FCC structure



Note. Copied from *The Structure and Properties of Engineering Materials* by S. H. Royce, 2002, (<https://www.princeton.edu/~maelabs/mae324/glos324/b103.gif>). Copyright by S. H. Royce, 2002.

2.2.5.2 Germanium Semiconductor Doping

Germanium has an atomic number of 32 and thus only four valency electrons. Germanium uses these atoms to form a covalent bond. Since the electrons are positioned stably, they do not act as a conductor. As a result, the Germanium element exhibits the aforementioned properties (Britannica, n.d). It is also devoid of any impurities. These are referred to as intrinsic semiconductors and their electrical characteristics fall somewhere between those of a

metal and an insulator (PHYWE, n.d). This metalloid is crystalline, brittle, and retains its lustre in the air at room temperature in its pure state. For semiconductors with an impurity of just one part in 10^{10} , zone refining methods have produced crystalline germanium (Ross, 2016).

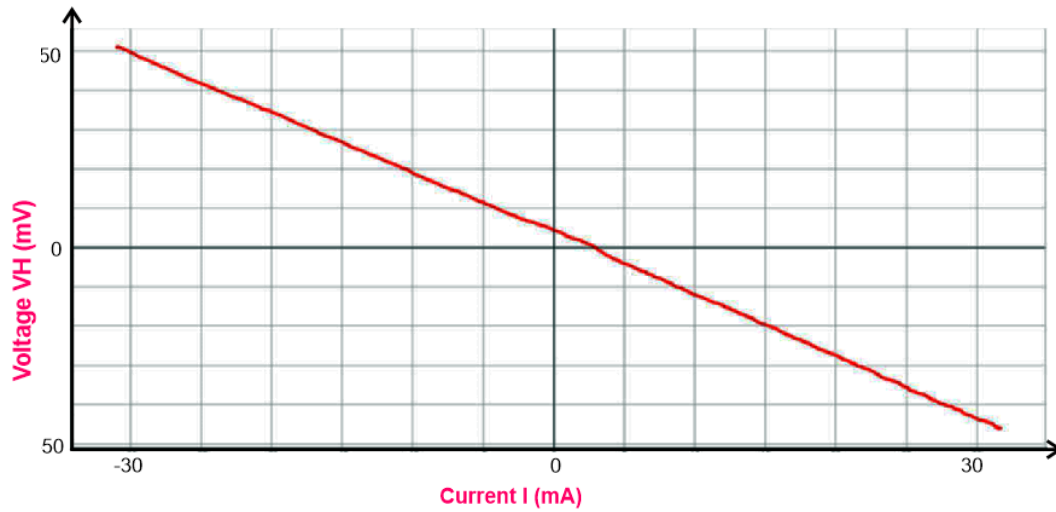
Wittmann (2011) describes doping as the technique by which impurity atoms are introduced into a semiconductor by ion implantation in the fabrication of modern semiconductor devices. The goal of semiconductor doping is to characterize the number and type of free charges that can be moved by introducing an external voltage to a crystal region. When impurities are doped into a semiconductor, the semiconductor becomes extrinsic, and impurity energy levels are introduced. p-type and n-type semiconductors are produced by doping an intrinsic semiconductor with an electron acceptor and an electron donor element, respectively (Libretexts, 2021b), during the manufacturing process. The term n-type refers to the electron's negative charge. In p-type semiconductors, holes are the majority carriers, while electrons are the minority carriers in n-type semiconductors.

2.2.5.3 Electrical Properties of Germanium

In an experiment aimed at studying the Hall Effect in n-type and p-type germanium by PHYWE (n.d), with Magnetic field strength (\vec{B}) of 250 mT and at a temperature (T) of 300 K., it was noted that;

- i. There was a linear relationship between V_H and I, but the linear trend between the two variables was inverted because the charge carriers in n-type and p-type Ge were different. A graph of V_H against I had a negative gradient in the n-type and a positive gradient in the p-type shown in Figures 8 and 9.

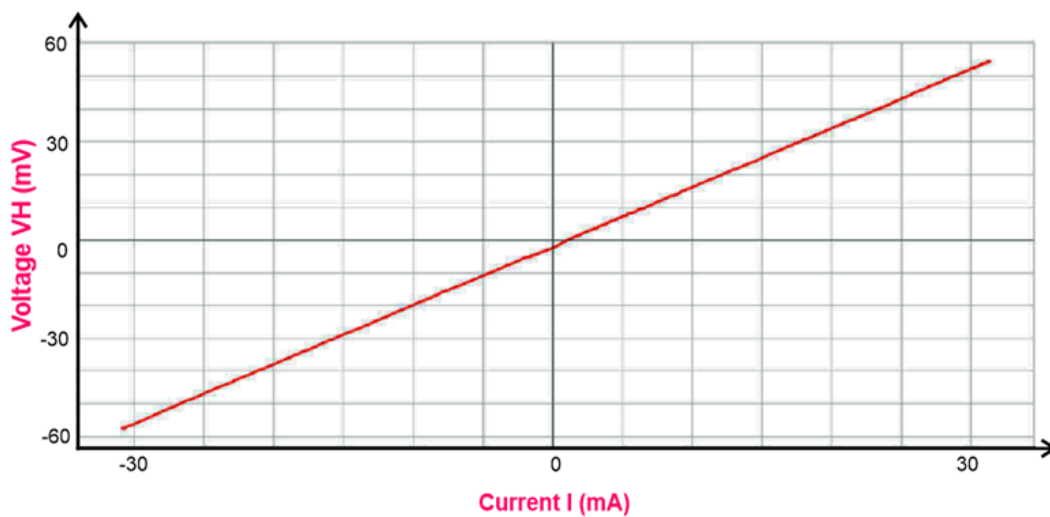
Figure 8.



A graph of V_H against I for n - Ge

Note. Reprinted from *Hall Effect in n- and p-germanium* by PHYWE, n.d, (https://www.phywe.com/experiments-sets/university-experiments/hall-effect-in-n-and-p-germanium_11052_12085/). Copyright PHYWE, n.d.

Figure 9.



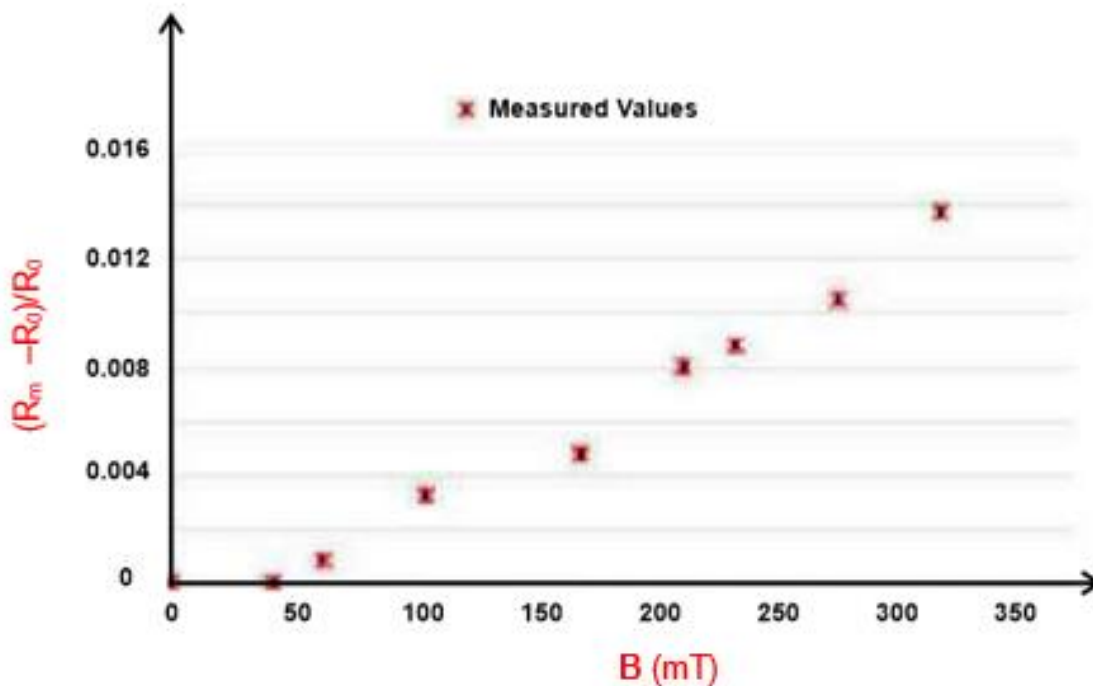
A graph of V_H against I for $p - Ge$

Note. Reprinted from *Hall Effect in n- and p-germanium* by PHYWE, n.d, (https://www.phywe.com/experiments-sets/university-experiments/hall-effect-in-n-and-p-germanium_11052_12085/). Copyright PHYWE, n.d.

- ii. With $I = 30\text{mA}$ and $T = 300\text{K}$ treated as constants, there was a non-linear variation in resistance as \vec{B} increased for both the n-type and p-type Ge as shown in Figures 10 and 11.

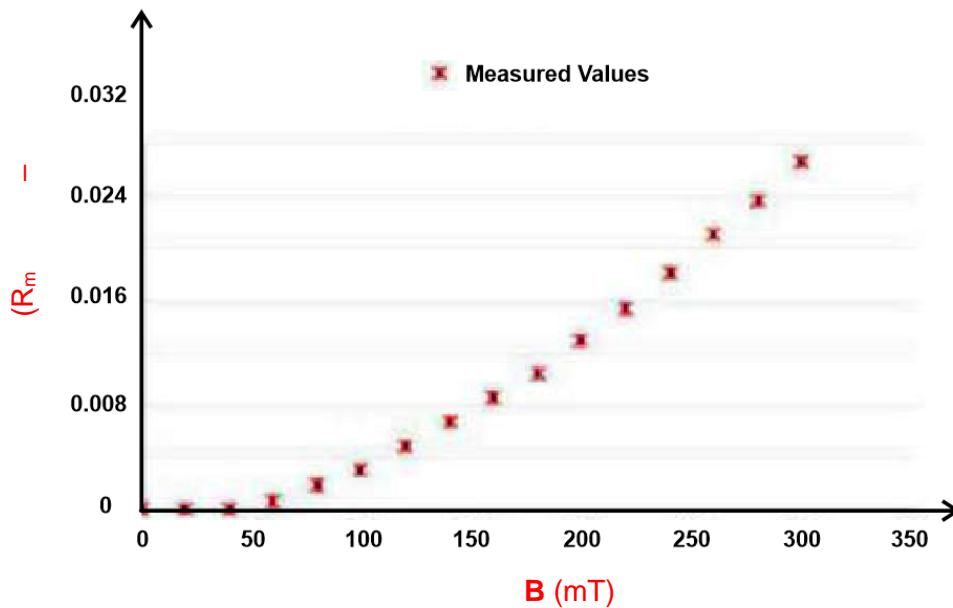
Figure 10.

A graph of $(R_m - R_0)/R_0$ against (\vec{B}) for n - Ge



Note. Reprinted from *Hall Effect in n- and p-germanium* by PHYWE, n.d, (https://www.phywe.com/experiments-sets/university-experiments/hall-effect-in-n-and-p-germanium_11052_12085/). Copyright PHYWE, n.d.

Figure 11.



A graph of $(R_m - R_0)/R_0$ against (\vec{B}) p - Ge

Note. Reprinted from *Hall Effect in n- and p-germanium* by PHYWE, n.d, (https://www.phywe.com/experiments-sets/university-experiments/hall-effect-in-n-and-p-germanium_11052_12085/). Copyright PHYWE, n.d

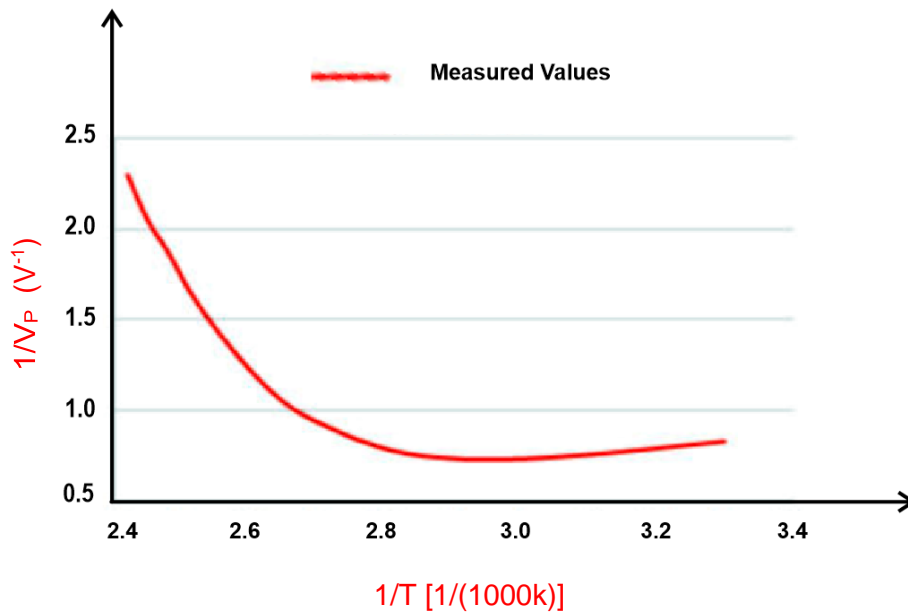
The slopes of the regression lines drawn are given by;

$$b = - \left(\frac{E_g}{2k} \right) \quad [2.15]$$

where E_g = energy of band gap and k = Boltzmann constant.

- iii. There was a non-linear relationship in the inverse of a sample voltage $1/V_P$ with the inverse of temperature $1/T$ with $I = 30\text{mA}$ and $B \rightarrow 0$ for both the n-type and p-type Germanium as shown in Figures 12 and 13

Figure 12.

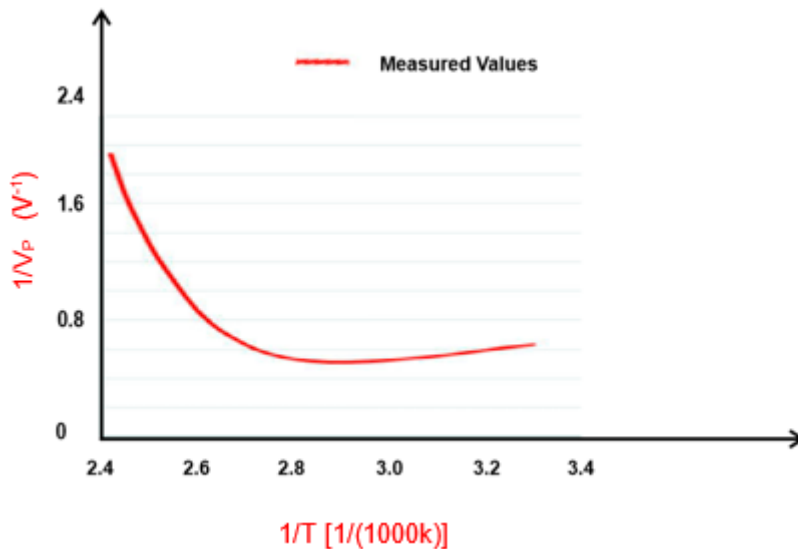


A graph of $1/V_p$ against $1/T$ for n - Ge

Note. Reprinted from *Hall Effect in n- and p-germanium* by PHYWE, n.d, (https://www.phywe.com/experiments-sets/university-experiments/hall-effect-in-n-and-p-germanium_11052_12085/). Copyright PHYWE, n.d.

Figure 13.

A graph of $1/V_p$ against $1/T$ for p - Ge

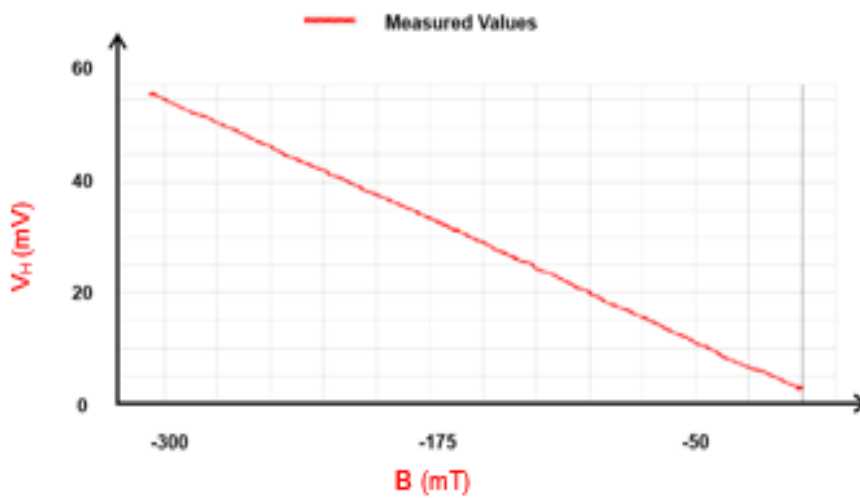


Note. Reprinted from *Hall Effect in n- and p-germanium* by PHYWE, n.d, (https://www.phywe.com/experiments-sets/university-experiments/hall-effect-in-n-and-p-germanium_11052_12085/). Copyright PHYWE, n.d.

- iv. For both the n-type and p-type Ge, there was a linear relationship between the Hall voltage V_H and the magnetic field \vec{B} as shown in Figures 14 and 15.

Figure 14.

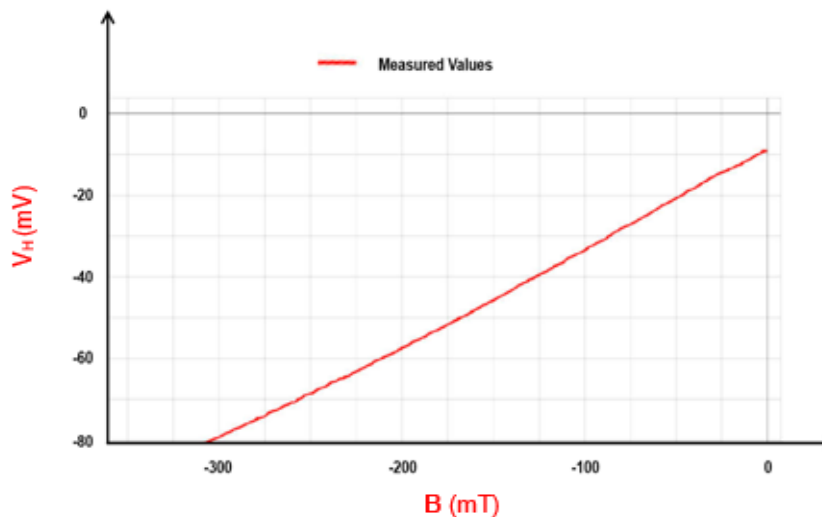
A graph of V_H against \vec{B} for n - Ge



Note. Reprinted from *Hall Effect in n- and p-germanium* by PHYWE, n.d, (https://www.phywe.com/experiments-sets/university-experiments/hall-effect-in-n-and-p-germanium_11052_12085/). Copyright PHYWE, n.d.

Figure 15.

A graph of V_H against \vec{B} for p -Ge



Note. Reprinted from *Hall Effect in n- and p-germanium* by PHYWE, n.d, (https://www.phywe.com/experiments-sets/university-experiments/hall-effect-in-n-and-p-germanium_11052_12085/). Copyright PHYWE, n.d.

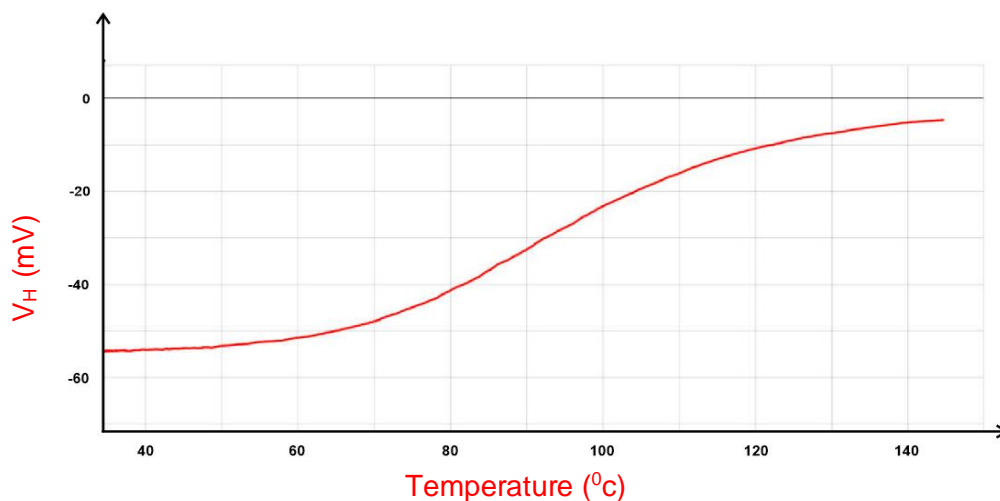
Using the values obtained in Figures 14 and 15 above, the regression line had the formula

$$V_H = V_0 + b \cdot \vec{B} \quad [2.16]$$

- v. The Hall voltage V_H is displayed as a function of the temperature T with $I = 300 \text{ mA}$ and $\vec{B} = 300 \text{ mT}$. The Hall voltage for both n-type and p-type Ge decreases with rising temperature, according to graphs obtained and illustrated in Figures 16 and 17. This was because there was an increase in charge carriers (a change from extrinsic to intrinsic conduction) and a corresponding decrease in drift velocity. After all, the experiment was conducted with a constant current.

Figure 16.

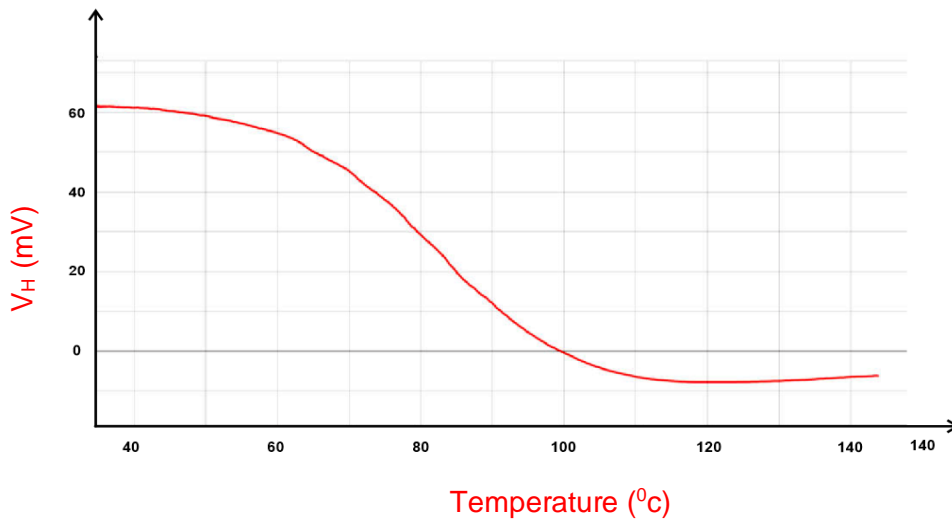
A graph of V_H against T for n - Ge



Note. Reprinted from *Hall Effect in n- and p-germanium* by PHYWE, n.d, (https://www.phywe.com/experiments-sets/university-experiments/hall-effect-in-n-and-p-germanium_11052_12085/). Copyright PHYWE, n.d.

Figure 17.

A graph of V_H against T for p - Ge



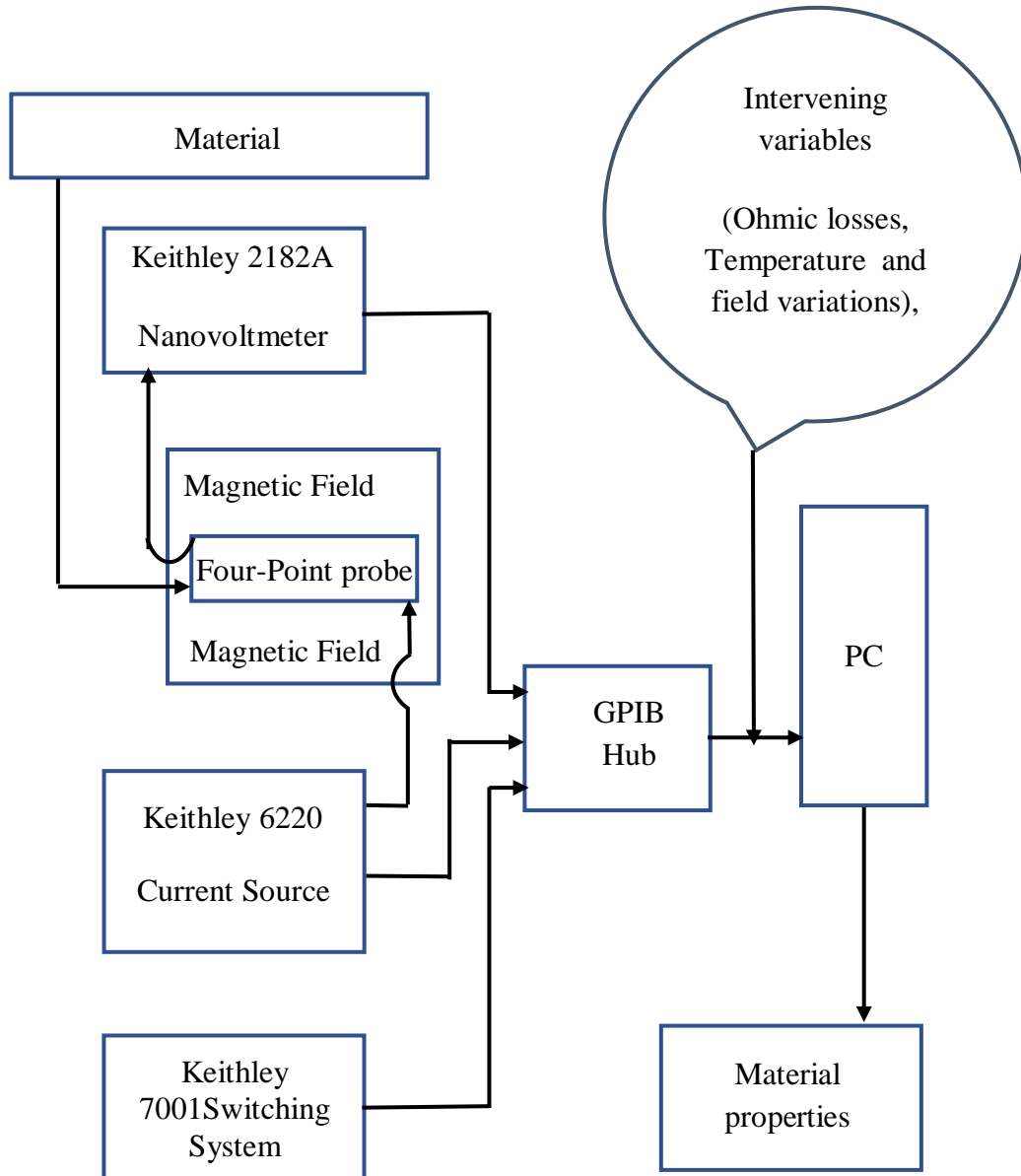
Note. Reprinted from *Hall Effect in n- and p-germanium* by PHYWE, n.d, (https://www.phywe.com/experiments-sets/university-experiments/hall-effect-in-n-and-p-germanium_11052_12085/). Copyright PHYWE, n.d.

2.2.6 Conceptual Framework

The diagrammatic representation of the setup and study is shown in Figure 18.

Figure 18.

Schematic diagram of the system



Note. Illustration done by the author.

2.3 Empirical Review

This section elaborates on the relevant previous research that is correlated with the methods used in this research. These previous studies were used as references to develop the methods and solve the problems in this research.

Agumba *et al.* (2011) set out to create a simple, effective, and portable computer-aided four-point probe system for measuring thin film sheet resistivity. For holding samples, a four-point probe head was designed and built. A relay-switching device was also designed and built to switch the probe tips on the sample surface according to the Van der Pauw setup. A Keithley Source Meter 2400 model was connected to a LabVIEW-running computer via the serial port (RS-232 port) for full computer control. The printer port has also been used to connect the relay-switching device to the computer (LPT1 port). The Van der Pauw probe head, relay switching device, and Keithley Source Meter were used to probe the samples. The sheet resistivity of Cu₂O semiconductor thin films prepared using the DC reactive magnetron sputtering technique was measured to test the workability and reliability of the fabricated system for thin film sheet resistivity measurement. The study discovered that the system provides a reliable, effective, and simple technique for thin film sheet resistivity measurements based on the measurements obtained.

Cervantes *et al.* (2018), in a study on the search and development of new materials to produce energy from heat, recognized the need to characterize the thermal and electrical properties. To achieve this, a system that can measure these characteristics for semiconductor material sample tablets was created. In the temperature range of 25 to 100 °C, the system measured the Seebeck coefficient. Additionally, it made it possible to collect JV curves at various temperatures, which were then used to estimate the conductivity (resistivity) of an electrical material. LabVIEW software and Arduino were used to automate the system. RS232 serial port was used for the Keithley model 2410-C 1100V Sourcemeter® interface. Using the

Slave/Master configuration and USB communication, the temperature at the sample's sides was measured using the Arduino platform (Arduino Uno Board). The Arduino board and the Keithley sourcemeter were used as "Slaves" to the computer running the LabVIEW software, which served as the "Master." Peltier cells and a preprogrammed pulse width modulation control were used to heat the samples.

Garnica *et al.* (2019) used a completely automated procedure to identify and electrically characterize those graphene flakes with as little human interaction as possible, improving on current methods' limitations. The micro-robotic automation sequence was divided into three major steps. To begin, a sample surface plane was calculated using multiple foci points distributed across the substrate. Secondly, the flakes on the substrate are identified in the hue, saturation, and value colour space, with an implementation tailored to fit the measurement probe, which is used to avoid undersized samples and adjust flake orientation. Finally, electrical characterization is carried out using the Van der Pauw method and four-point probe measurements. Throughout the experiments, a semiconductor device analyzer (Keysight B1500A) was used as the sourcing and measuring equipment. The device was chosen for the flexibility it provided when setting a measuring step, as different channels can be used in either current or voltage mode, allowing the electrodes to act as either sources or monitor channels.

In a research to characterize ceramic materials, Valladares *et al.* (2019) used the non-destructive method of complex impedance spectroscopy, to develop a system for automatic dielectric characterization. The technique allowed for the determination of the complex impedance and dielectric constant for a wide range of temperatures and applied field frequencies. Two impedance analyzers' configurations and the characterization test setup were made simpler by the user interface developed by LabVIEW IDE. The test reports were also generated automatically from the measurements, which facilitated the experimental analysis

by plotting the more crucial parameters in the dielectric characterization. To demonstrate the system's proper operation, one of these parameters - the peak of the graph ϵ_r' (the real part of the dielectric constant) vs. temperature, which is the temperature at which ceramic materials transition from the ferroelectric to the paraelectric state was obtained and compared to reference values. The design utilized a heating subsystem consisting of a Eurotherm 2404 temperature controller, a solid-state power controller actuator, an electric oven and a temperature sensor.

2.4 Research Gap

Table 2 below presents the summary of previous related research, their key outputs and the limitations that this research aimed to address.

Table 2.

Summary of previous related research and their limitations

Research	Key Output	Limitation
Design And Fabrication of a Simple Four Point Probe System for Electrical Characterization of Thin Films. (Agumba <i>et al.</i> , 2011)	Developed a computer-aided four-point probe system for measuring thin film sheet resistivity	<ul style="list-style-type: none"> i. It was limited to resistivity measurements. ii. Accuracy was lowered due to the induced Schottky effect by the aluminium probe tips used.
Development and Automation of a Thermoelectric Characterization System. (Cervantes <i>et al.</i> , 2018)	Developed an automated thermoelectric characterization system	<ul style="list-style-type: none"> i. It was limited to resistivity and conductivity measurements at various temperatures.

Research	Key Output	Limitation
Automatic Micro-Robotic Identification and Electrical Characterization of Graphene (Garnica <i>et al.</i> , 2019)	Automated a procedure to identify graphene flakes electrically and characterize them	i. It was limited to conductivity measurements.
Design and Implementation of an Automatic System for Dielectric Characterization of Ceramic Materials. (Valladares <i>et al.</i> , 2019)	Designed an automatic characterization system to calculate the complex impedance and dielectric constant at various temperatures.	i. It was limited to capacitance and conductance measurements.

CHAPTER THREE

RESEARCH DESIGN AND METHODOLOGY

3.1 Introduction

This chapter presents the apparatus, software, and method to be used in interfacing and setting up the components to obtain the data. The methods include setting up the four-point probe, connecting the Keithleys' apparatus, interfacing the apparatus with LabVIEW via the computer, and collecting and analyzing the obtained data.

3.2 Research Design

This research was experimental and was carried out in the laboratory at room temperature since primary quantitative multivariate data was required. A flowing current from Keithley 6120 was used as an independent variable and the resulting voltage from Keithley 2182A was used as the independent variable. The sample dimensions and the magnetic field strength were taken as constants.

3.3 Location of the Study

The research was carried out at the University of Eldoret in Uasin Gishu County, Kenya, in the Photovoltaics Laboratory. The choice was made because the laboratory was well-equipped and was in close proximity to Kabarak University.

3.4 Instruments Used in Electrical Characterization

Dedicated instruments were used to collect the data which was then stored and analyzed using a computer program to obtain the electric properties of a germanium sample. The whole process of data acquisition and analysis was automated by the use of the following instruments and software.

3.4.1 A Fabricated Four-Point Probe

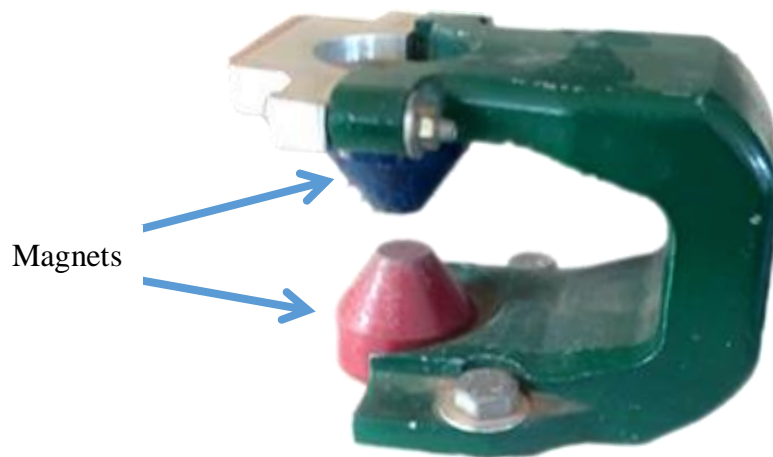
The research utilized a fabricated four-point probe that was used to hold the semiconductor sample.

3.4.2 Fixed Magnets

Consisting of two permanent magnets, this was used to generate the magnetic field required for the experiment. It produced a magnetic field of 258.125mT. The magnet used is presented in Figure 19.

Figure 19.

Fixed magnets used in the experiment



Note. Photograph sourced by the author.

3.4.3 NI Keithley 2182A Nanovoltmeter

This is a two-channel voltmeter designed for producing stable, low-noise voltage measurements and reliably and consistently characterizing low-resistance materials and

devices. It is suitable for this study since it offers substantially faster measurement speed and lower noise performance than other low-voltage measuring options (Keithley, 2022b)

3.4.4 NI Keithley 6220 Precision Current Source

This is a DC source that combines the simplicity of use with extremely low current noise, built-in control capabilities, and high sourcing accuracy, all of which are crucial in test settings, particularly in semiconductor, nanotechnology, and superconductor sectors. It is perfect for Hall measurements, resistance measurements in delta mode, pulsed measurements, and differential conductance measurements, among other things (Keithley, 2004).

3.4.5 NI Keithley 7001 Switching System

This is a high-density, two-slot mainframe for the test and measurement industry that supports the largest variety of signals. It supports DC switching from nanovolts to 1100 volts and femtoamps to 5 amps, as well as radiofrequency and optical switching, inbuilt scan control, non-volatile memory, and up to 80 channels of 2-pole switching (Keithley, 2022a)

3.4.6 Semiconductor Sample

A P-Type doped Germanium (Ge) thin-film semiconductor sample 1.00cm wide, 2.00cm long, and 1.00 mm thick was used for validation.

3.4.7 PC

An i3-10100, 4-core 2GB RAM. 320GB HDD desktop PC with Intel® UHD Graphics 630 running on Windows 7 32-bit Architecture OS was used.

3.4.8 Micrometer Screw Gauge and a Vernier Calliper

A Micrometer screw gauge was used to measure the thickness of the samples whereas a Vernier calliper was used to measure the length and width

3.5 Devices Set-up and Configuration

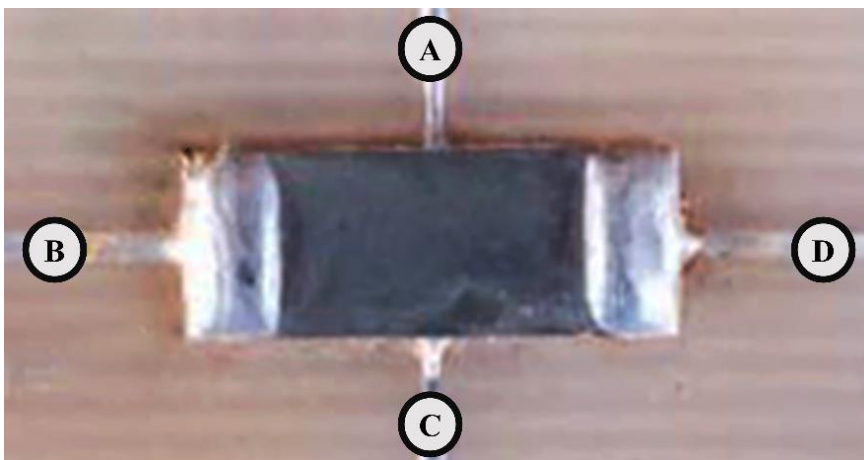
Communication between the Keithley measurement instruments and the PC was carried out interchangeably using USB and GPIB protocol. Copper wires were used in closing the circuits. The Four-point probe, the PC, and the Keithley instruments were set as discussed in the following sub-sections.

3.5.1 Four-Point Probe Set-Up

A four-point probe is made up of four silver metal points that are evenly spaced and have a defined radius. To avoid harming the thin-film sample during probing and to make mounting and unmounting easier, each tip was held by a soldered probe. Probes A and C were connected to the precise current source while probes B and D were connected to Model 2182A as depicted in Figure 20. The current source provides current to the outer two probes, while the voltmeter measures the voltage between the inner two probes. When using a thin film sample whereby the thickness is less than the inter-probe distance, rings are formed instead of spheres (Anjum *et al.*, 2019).

Figure 20.

Probed Germanium sample



Note. Photograph supplied by the author.

The Probed sample presented in Figure 20 is placed perpendicularly to a magnetic field provided by two fixed magnets. The magnets are presented in Figure 19.

3.5.2 PC Setup

As defined by HP (2019), a driver is a group of files that instructs hardware on how to interact with an operating system on a computer. They are necessary for every piece of hardware, including those built into a computer. NI application software, Add-ons, programming environments, utilities, and drivers listed were installed on the PC to facilitate data access, acquisition, transfer calculation, display, manipulation, and analysis.

A USB port USB to GPIB cables and a GPIB Hub were used to connect the instruments to the PC. As a standard tool for creating interfaces, NI-VISA enables the configuration, programming, and debugging of instruments and equipment as well as the acquisition of data from external sensors using any type of communication port, including Ethernet, GPIB, USB, and others (Villarreal *et al.*, 2022).

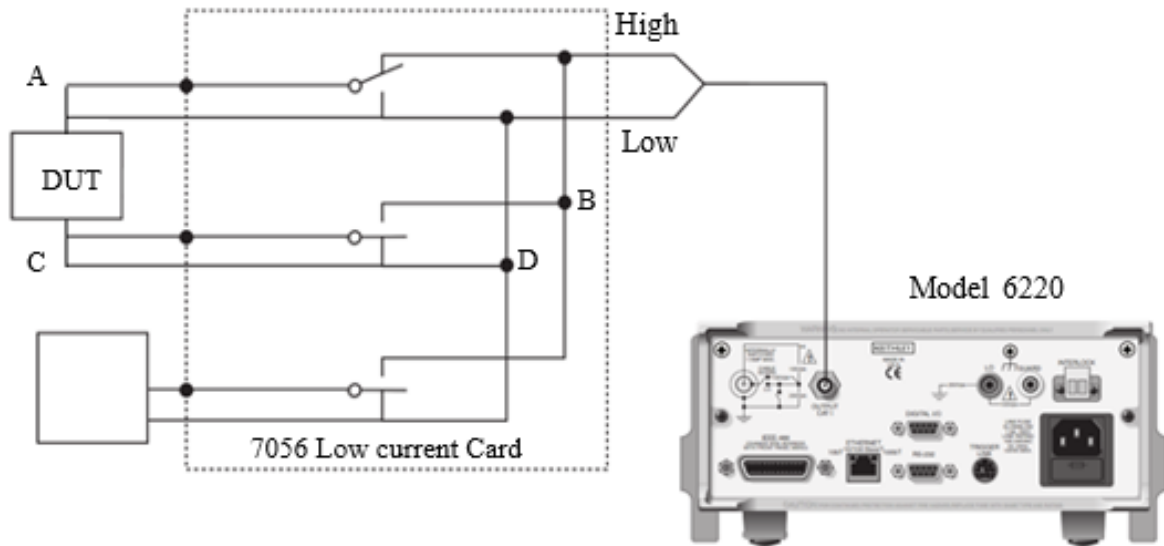
3.5.3 Keithley's Setup

3.5.3.1 Keithley 7001 Switching System

The 7001 switch employs cards that can accommodate a wide range of signals while maintaining high accuracy and signal quality. These cards reduce signal errors and protect against signal degradation caused by offset voltage, isolation resistance, and leakage current. 7065 low current scanner card model: an 8-channel, 2-pole card with a thermal offset of 30nV. In the card 1 slot of the 7001-switch system, a 25-channel pA-Multiplexer with BNC socket was installed. The test sample was connected to channel two of the multiplexer card and the 6220 Current source output was connected to channel one as shown in Figure 21.

Figure 21.

Keithley 7001 External Connection



Note. Model 6220 photo adapted from *AC / DC Low Resistance Digital Multimeters* by Linktronix, n.d, (https://www.linktronix.ch/resources/public/liveedit/media/1404721789_53ba5a7de0600.jpg). Copyright Linktronix, n.d.

Model 7065 Hall Effect card facilitated switching digital output using assigned channels by model 7001 (see appendix IV)

3.5.3.2 Keithley 2182A Nanovoltmeter

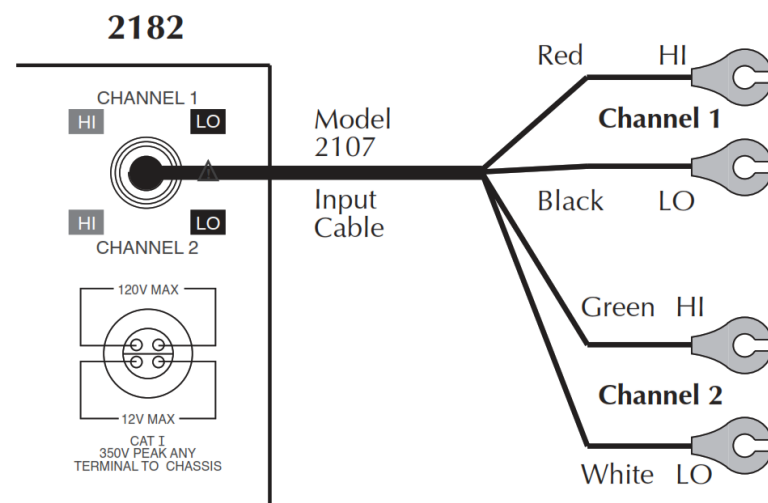
The Model 2182A is a high-performance digital nanovoltmeter with $7\frac{1}{2}$ digits. It has two voltage and temperature input channels, channels 1 and 2. (See Appendix IV) Channel 1 is the primary measurement channel, while Channel 2 is used for sense measurements. Temperature measurements were not taken because Model 2182A can only measure one variable at a time. Channel 1 (DCV1) has five measurement ranges (10mV, 100mV, 1V, 10V, and 100V) and can measure voltage between 1nV and 120V, whereas Channel 2 (DCV2) has three measurement

ranges (100mV, 1V, and 10V) and can measure voltage between 10nV and 12V. The range chosen affects both the accuracy of the voltage measurement and the maximum voltage that can be measured.

The Model 2107 Input Cable, a supplied accessory made up of cable wires made of twisted silver wire and terminated with a LEMO plug on one end and copper lugs on the other, was used to connect the 2182A model and the four-point probe. When connected to the Model 2182, the cable was shielded to the chassis ground. In Figure 22, the input cable is displayed.

Figure 22.

Model 2107 input cable



Note. Reprinted from *Model 2182A Nanovoltmeter User's Manual* by Keithley, 2022, p. 4-5.

Copyright 2022 by Keithley Instruments, LLC

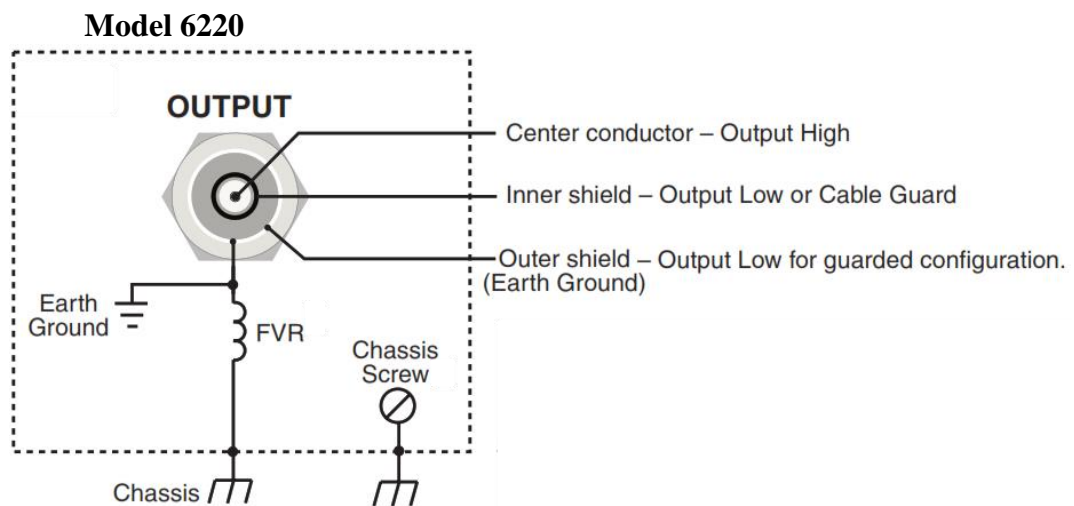
Using an external simulated reference junction and a thermocouple, this cable can be used to measure voltage and temperature. The copper lugs on the Model 2107 Input Cable were removed, and the wires were connected directly to the four-point probe with silver solder, which is considered to minimize thermal electromotive forces (EMFs). Keithley recommends using silver (Ag) with their low Emf connectors with 2182A nanovolt meters (Cigoy, 2010).

3.5.3.3 Keithley 6220 High Precision Current Source

The model 6220 has a DC source ranging from 0.1pA to 105mA and a voltage compliance limit ranging from 0.1V to 105V in 10mV steps, as well as an Analog filter to slow down output response and a Protective Triax Shield/Cap (CAP-28-1) - 237-ALG-2 Triax cable equipped with alligator clips solely on a single end. The current source output was accessed via the rear panel's 3-lug female Triax connector. (See Appendix IV) This was accomplished by connecting to this connector with a 3-slot male Triax cable. A Frequency Variable Resistor (FVR) isolated the Triax connector's Earth Ground from the Model 6220's chassis. The current source circuitry was isolated from high frequencies that might be present on the Model 6220 chassis using the FVR as shown in Figure 23.

Figure 23.

Model 237-ALG-2 Triax connector and ground point

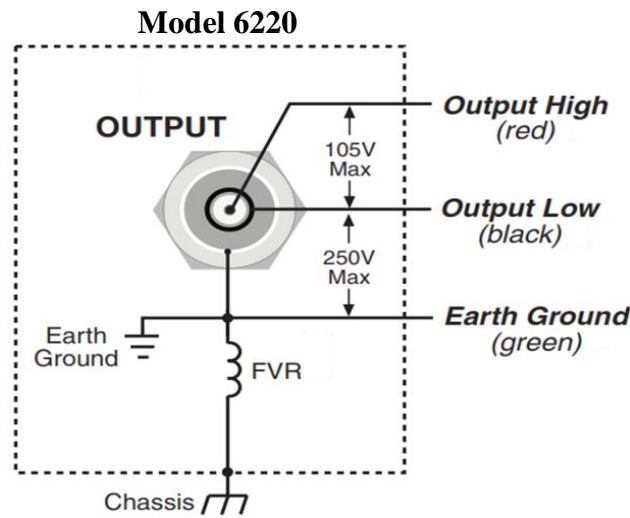


Note. Reprinted from *Model 6220/6221 Reference Manual*, by Keithley Instruments, 2004, p. 2-2, Copyright 2004 by Keithley Instruments, Inc

The resistance of the FVR rises to dampen the effects of rising frequencies on the chassis. Figure 24 illustrates how the Triax connector's centre conductor was connected to the current source's Output High, its inner shield to Output Low, and its outer shield to Earth Ground.

Figure 24.

Model 237-ALG-2 Output configuration



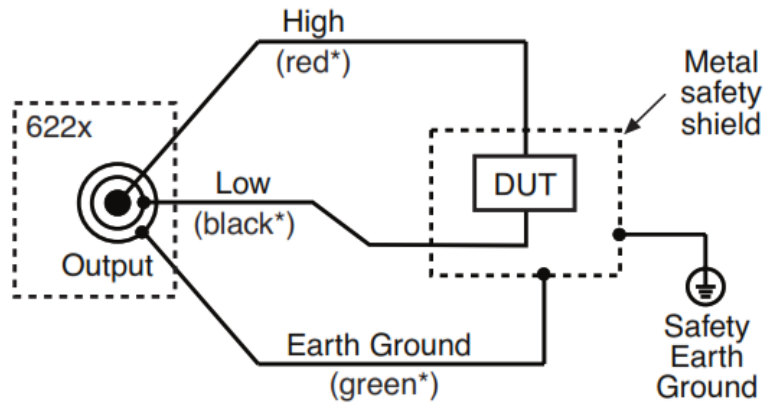
Note. Reprinted from *Model 6220/6221 Reference Manual*, by Keithley Instruments, 2004, p. 2-6, Copyright 2004 by Keithley Instruments, Inc

The interlock cable included with the instrument was attached to the interlock switch. When the interlock switch is open, the Model 6220's OUTPUT is disabled and cannot be turned on. If the OUTPUT is already turned on, pressing the Interlock switch turns it off. When the interlock switch is closed, the OUTPUT becomes active and can be activated.

A safety shield was used to connect the sample to the current source. As shown in Figure 25, the metal safety shield completely encircled the four-point probe test circuitry and was connected to a known Safety Earth Ground and Chassis. For the connection to the safety Earth Ground and Chassis, a #18 American wire gauge wire was used.

Figure 25.

Output connection and shielding



Note. Reprinted from *Model 6220/6221 Reference Manual*, by Keithley Instruments, 2004, p. 2-16, Copyright 2004 by Keithley Instruments, Inc

3.6 Data Input and Collection

3.6.1 Data Collection Procedure

At the start of this research project, a letter from Kabarak University's Institute of Postgraduate Studies was obtained, which facilitated the application of written clearance letters from the Kabarak University Research Ethics Committee (KUREC) and a research permit from the National Commission for Science, Technology and Innovation (NACOSTI), (See Appendix III) paving the way for data collection and report writing. An affiliation letter was also obtained from the University of Eldoret, which allowed the use of their laboratory equipment in the institution's School of Sciences.

3.6.2 Data Acquisition

LabVIEW is a full-featured programming language with a variety of data types, loops, data structures, conditional statements, string manipulation routines, arrays, and file Input/Output methods, among other things (Bress *et al.*, 2013). Hence floating-point numeric data types with double precision and associated physical quantities of measure were used for both data

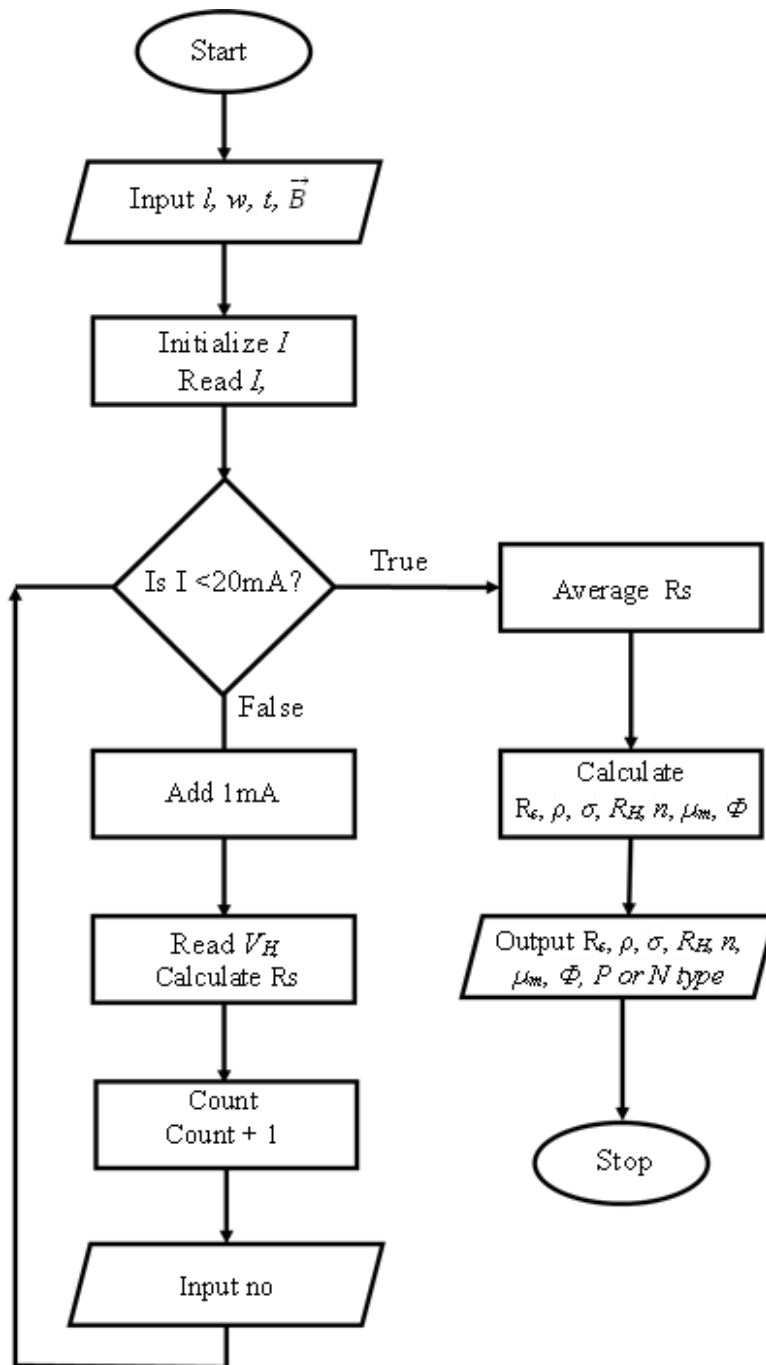
collection and input while string data types were used for output statements like simple text messages. LabVIEW-based VIs and sub-VIs coupled with SCPI commands were used for both data input and collection from the Instruments. Instruments data was observed, collated, evaluated, and analyzed within the LabVIEW software. The obtained data was exported as a Comma separated value (CSV) file giving an option of transferring to spreadsheets or any other application for further manipulations.

The Model 2182A and the ammeter readings were collected remotely from the Keithley instruments by coded data acquisition VIs via the NI-VISA architecture and SCPI commands. The NI-VISA facilitated the communication between the Keithley instruments and the PC while LabVIEW acted as the system controller operating all the devices simultaneously (Cai *et al.*, 2017). A test report was initially obtained and commenced by ensuring empirical data collection. Using the obtained data, the parameters discussed in section 2.2.4 were automatically computed using the coded Sub-VIs discussed in the subsequent section. To obtain precise and accurate information, the program iterated using execution structures by conducting a sweep in the DC source with the option of repeating the procedure at several defined times and intervals.

The data collected was stored in arrays then the average resistance followed by other parameters was calculated. The procedure continues until parameters within the user-defined range are obtained. Then the program stops, records, and analyzes the values obtained. The process followed the following algorithm in Figure 26.

Figure 26.

Data flow diagram for the automated test system



Note. Illustration done by the author.

3.7 Data Validation

Data was collected and recorded at increasing current thrice in predefined steps to check on the systems' consistency and repeatability. The first set of data was used to develop a mathematical model that connects the input data and the desired data while the second set was used to test the validity of the models. For valid data, the second part percentage error should not differ by more than a small amount, such as 2 or 3 per cent according to Yousif (2018).

3.8 Data Analysis

A wide range of data points was collected to minimize the effect of individual measurement errors. For error analysis, random errors were collected from the instruments' precision and the experiment was repeatedly done to check for systematic errors. The data automatically recorded for the available Germanium sample were tabulated and compared with manually done experimental values. The LabVIEW software used the least square regression analysis from the $V - I$ data recorded to determine the resistance of the sample and thereafter calculate the other parameters. Additional mathematical analysis and graphs were drawn and done using OriginPro™ application software.

3.9 Ethical Considerations

The research was experimental and was conducted inside a Laboratory hence, there was no human contact in any way during the entire period of the research. Moreover, low-risk ethical review permission was requested and granted as per the university guidelines (See Appendix II).

CHAPTER FOUR

DATA ANALYSIS, RESULTS, AND INTERPRETATIONS

4.1 Introduction

This chapter gives the findings. Interpretations and discussions of the research work. The configuration made, LabVIEW VIs and SubVIs used, PC Setup, fabricated four-point probe, electrical characterization of Germanium semiconductor, and the analysis of the results are hereby discussed and presented.

4.2 Results and Discussions of the Study

The sections below contain the configuration of Keithley's instruments, the PC setup, LabVIEW interfacing and data validation.

4.2.1 Configuration for Keithley'

Products from Keithley are intended for use with mains electricity and control using dedicated ports. Interconnection between the instruments was achieved by using a GPIB bus connector by stacking them to form a hub and then connecting to the PC via a GPIB to a USB cable. GPIB pin connections network requires a specific address for each instrument to facilitate control from LabVIEW sub-VIs (Angrisani *et al.*, 2020). Unique GPIB addresses were assigned to the Keithley instruments. Moreover, the instruments support varying programming languages. The selection to be done for interfacing, GPIB addresses assigned for remote operations and connections was done as in Table 3

Table 3.

Selects and addresses

Instrument	Interface	Address	Programming Language
Keithley 2182A Nano voltmeter	GPIB	09	SCPI
Keithley 6220 High precision current source	GPIB	21	SCPI
Keithley 7001 Switching system	GPIB	08	SCPI

4.2.2 PC Setup

Software installed to manage data collection, conversion, collation, computation and analysis, and presentation of electrical characterization is listed in Appendix III via the NI package manager. A light executable application was later packaged and exported for use.

4.2.3 LabVIEW Interfacing

Several VIs and SubVIs were coded using LabVIEW IDE for the three instruments then combined in a general user-friendly interface and compiled into a Windows executable file. The VIs and SubVIs used are discussed below.

4.2.3.1 Keithley 7001 Interfacing

The KUSB GPIB to USB adapter was used to interface this instrument with the computer's USB port. A straight-through GPIB cable ended with a GPIB port was used to link the instrument's GPIB port to the computer's serial port. As mentioned in section 2.2.1.2, the 7001 GPIB first needed to be initialized and configured for data transmission with the computer. The VIs and SubVIs used for total control are discussed below.

4.2.3.1.1 Initialization

Following the setting of the computer port and model 7001 GPIB address port, the initialization action was carried out using the VI shown in Figures 27, 28, and 29. The VI queries for Errors, Identity then reset the instrument.

Figure 27.

Block diagram for initializing model 7001 (a)

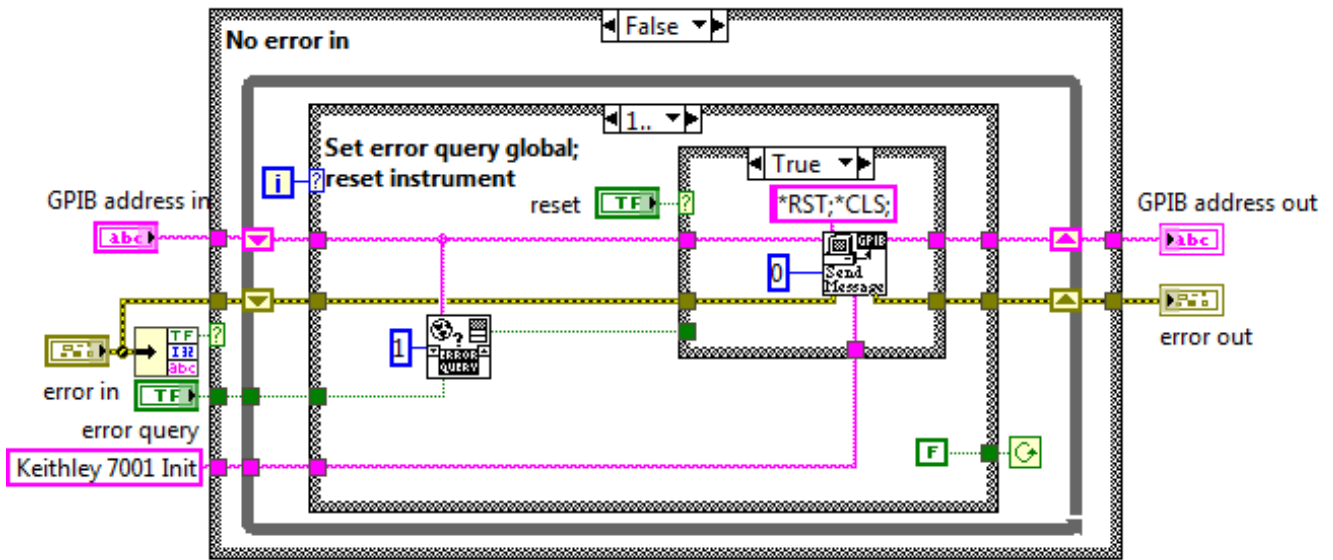


Figure 28.

Block diagram for initializing model 7001 (b)

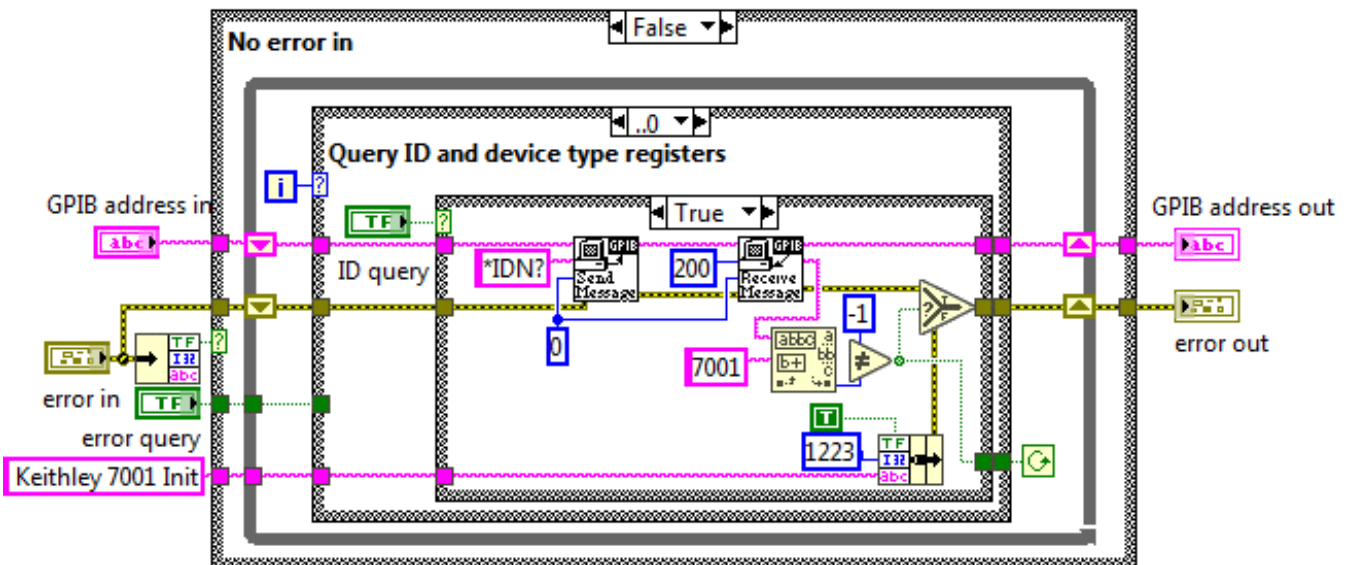
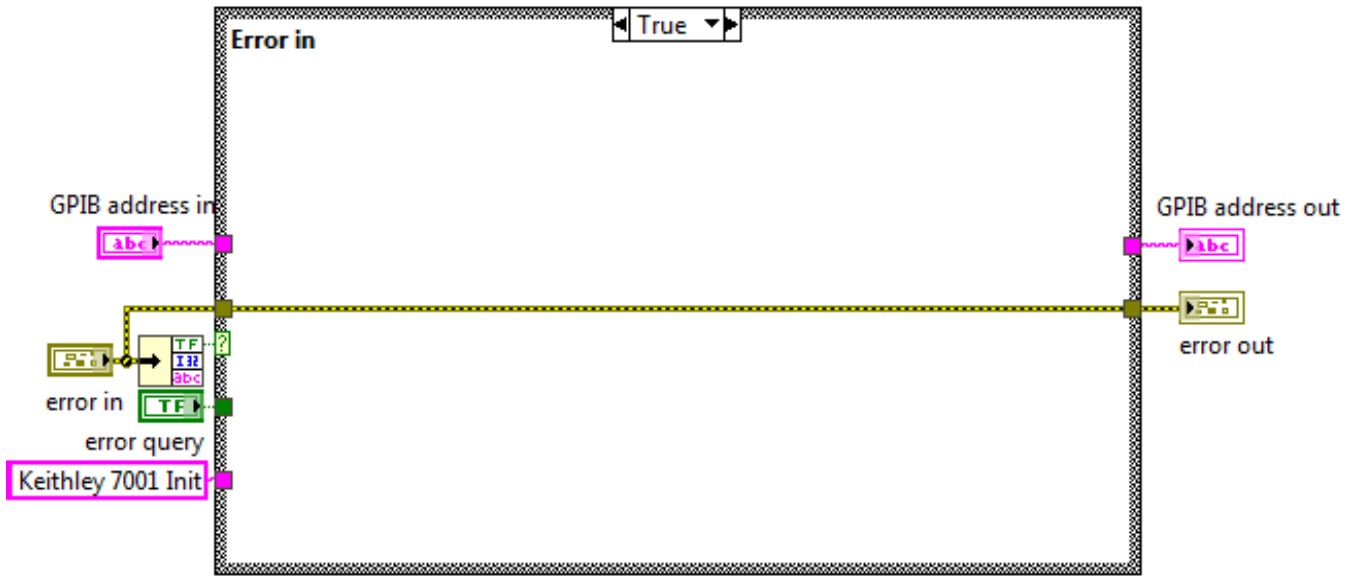


Figure 29.

Block diagram for initializing model 7001 (c)



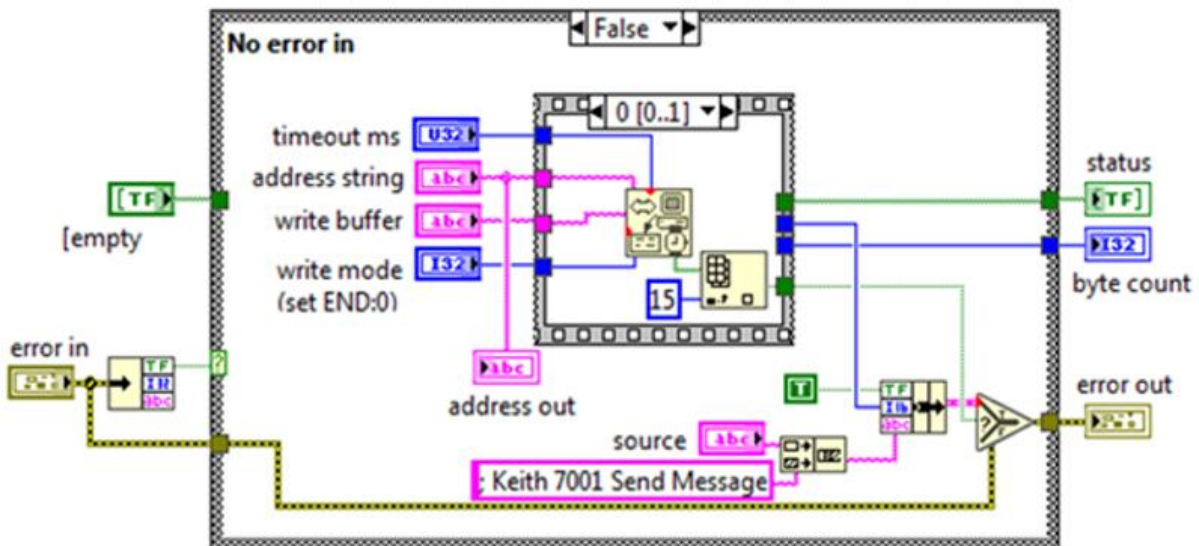
The initializing VI utilizes two subVIs discussed and Global Error Query VI discussed in section 4.2.3.1.4.1

4.2.3.1.1.1 Send Message SubVI

This SubVI was used to relay string messages from LabVIEW to model 7001. The code is represented in Figures 30, 31 and 32

Figure 30.

Block diagram for sending a message to model 7001 (a)

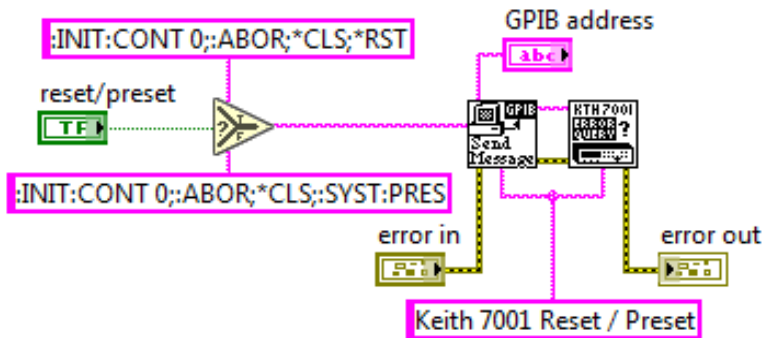


4.2.3.1.2 Resetting the Instrument

For the ensuing operations, Model 7001 was first to reset to its default scan configuration using the VI in Figure 36.

Figure 36.

Block diagram for resetting model 7001



The reset VI had two SubVIs for error querying and sending messages. The code for sending a message is discussed in section 4.2.3.1.1.1 while the code for error querying is illustrated in Figures 37 and 38.

Figure 37.

Block diagram for error querying model 7001(a)

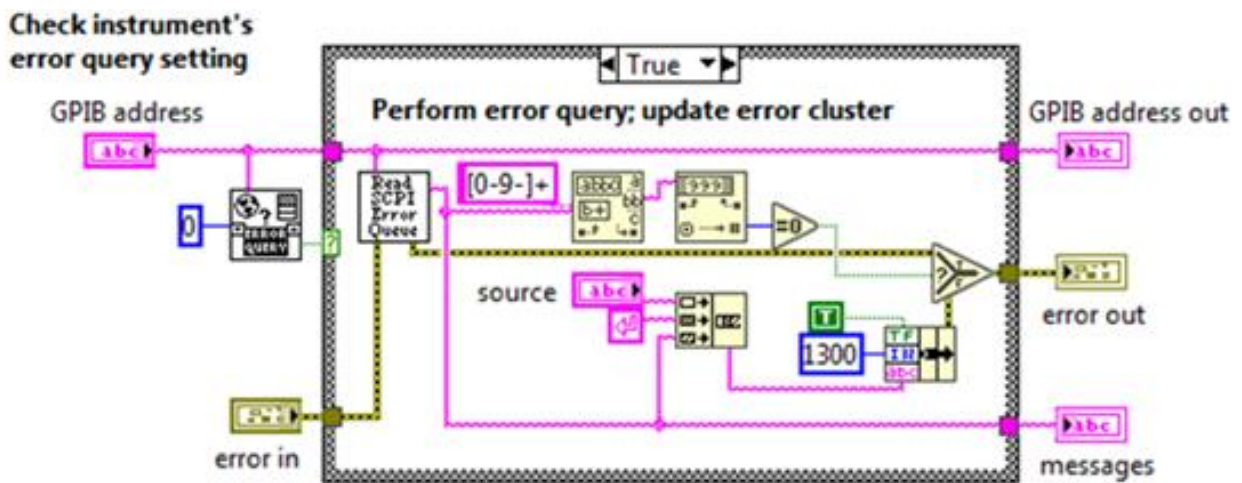
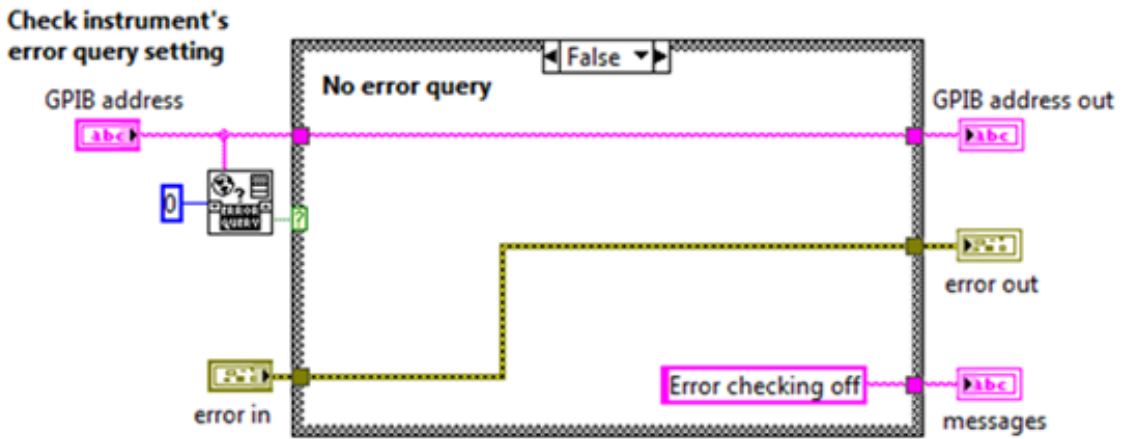


Figure 38.

Block diagram for error querying model 7001(b)

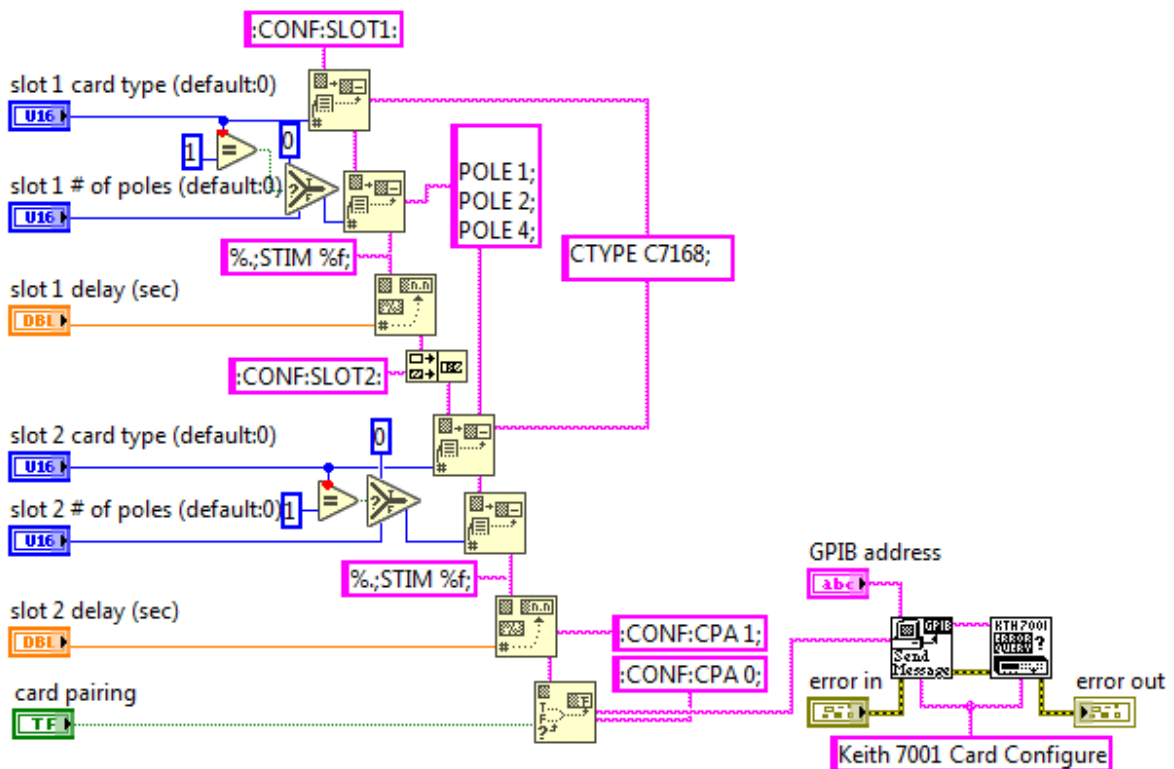


4.2.3.1.3 Card Configuration

The 7065, 40-channel multiplex low current scanner card model installed was configured using the code in Figure 39.

Figure 39.

Block diagram for configuring 7168 scanner card in model 7001



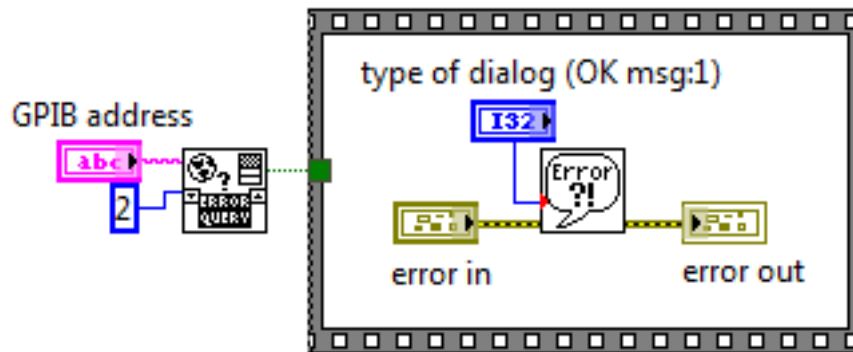
The VI comprised also the Send message VI and Error querying VI. The codes for these VIs are illustrated in the subsequent sections

4.2.3.1.4 Closing the Session

This code queried for instrument error(s) then sequentially outputs the error else terminates the session. The code is presented in Figure 40.

Figure 40.

Block diagram for session closure in model 7001

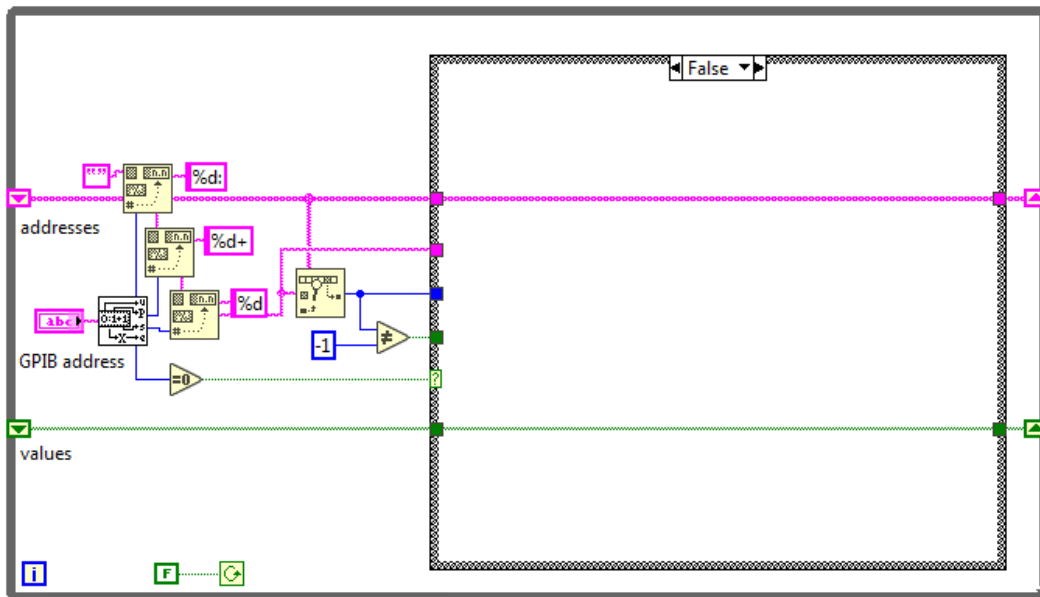


The Close VI utilized the global error querying VI and the simple error handler VI discussed as follows.

4.2.3.1.4.1 Global Error Querying

This VI is made up of a shift register composed of a case structure that keeps checking for errors across all the instruments connected and defined within the LabVIEW application package. It has several instances as shown in Figures 41, 42, 43, 44, 45, 46 and 47.

Figure 41.



Block diagram for Global Error querying (a) in model 7001

Figure 42.

Block diagram for Global Error querying (b) in model 7001

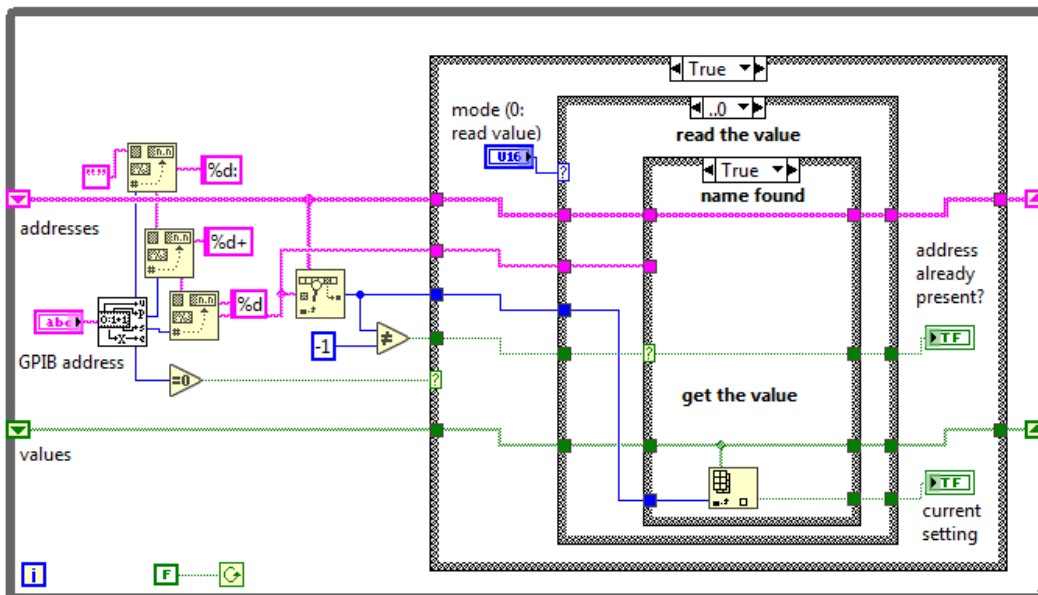


Figure 43.

Block diagram for Global Error querying (c) in model 7001

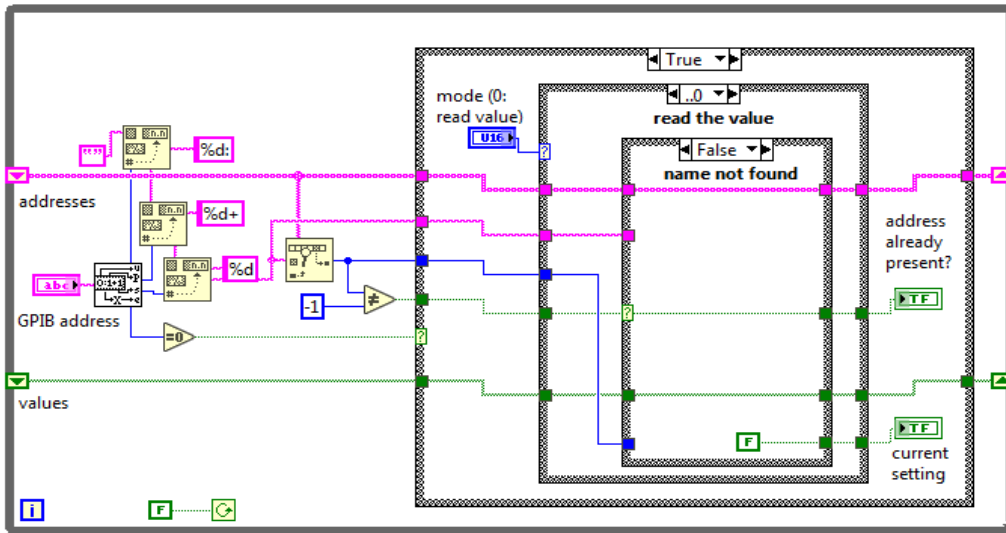


Figure 44.

Block diagram for Global Error querying (d) in model 7001

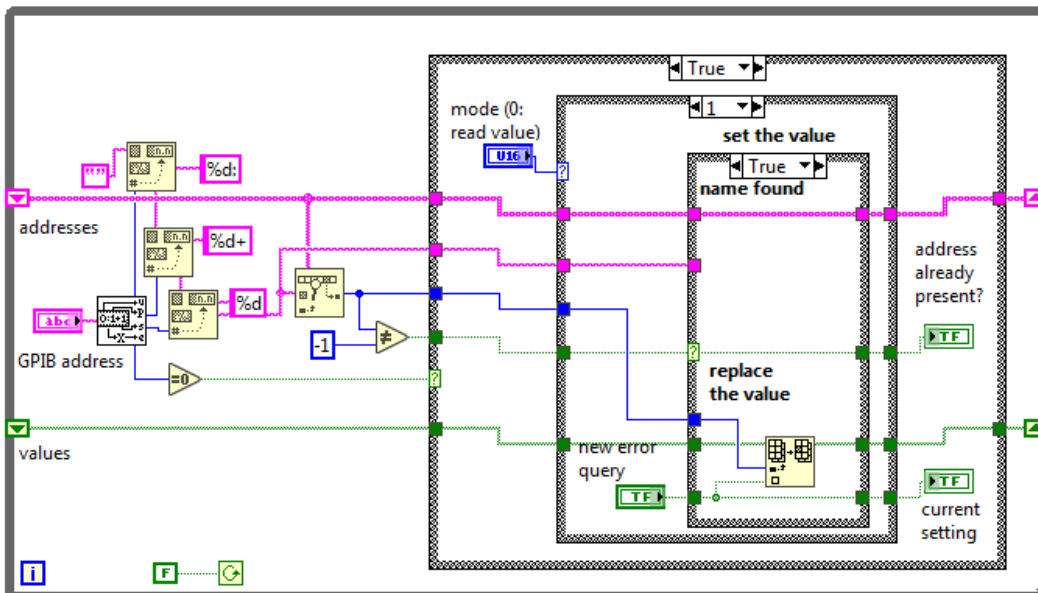
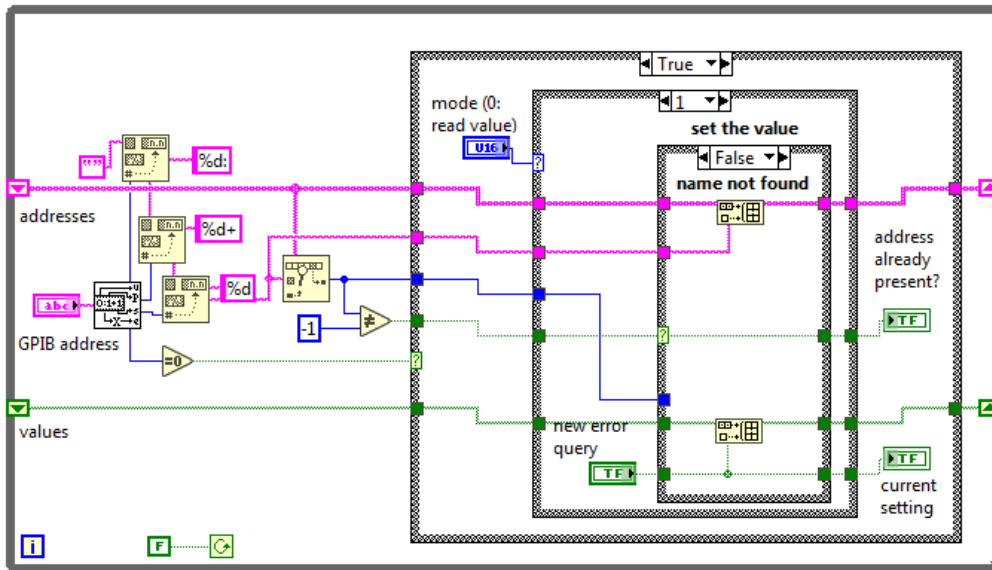
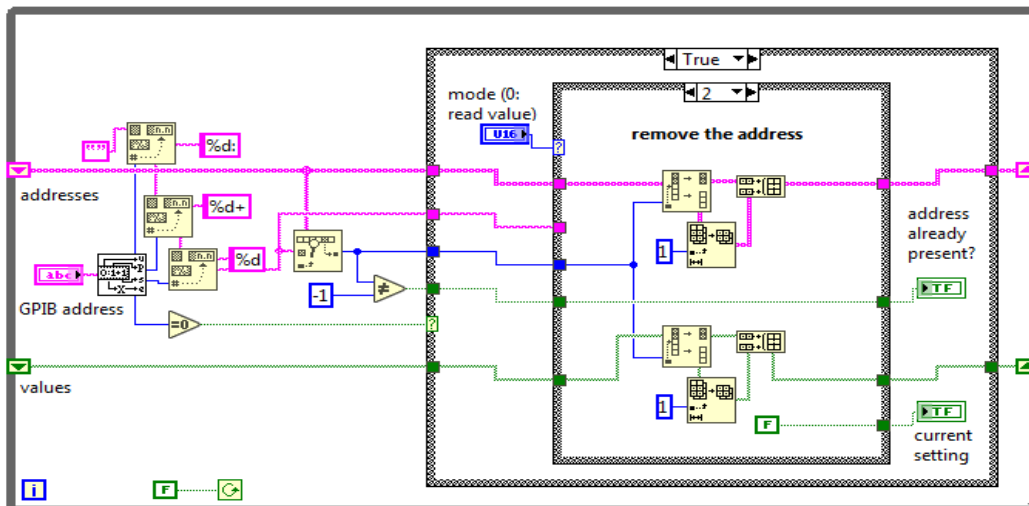


Figure 45.



Block diagram for Global Error querying (e) in model 7001

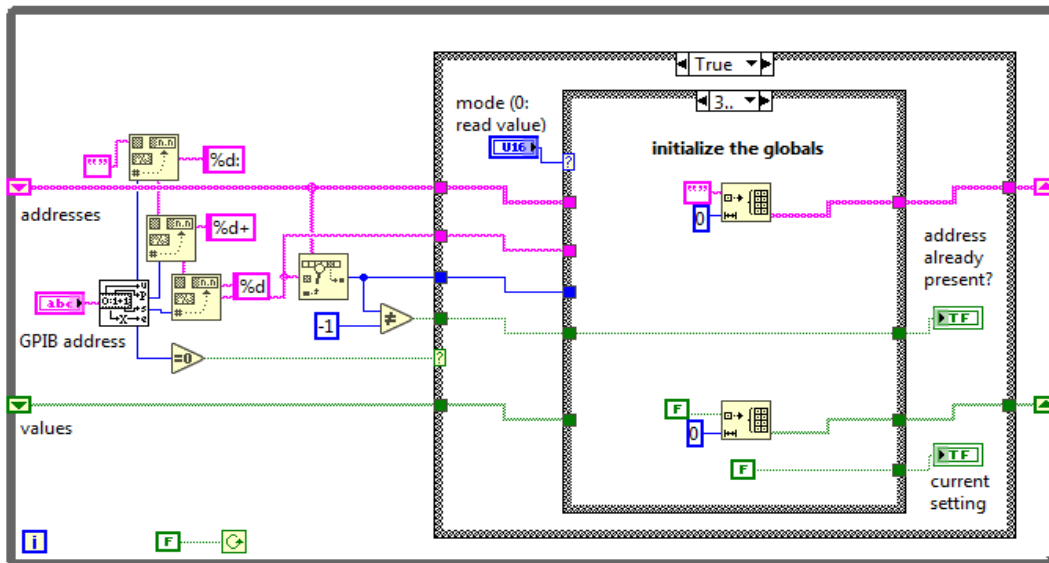
Figure 46.



Block diagram for Global Error querying (f) in model 7001

Figure 47.

Block diagram for Global Error querying (g) in model 7001

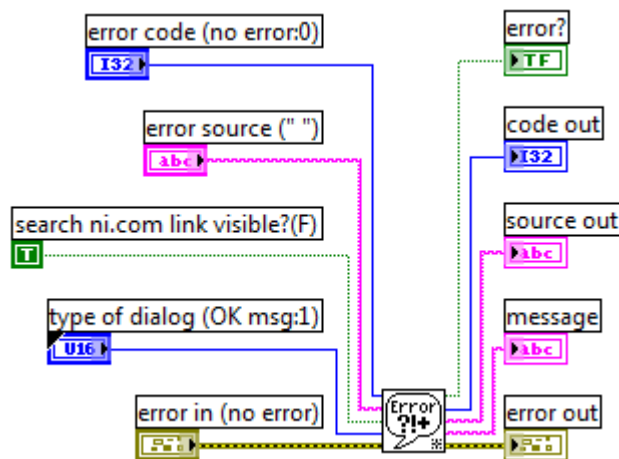


4.2.3.1.4.2 Simple Error Handler

Whenever an error occurs, it is indicated with this VI in Figure 48. This VI returns an error explanation and displays a dialogue box. This calls for the General Error Handler VI. It offers fewer choices but the same fundamental functionality as the General Error Handler.

Figure 48.

Block diagram for Simple Error querying

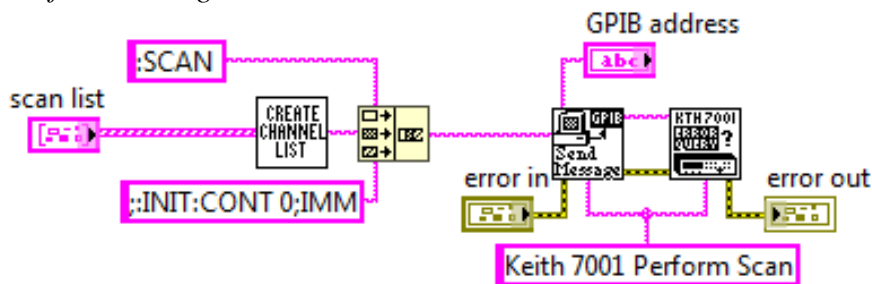


4.2.3.1.5 Arming and Scanning of Channels

Model 7001 requires an arming event before proceeding to the scan layer. The operation transitioned into the scan layer after the instrument left the arm layer. The following code in Figure 49 was used to achieve this.

Figure 49.

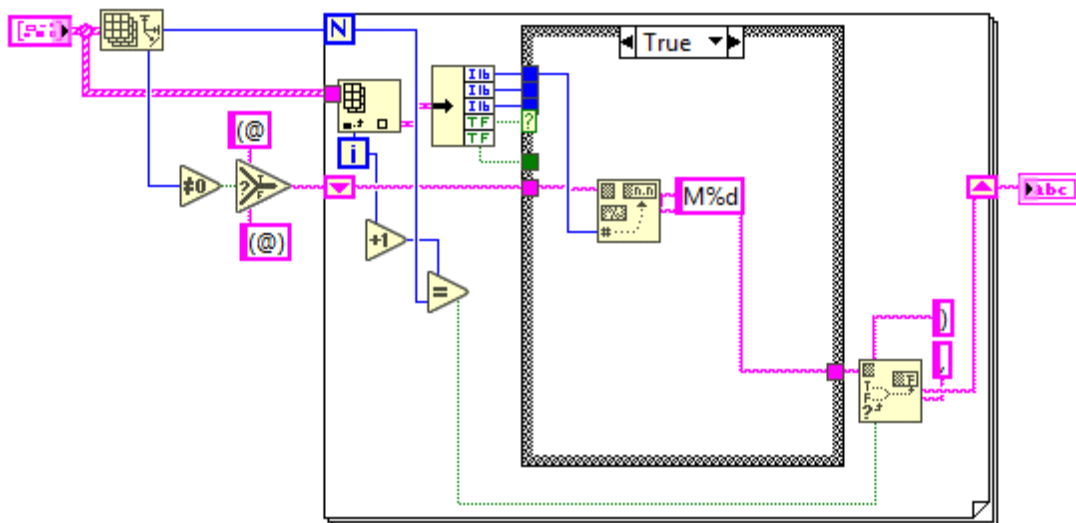
Block diagram for scanning channels in model 7001



The VI is composed of three SubVIs for creating a channel list, sending a message, and querying for errors. The send message code is highlighted in section 4.2.3.1.1.1 while the error querying is discussed in sub-section 4.2.3.1.2. The code used for populating the channel lists is shown in Figure 50. Arming is useful since it disables the instrument front panel buttons from functioning to avoid interruption and confusion with the remote command.

Figure 50.

Block diagram for populating channel list in model 7001

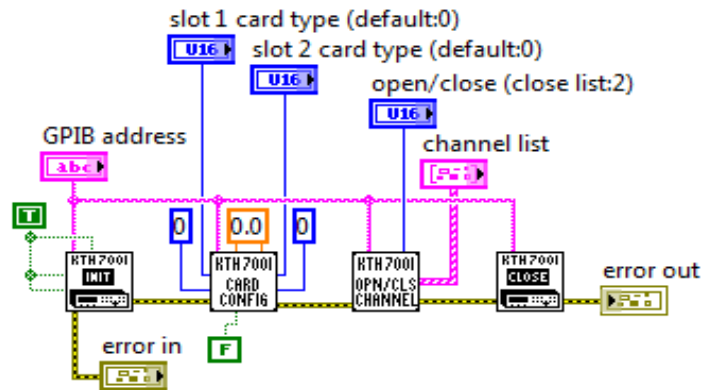


4.2.3.1.6 Opening and Closing Channels

Each model 7001 slot can support up to 40 channels. These channels were closed and opened using the code in Figure 51

Figure 51.

Block diagram for Opening/Closing Channels in model 7001



The VI comprised the initialize VI, the Card configuration VI, the Open/Close channel VI, and the Close VI. These VIs were executed sequentially.

4.2.3.1.7 Reading SCPI Error Queue

The code in Figures 52 and 53 was used in reading errors obtained from syntax or spelling errors made when querying the instrument using the SCPI language.

Figure 52.

Block diagram for Reading SCPI Error Queue in model 7001 (a)

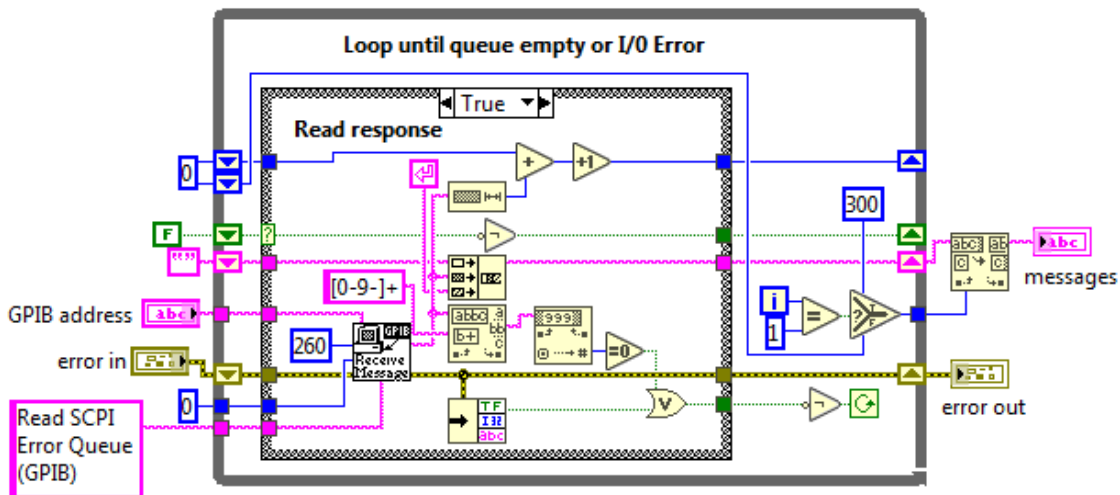
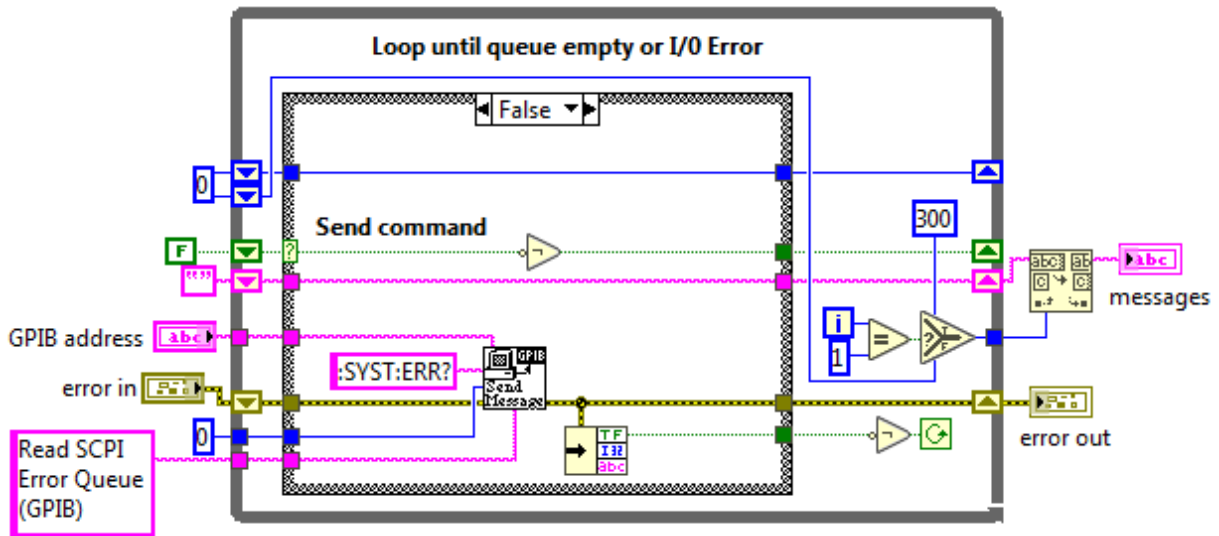


Figure 53.

Block diagram for Reading SCPI Error Queue in model 7001 (b)



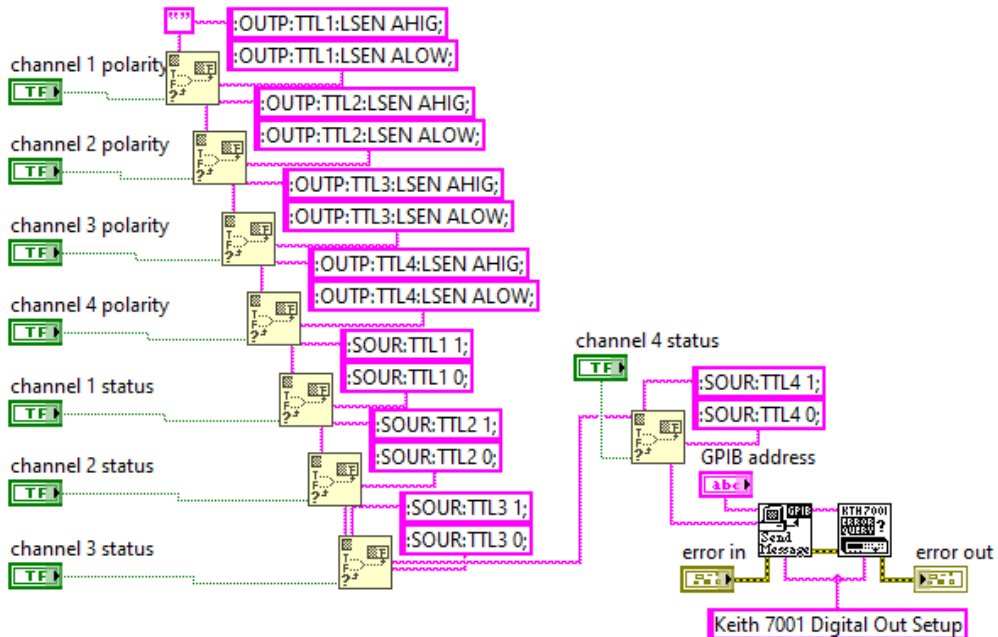
The VI also used the send message subVI discussed in section 4.2.3.1.1.1.

4.2.3.1.8 Digital Output Relay Switching

The VI illustrated in Figure 54 was used sequentially to switch the digital output of the 7065 Hall Effect card.

Figure 54.

Block diagram for Switching digital output in 7056 card



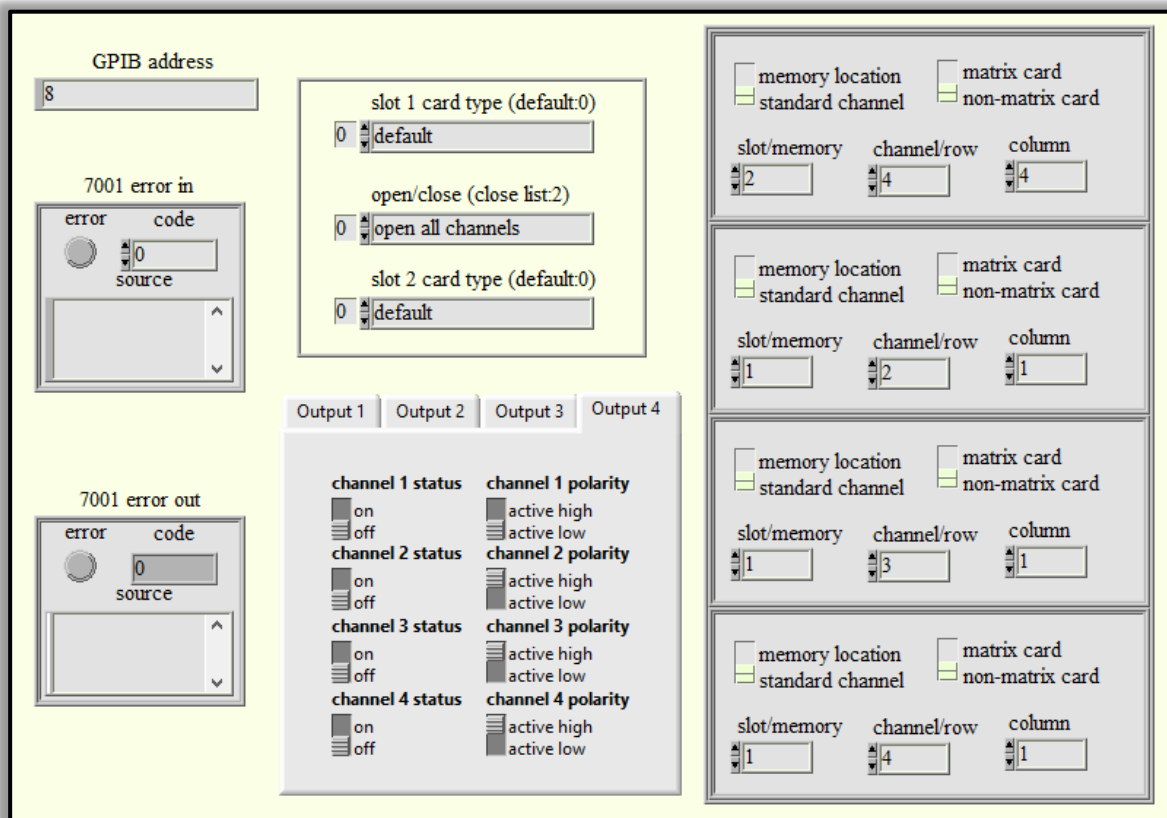
The VI utilized the send message VI and the Error query previously discussed.

4.2.3.1.9 Front Panel for Model 7001

The front panel for controlling Model 7001 is presented in Figure 55.

Figure 55.

Front panel diagram for controlling model 7001



4.2.3.2 Keithley 2182A Interfacing

Model 2182A was connected via a stacked GPIB hub to the USB computer port for complete control. The following VIs and SubVIs were used to control the instrument.

4.2.3.2.1 Initialization

Similar to Model 7001, model 2182A had to be connected to a power supply to be initialized first. The code was used in initialization. The VI sequentially opens the instrument, Queries

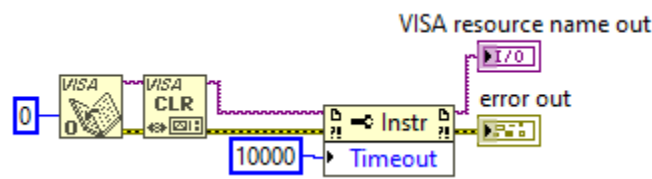
the instrument ID, Resets the instrument to the default setup checks for errors and then terminates the program as discussed

4.2.3.2.1.1 Opening the Instrument

The VI in Figure 56 was used in opening the Instrument

Figure 56.

Block diagram for opening session in model 2182A

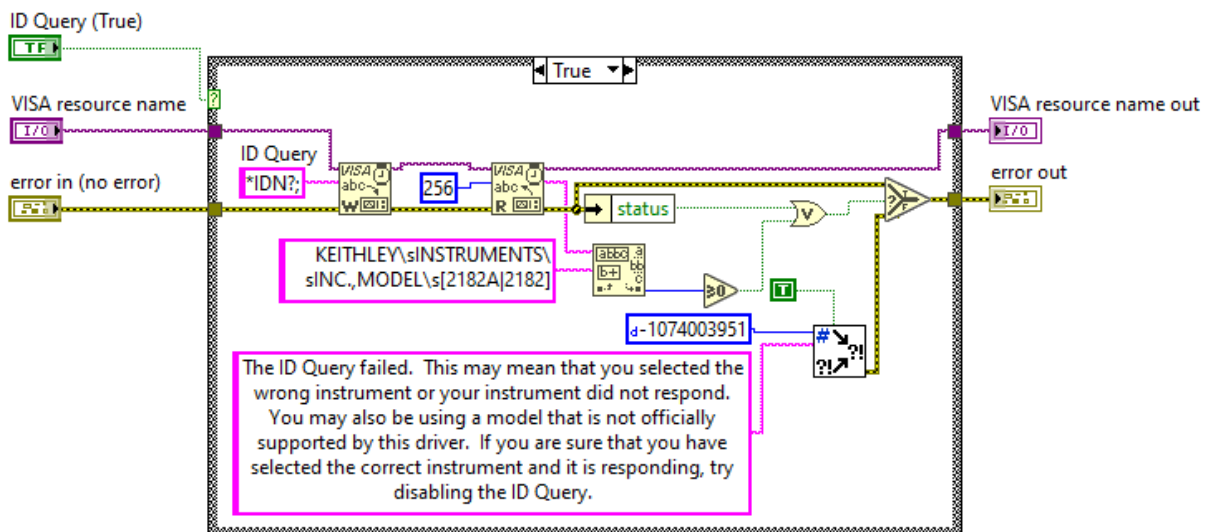


4.2.3.2.1.2 Querying Instrument ID

This code illustrated in Figure 57 was used to check if the instrument responds or else returns an error message string. If the instrument responded, the instrument was reset to default.

Figure 57.

Block diagram for querying instrument ID in model 2182A



4.2.3.2.1.3 Resetting Instrument to Default Setup

If the instrument responds positively, it is then reset and then a set of default setup commands is sent to the instrument using the piece of code shown in Figure 58.

Figure 58.

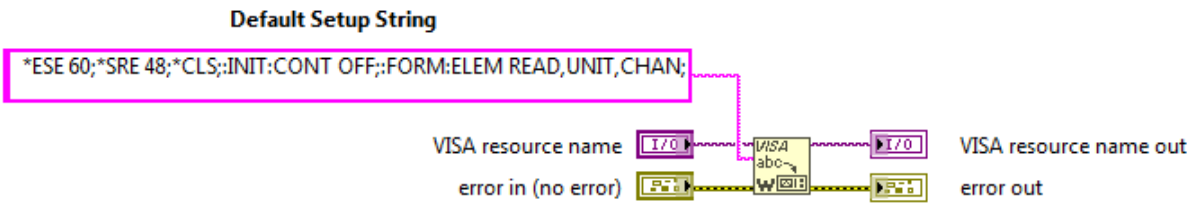
Block diagram for resetting model 2182A



The VI calls for the default setting VI presented in Figure 59.

Figure 59.

Block diagram for restoring model 2182A to the default setting



The default setup is presented in Table 4.

Table 4.

The default setup for 2182A

Command	Description
HEADER OFF	instrument no longer returns headers with responses to queries
*ESE 60	enables command, execution, query, and device errors in the event status register
*SRE 48	enables message available, standard event bits in the status byte
*CLS	clears status
INIT: CONT OFF	Disables continuous triggering after a restart
FORM: ELEM READ, UNIT, CHAN	enables metadata for correct parsing of the return string

4.2.3.2.1.4 Terminating Session

The code in Figure 60 was used to terminate the session

Figure 60.

Block diagram for error Session termination in model 2182A

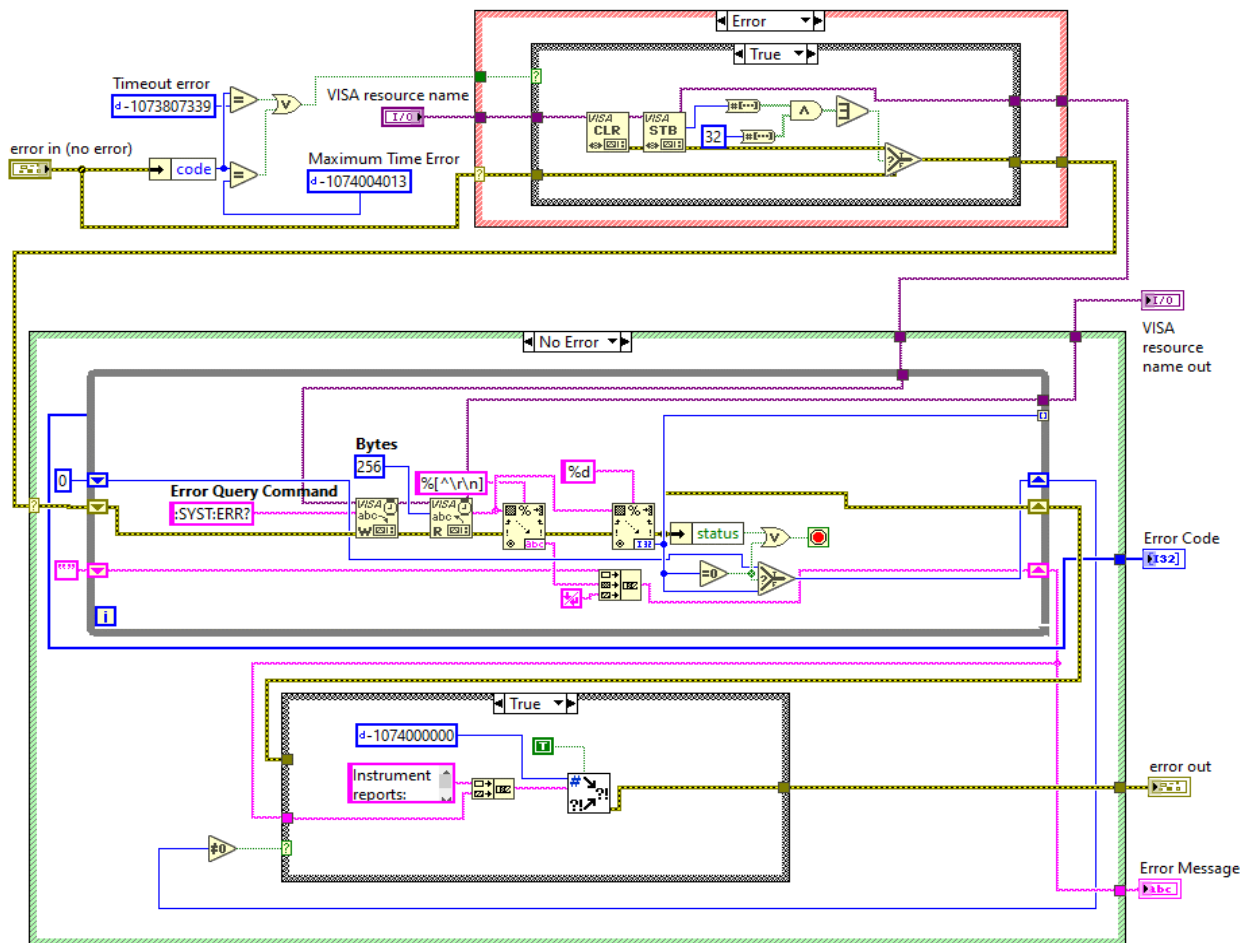


This occurs after error checking and reporting have been done and no error has been returned

4.2.3.2.2 Error Querying

The following VI in Figure 61 was used in error querying and reporting.

Figure 61.



Block diagram for Error querying and reporting in model 2182A

The VI checks if the error code indicates a timeout, to inform the user; otherwise, it determines if a timeout or maximum time error has occurred. If yes, it next determines whether the instrument has reported an error. After a timeout, VISA Clear is then used to halt the present process and flush the I/O buffer. The next step proceeded to read the service request status byte (STB) from the message-based device identified by the VISA resource name. This enabled the STB call's results to be accurately read. The Event Status bit is checked by the STB to see if it is set. If true, an instrument error exists and the error query instruction is sent. It, therefore, returns the timeout error that was sent into the VI if the Event

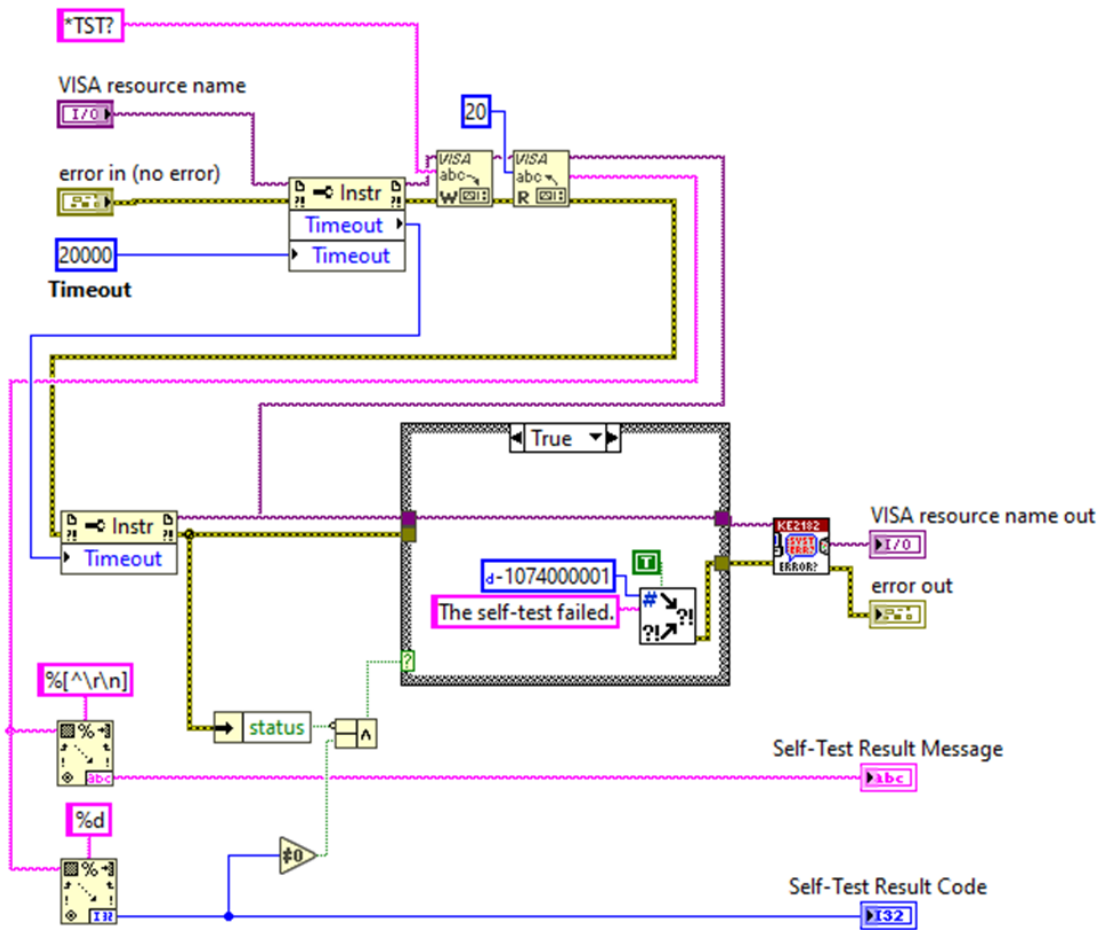
Status bit is not set (no instrument error). If the code is ever non-zero, an instrument error is reported as the cause of the problem.

4.2.3.2.3 Self-Testing

The self-test function for the instrument was executed using the code in Figure 62, which also returns the test results and the instrument's self-test answer string.

Figure 62.

Block diagram for self-testing model 2182A



This VI checks the instruments' error queue to see whether there are any issues. Until all errors have been read from the instrument, it keeps reading errors. Any issues were reported in

the error out of control, which can then check the ROM's checksum. The command adds the output queue with the coded result (0 or 1).

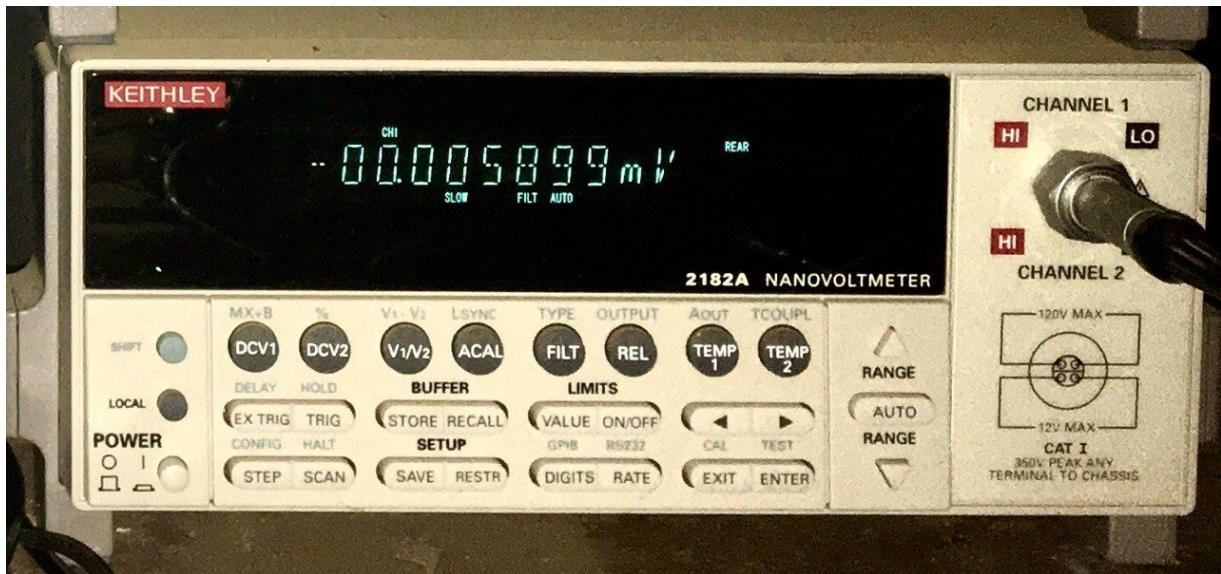
If Model 2182A is asked to speak. The computer receives the coded result from the output queue. If a value of zero (0) is returned, the test was successful and a result of one (1) means the test was unsuccessful.

4.2.3.2.4 Obtaining Voltage and Time Interval Readings

Voltage readings were measured as soon as model 6220 started sweeping the current. The voltage measurements were queried in every step interval and recorded. The collected data was held in data containers awaiting manipulation. The VI used to achieve this is presented in Figure 64. The VI utilized Error querying subVI discussed in section 4.2.3.2.1 The array sizes depended on the sweep steps covered by model 6220.

Figure 63.

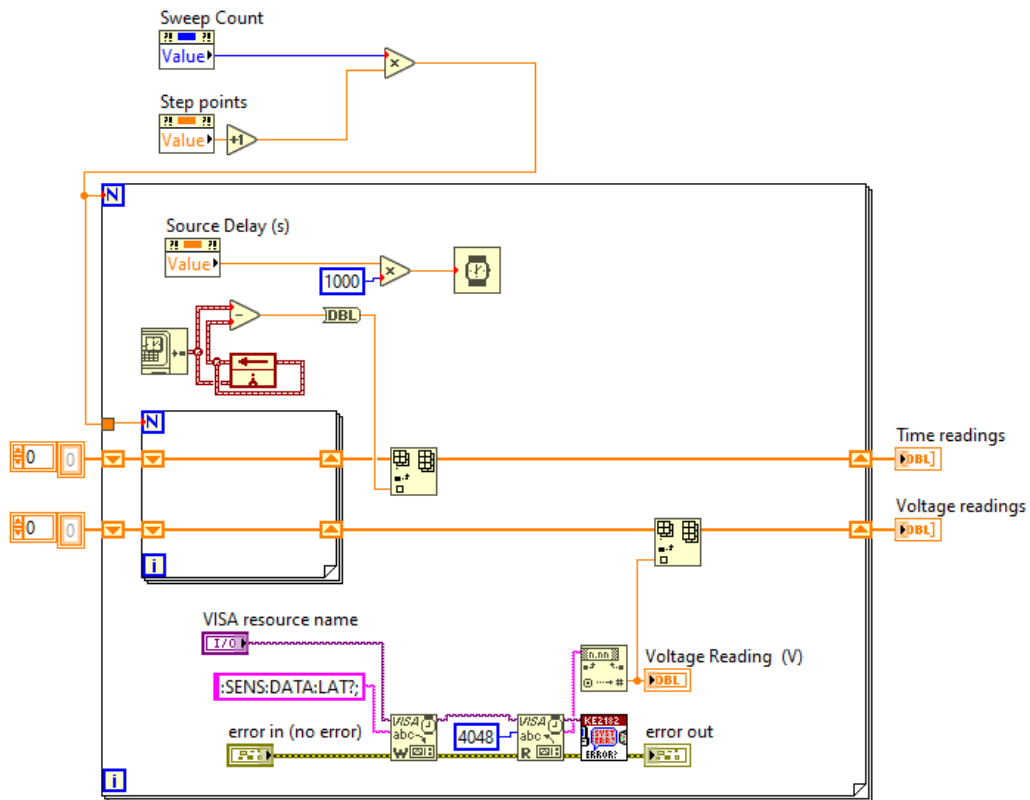
Front panel photo of model 2182A displaying a voltage reading



Note. Photograph taken by the author.

Figure 64.

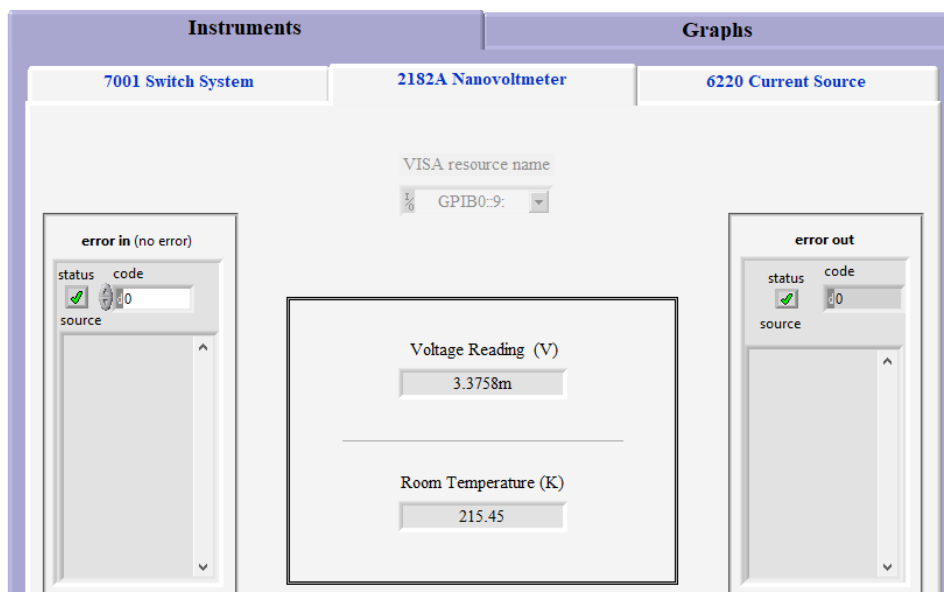
Block diagram of voltage and time interval measurements in model 2182A



The front panel used to view model 2182A voltmeter and temperature readings were as shown in Figure 65.

Figure 65.

Screenshot of front panel interface for model 2182A



4.2.3.3 Keithley 6220 Interfacing

4.2.3.3.1 Initialization

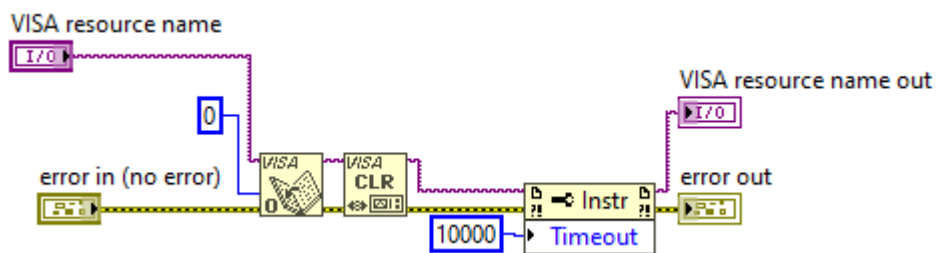
Initializing model 6220 comprised of three sequential steps highlighted below;

4.2.3.3.1.1 Opening the Instrument

The following code in Figure 66 was used to open the instrument. GPIB was set as the default interface type.

Figure 66.

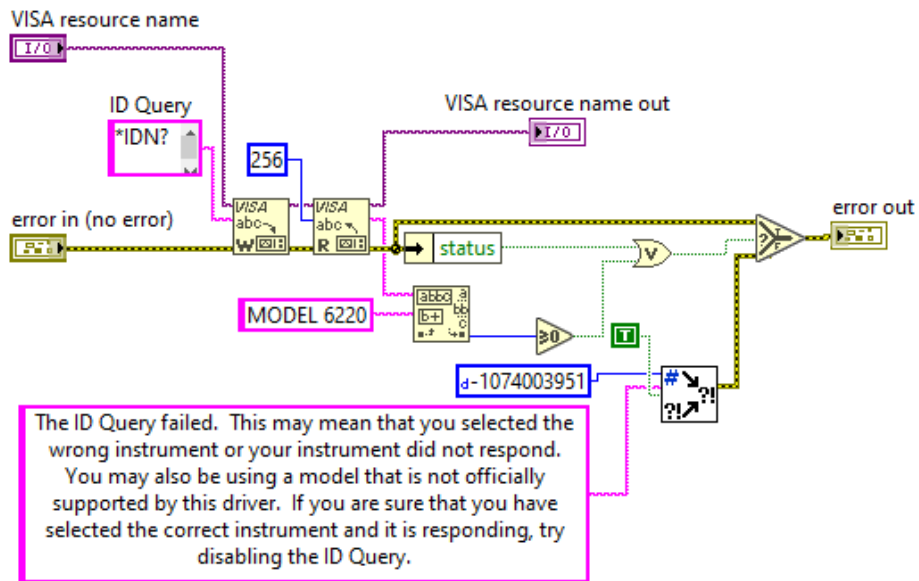
Block diagram for opening model 6220



4.2.3.3.1.2 Querying Instrument ID

This code illustrated in Figure 67 was used to check if the instrument responds or else returns an error message string. If the instrument responds, it is then reset in the subsequent initialization step.

Figure 67.



Block diagram for querying model 6220 ID

4.2.3.3.1.3 Resetting Instrument to a Default Setup

The code illustrated in Figures 68, 69, and 70 was used in resetting the instrument to its default setup.

Figure 68.

Block diagram for resetting model 6220 (a)

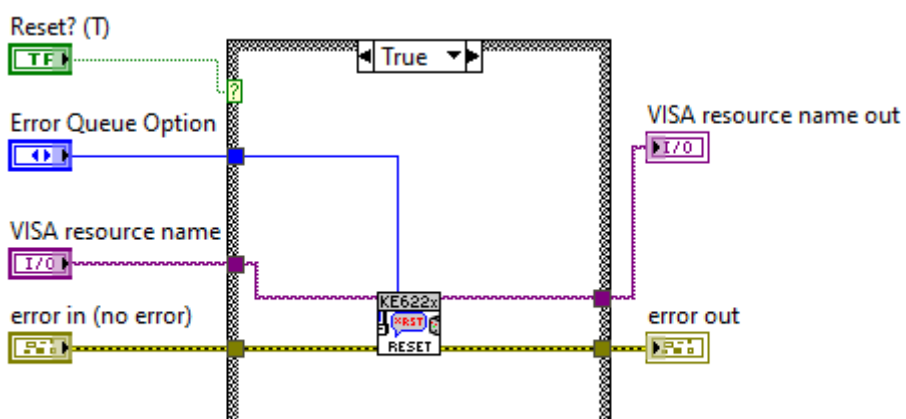
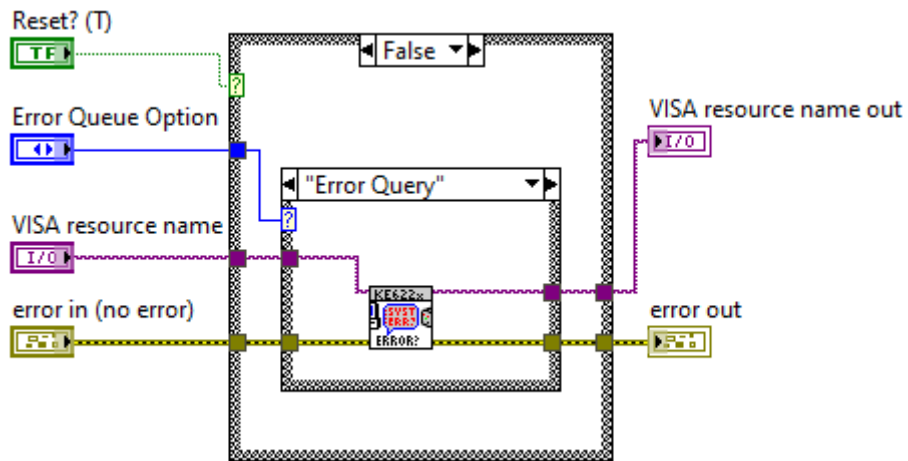
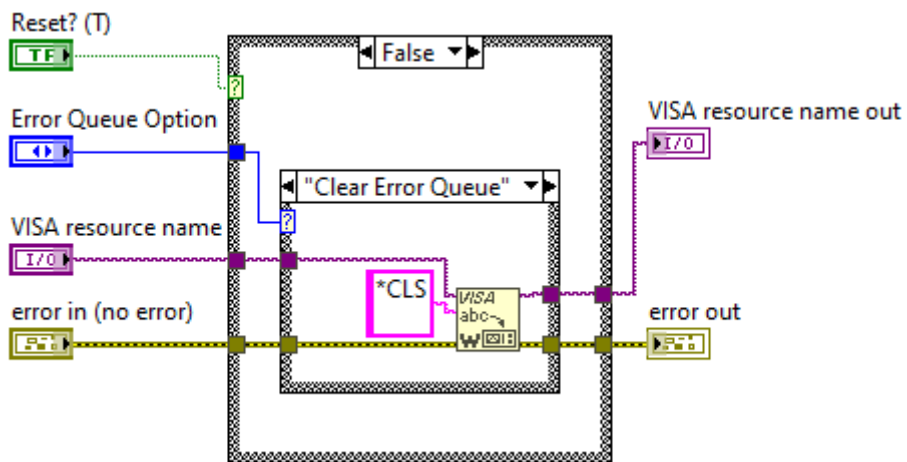


Figure 69.



Block diagram for resetting model 6220 (b)

Figure 70.



Block diagram for resetting model 6220 (c)

If the ID query fails, the VI resets the instrument by calling the reset SubVI discussed in section 4.2.3.3.1.3. Otherwise, errors in the error queue were checked and cleared if any. The errors were checked using the error checker VI discussed in 4.2.3.3.3

4.2.3.3.1.4 Terminating the Session

If an error is reported from the instrument, it is closed by invoking the close SubVI discussed in section 4.2.3.3.1.4. The code to achieve this is illustrated in Figures 71 and 72.

Figure 71.

Block diagram for error checking and terminating session in model 6220 (a)

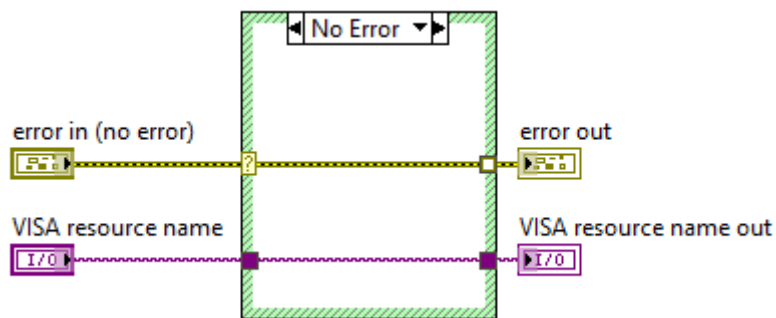
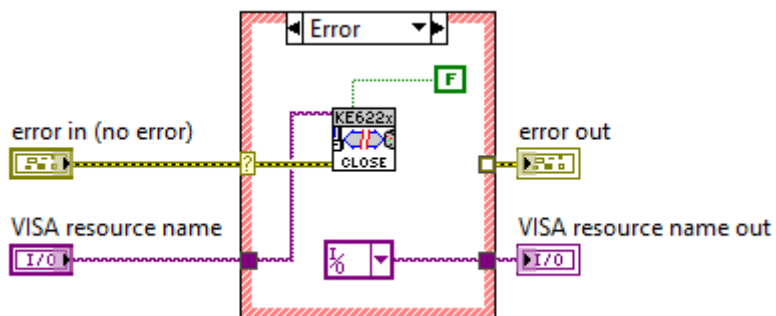


Figure 72.

Block diagram for error checking and terminating session in model 6220 (b)



4.2.3.3.2 Sweeping

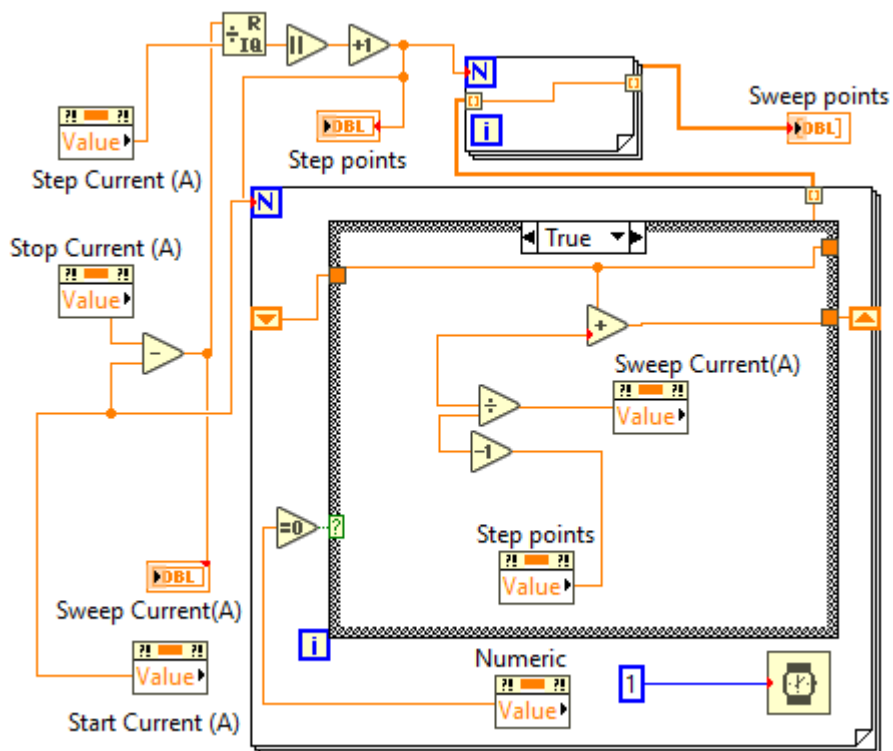
The following VIs were used to conduct a DC sweep in model 6220. All VIs had to be checked for SCPI errors using the error checker discussed in section 4.2.3.3.3. If there is an error, the VI aborts and returns the error string else triggers the next command.

4.2.3.3.2.1 Sweep Type

The current source generated two types of sweeps, Linear (Lin) and logarithmic (log) staircase DC sweeps. The formulas for the two types of sweeps are built into model 6220. The current increases or decreases in discrete steps in a linear staircase sweep type, starting with a start current and completing with a stop current. The fixed current setting just before the sweep begins is known as the bias current. After the sweep is finished, the current output stays at the final position. The VI used in generating the linear sweep points is presented in Figure 73

Figure 73.

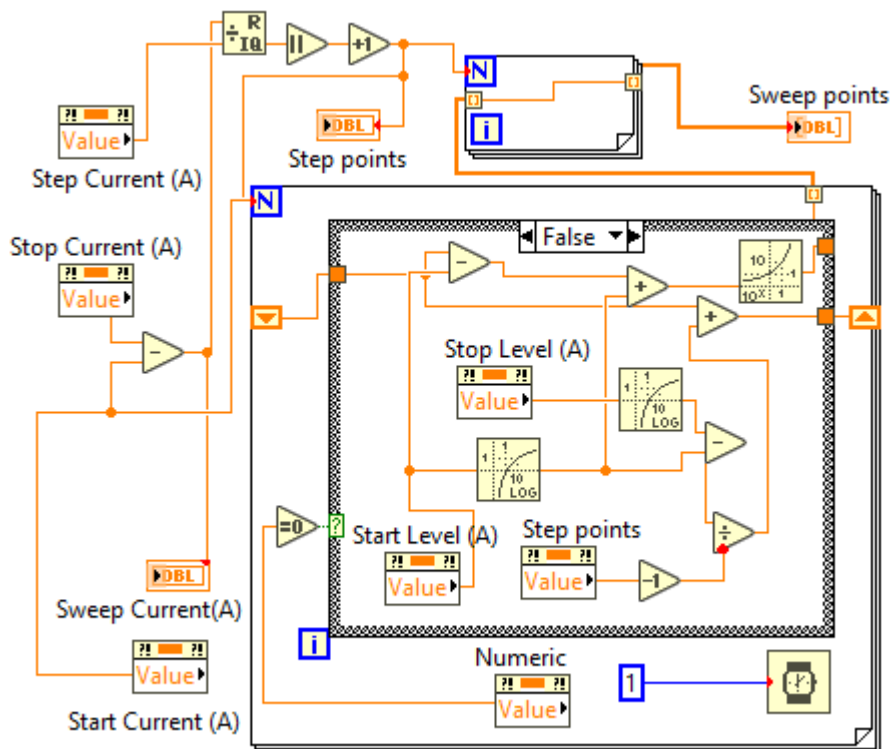
Block diagram for obtaining linear staircase points



In the case of the logarithmic staircase sweep, the current increases or decreases logarithmically and starts and stops with logarithmic steps. Once more, the bias current is the fixed current setting immediately before the sweep begins. After the sweep is finished, the current output remains where it was at the previous point. The VI used in generating the logarithmic sweep points is presented in Figure 74.

Figure 74.

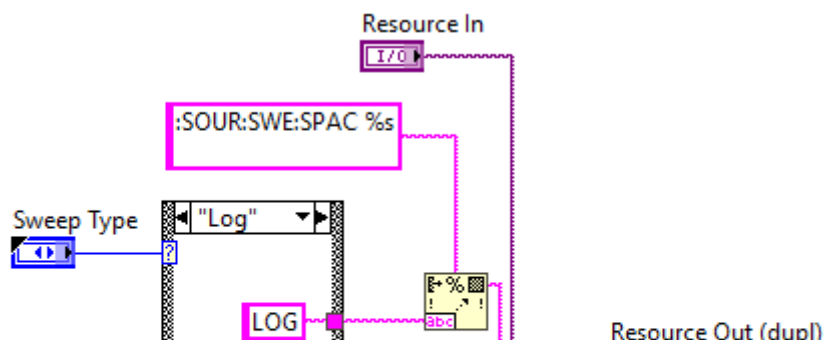
Block diagram for obtaining logarithmic staircase points



The sweep type selection is made from the front panel of the 6220 presented in Figure 79, and the VI for setting the sweep type is presented in Figure 75.

Figure 75.

Block diagram for setting the sweep type in model 6220



4.2.3.3.2 Arm and Initialize Sweep.

Before the model 6220 can conduct a sweep, it has to be armed first. Arming disables any operation on the front panel of the instrument to avoid interruptions. The code illustrated in Figures 76 and 77 was used to achieve this.

Figure 76.

Block diagram for arming and initializing sweep in model 6220 (a)

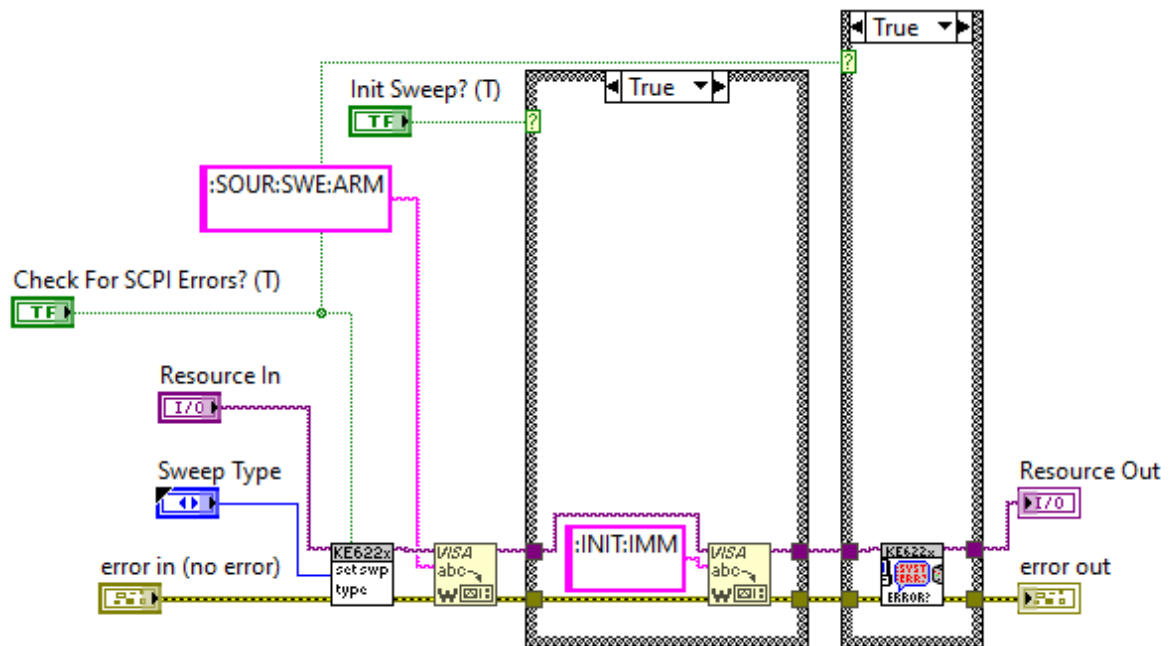
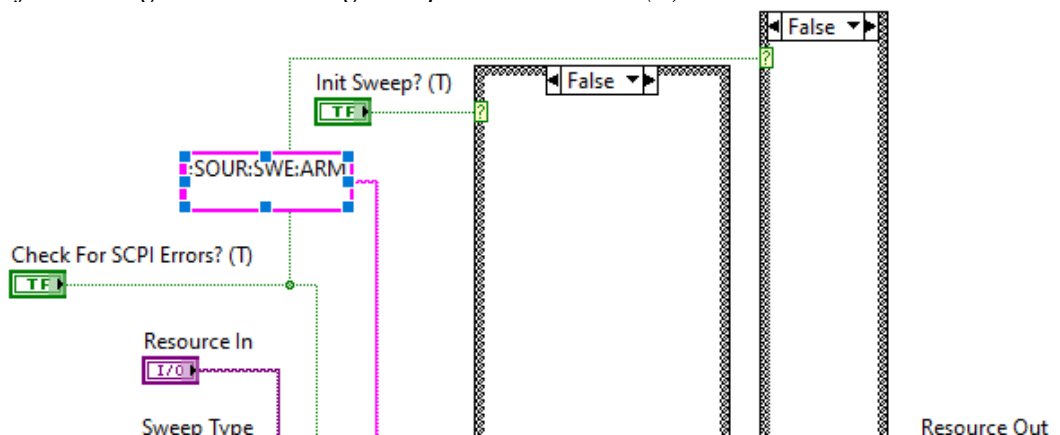


Figure 77.

Block diagram for arming and initializing sweep in model 6220 (b)

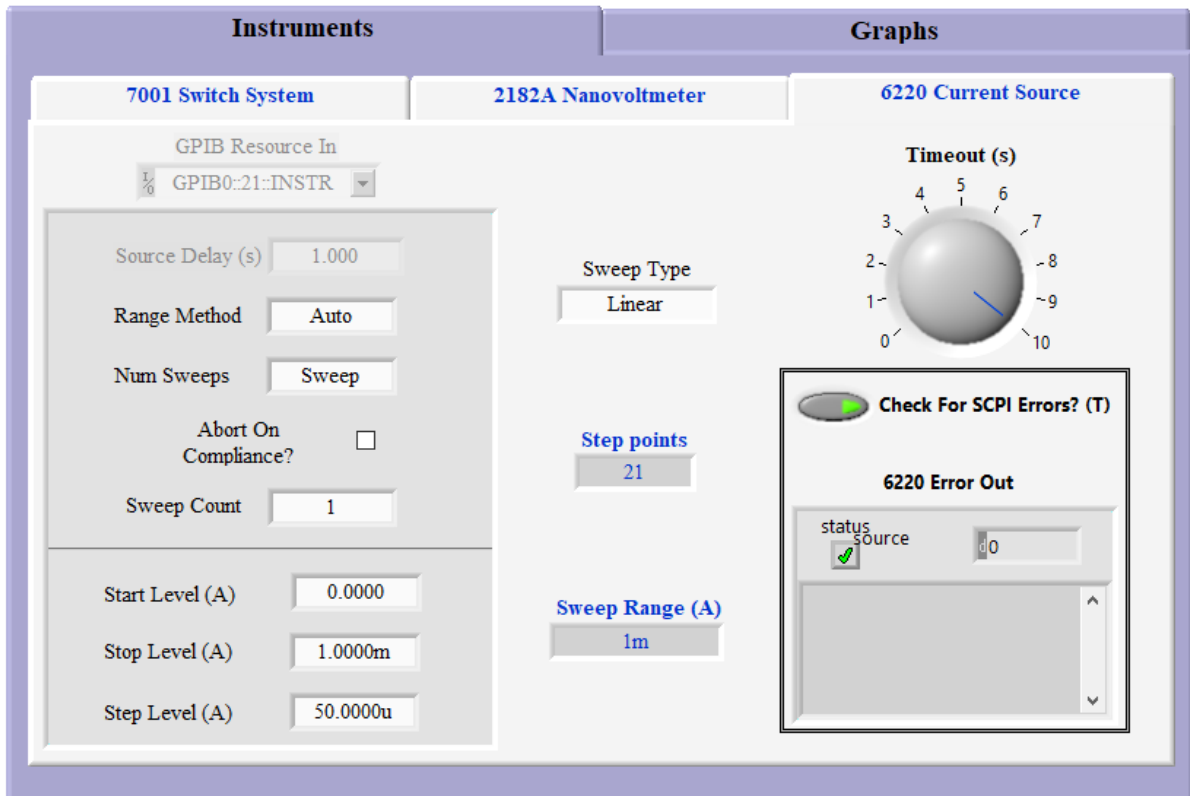


4.2.3.3.2.3 Setting Lin Log Parameters

Lin Log parameters include; source delay, the Number of sweep steps, the sweep type, the range method, the number of sweeps, and the sweep count. These were set from the front panel of model 6220 presented in Figure 78.

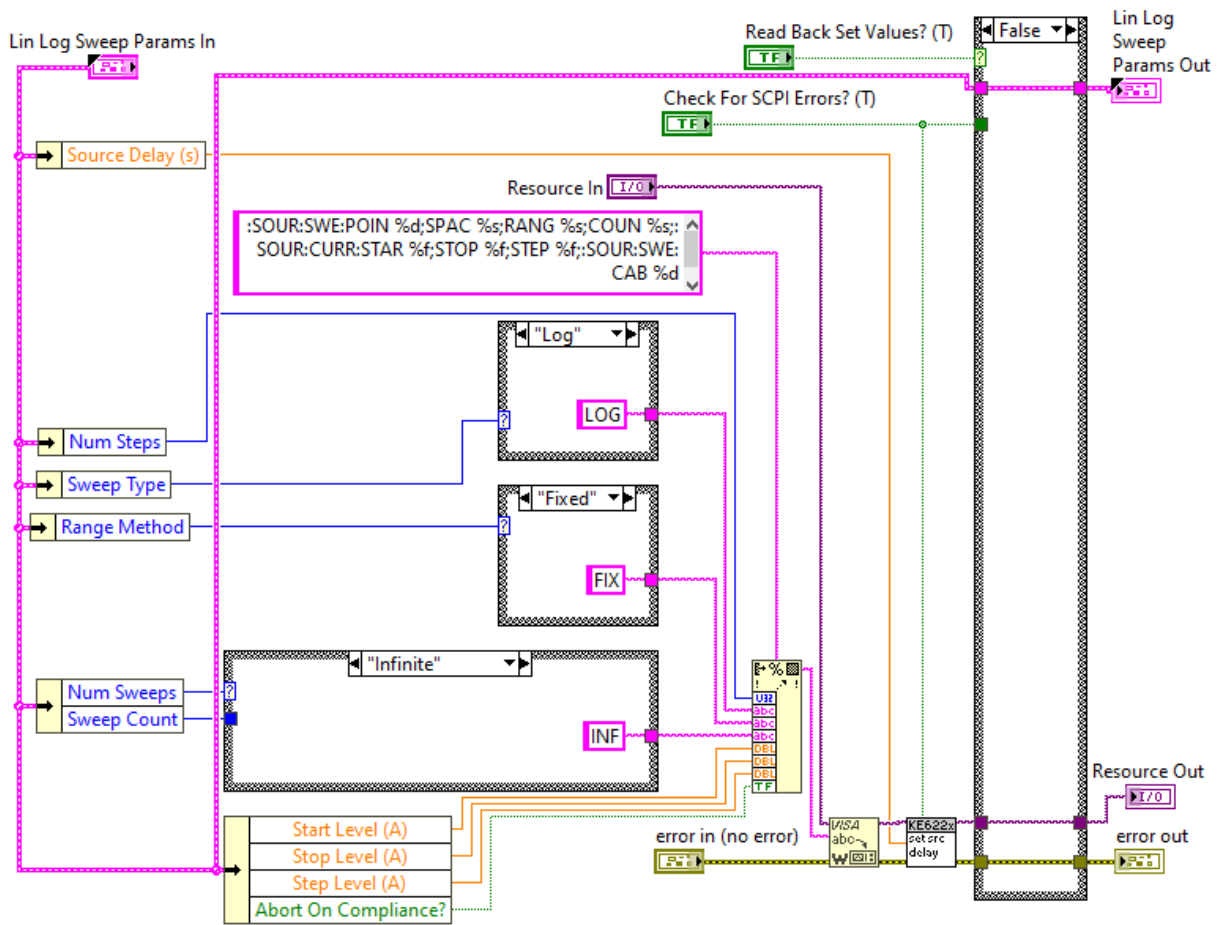
Figure 78.

Front panel for setting sweep parameters in model 6220



The settings were managed by the VI in Figure 79.

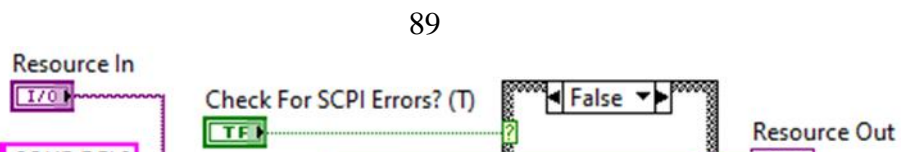
Figure 79.



Block diagram for setting Lin Log parameters in model 6220

The VI called for the source delay VI presented in Figure 80. The delay represents the time taken between two step points. All steps of linear and log sweeps use this delay.

Figure 80.



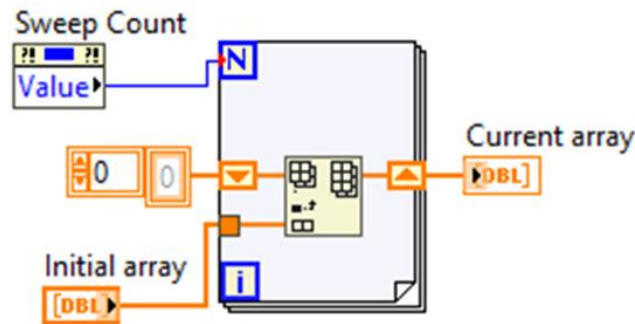
Block diagram for setting source delay in model 6220

Model 6220 supports three range methods, best, auto, and fixed. The best option uses the largest sweep step at the best range, the auto option is based on individual sweep step and the fixed option always stay within the fixed source range.

The sweep array was built by concatenating the initial array using the piece of code presented in Figure 81 depending on the number of sweeps.

Figure 81.

Block diagram for concatenating current array



4.2.3.3.2.4 Getting Operation Event Register

For monitoring sweep progress in model 6220, three status model events are available, all of which are set bits in the operation condition register. These events are summarized in Table 5. At each stage of the sweep, the Device sweeping event is set. This bit set remains set throughout the entire sweep according to queries of the operation event register. When a

sweep is stopped before it can finish, it raises the Sweep aborted event, and when the specified number of sweeps have been finished, it raises the Sweep done event.

Table 5.

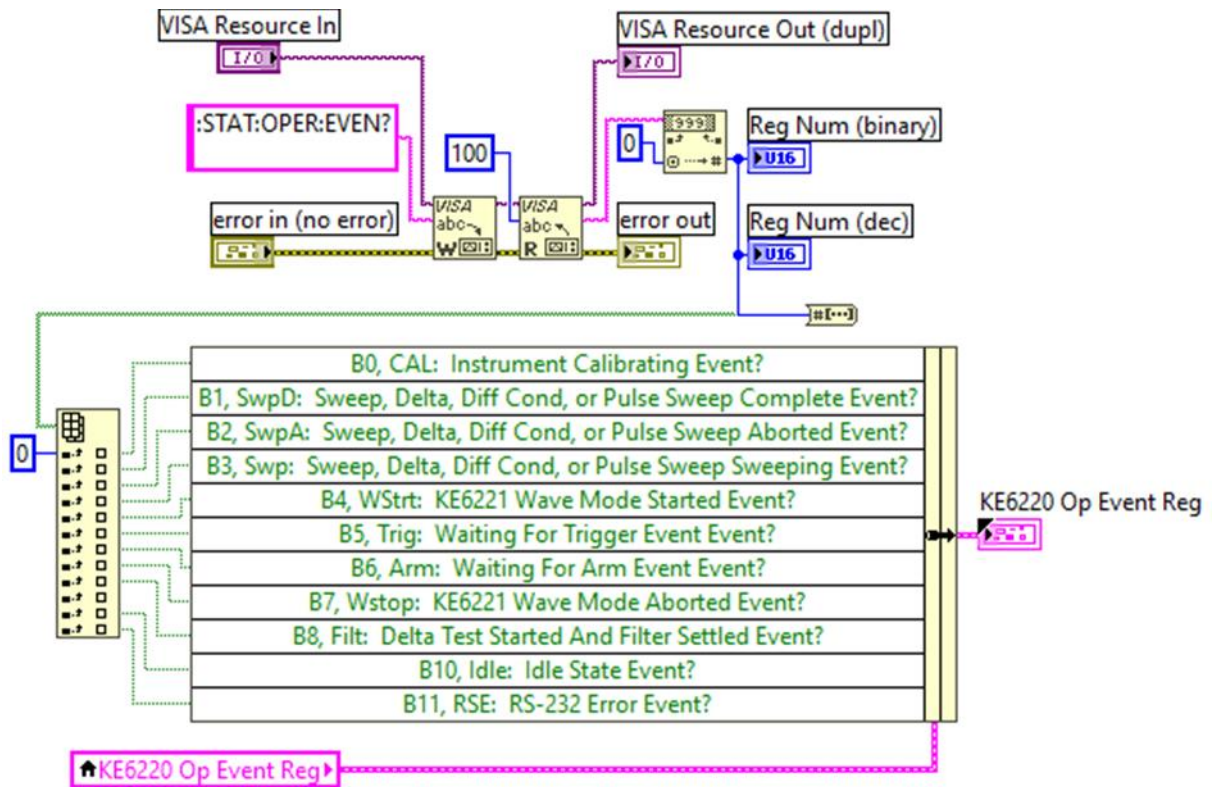
Sweep status model bits in model 6220

Bit	Status Event
1	+ 122 “Sweep Done”
2	+ 123 “Sweep Aborted”
3	+ 124 “Device Sweeping”

The following detailed events were obtained using the VI in Figure 81

- i. Instrument Calibrating Event?
- ii. Sweep, Delta, Diff Cond, or Pulse Sweep Complete Event?
- iii. Sweep, Delta, Diff Cond, or Pulse Sweep Aborted Event?
- iv. Sweep, Delta, Diff Cond, or Pulse Sweep Sweeping Event?
- v. KE6221 Wave Mode Started Event?
- vi. Waiting For Trigger Event?
- vii. Waiting For Arm Event?
- viii. KE6221 Wave Mode Aborted Event?
- ix. Delta Test Started and Filter Settled Event?
- x. Idle State Event?

Figure 82.



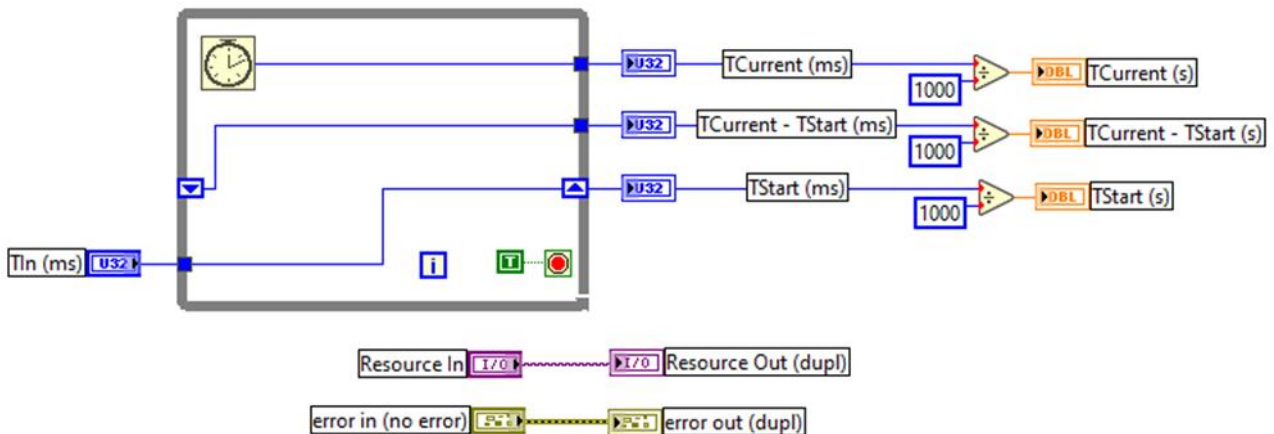
Block diagram for getting operation event register in model 6220

4.2.3.3.2.5 Timing

The timing between step points was achieved using the VI in Figure 83

Figure 83.

Block diagram for getting operation event register in model 6220

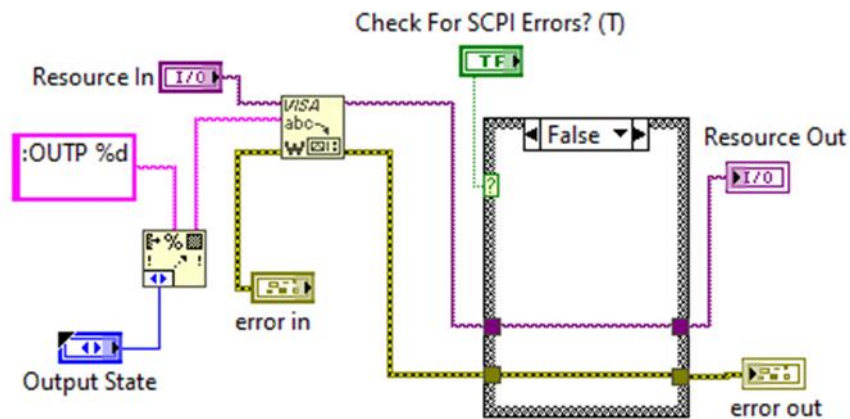


4.2.3.3.2.6 Setting the Output State

For current to flow from the instrument, the interlock switch must be connected and closed, moreover, the output state must be toggled ON. The VI in Figure 84 was used to toggle model 6220 ON and OFF at the beginning and the end of the sweep respectively.

Figure 84.

Block diagram for toggling the output state in model 6220



4.2.3.3.3 Error Handling

A simple error handler was used as the program's final action at the end of the I/O data path, to alert the user to an error while the general error handler was used to check the instrument's error queue to see if there were any errors. Until all errors were read from the instrument, it kept reading errors. The error-out indicator contained any errors that were discovered.

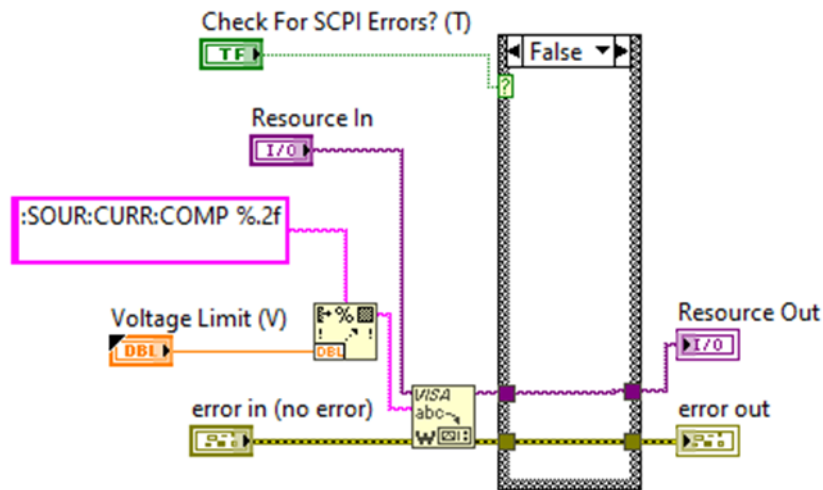
4.2.3.3.4 Compliance

The Model 6220's output voltage is limited by the compliance setting. The voltage compliance limit can be adjusted in 10mV steps from 0.1V to 105V. The output won't go over the level of

programmed compliance. The piece of code presented in Figure 85 was used for compliance setting.

Figure 85.

Block diagram for setting compliance in model 6220



The VI checks for SCPI errors and returns an error if any else sets the voltage limit.

4.2.3.4 Data Collection

Whereas voltage, time, and current data were collected from models 2182A and 6220 from the VIs discussed in sections 4.2.3.2.4 and 4.2.3.3.2.1, the dimensions of the thin film sample were measured by a Vernier calliper, and the magnetic field strength was keyed in as inputs in the LabVIEW program. Figure 86 shows a screenshot of the front panel of the input design diagram used to show the values of the model data input.

Figure 86.

Front panel for inputting sample size, compliance and the magnetic field strength

Voltage Limit	Length between voltage contact points	Sample Width	Sample Thickness	Magnetic Field
10.00 v	1.00 cm	2.00 cm	1.00 mm	258.125000 mT

The voltage and time data collected were exported as a CSV file for further analysis. Table 6 shows the I-V data recorded and exported.

Table 6.

Hall Effect I – V data

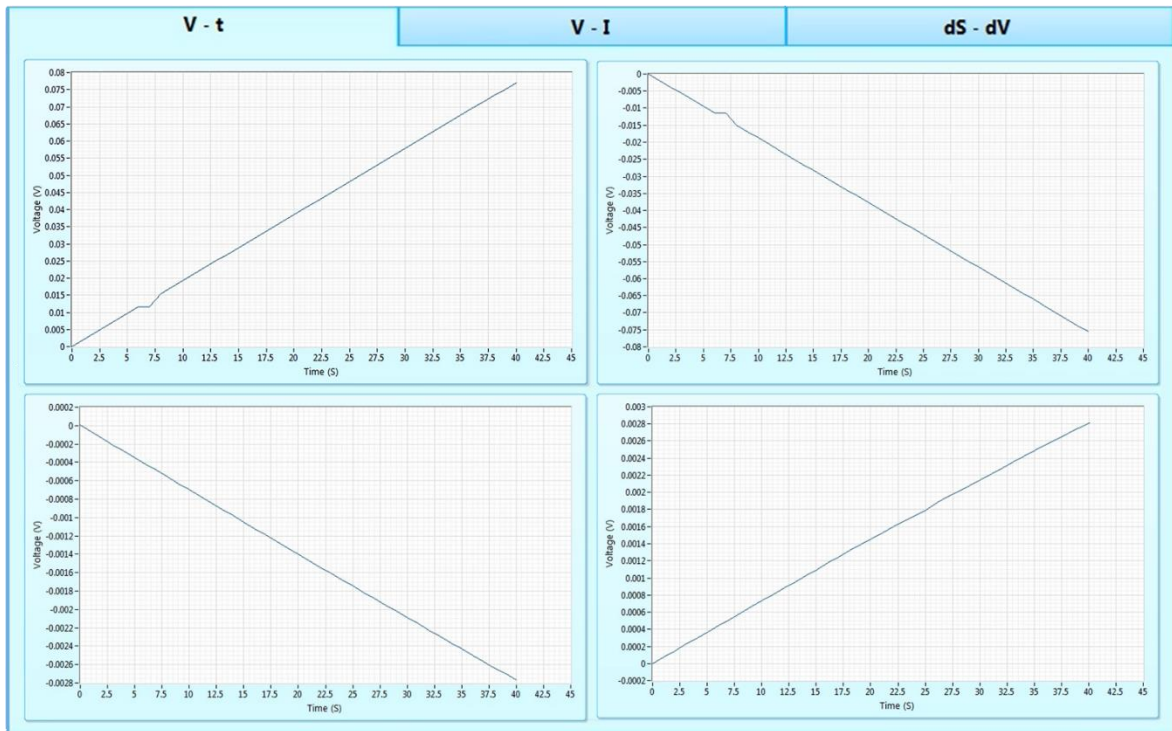
Time (S)	I (A)	V _{BD} B+ (V)	V _{DB} B- (V)	V _{BD} B- (V)	V _{DB} B+ (V)
0	0.0000	0.000000	0.000000	0.000000	0.000000
1	0.0005	0.001990	-0.000068	-0.001939	0.000072
2	0.0010	0.003901	-0.000138	-0.003806	0.000146
3	0.0015	0.005826	-0.000208	-0.005681	0.000220
4	0.0020	0.007751	-0.000279	-0.007558	0.000295
5	0.0025	0.009680	-0.000349	-0.009433	0.000369
6	0.0030	0.011591	-0.000418	-0.011309	0.000443
7	0.0035	0.011591	-0.000489	-0.011310	0.000516
8	0.0040	0.015441	-0.000559	-0.015064	0.000592
9	0.0045	0.017374	-0.000630	-0.016949	0.000668
10	0.0050	0.019293	-0.000699	-0.018812	0.000740
11	0.0055	0.021220	-0.000769	-0.020693	0.000809
12	0.0060	0.023145	-0.000839	-0.022574	0.000885
13	0.0065	0.025073	-0.000910	-0.024459	0.000957
14	0.0070	0.026986	-0.000980	-0.026368	0.001027
15	0.0075	0.028918	-0.001049	-0.028247	0.001099
16	0.0080	0.030843	-0.001119	-0.030132	0.001174
17	0.0085	0.032777	-0.001190	-0.032026	0.001244
18	0.0090	0.034691	-0.001260	-0.033894	0.001319

Time (S)	I (A)	V _{BD} B+ (V)	V _{DB} B- (V)	V _{BD} B- (V)	V _{DB} B+ (V)
19	0.0095	0.036619	-0.001331	-0.035779	0.001388
20	0.0100	0.038548	-0.001400	-0.037709	0.001459
21	0.0105	0.040481	-0.001469	-0.039594	0.001530
22	0.0110	0.042406	-0.001538	-0.041485	0.001597
23	0.0115	0.044317	-0.001607	-0.043369	0.001663
24	0.0120	0.046253	-0.001675	-0.045254	0.001730
25	0.0125	0.048178	-0.001745	-0.047151	0.001794
26	0.0130	0.050111	-0.001814	-0.049038	0.001878
27	0.0135	0.052022	-0.001882	-0.050910	0.001954
28	0.0140	0.053964	-0.001953	-0.052804	0.002015
29	0.0145	0.055892	-0.002021	-0.054736	0.002084
30	0.0150	0.057819	-0.002090	-0.056626	0.002150
31	0.0155	0.059730	-0.002157	-0.058517	0.002214
32	0.0160	0.061660	-0.002227	-0.060398	0.002284
33	0.0165	0.063588	-0.002294	-0.062296	0.002352
34	0.0170	0.065521	-0.002364	-0.064195	0.002427
35	0.0175	0.067437	-0.002430	-0.066074	0.002495
36	0.0180	0.069364	-0.002500	-0.067982	0.002562
37	0.0185	0.071300	-0.002568	-0.069870	0.002619
38	0.0190	0.073232	-0.002635	-0.071772	0.002687
39	0.0195	0.075150	-0.002698	-0.073660	0.002754
40	0.0200	0.077086	-0.002765	-0.075555	0.002811

The V – t graph was drawn within the application package to relate how the Hall voltage evolved. The graph is represented in Figure 87. The code used to draw this is presented in Figure 92.

Figure 87.

Front panel showing $V - t$ graphs



The exportation of the I-V data and the input and output parameters in CSV format was executed by the VIs in Figures 88 and 87 respectively.

Figure 88.

Block diagram for exporting I-V data

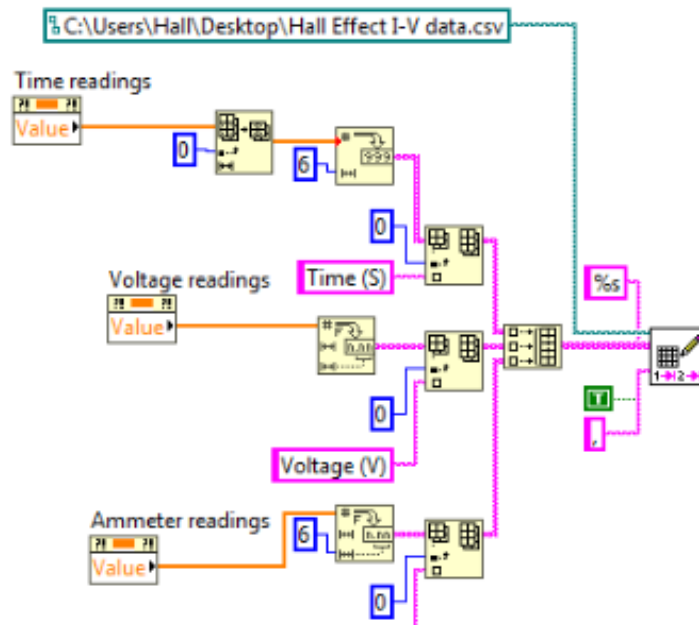
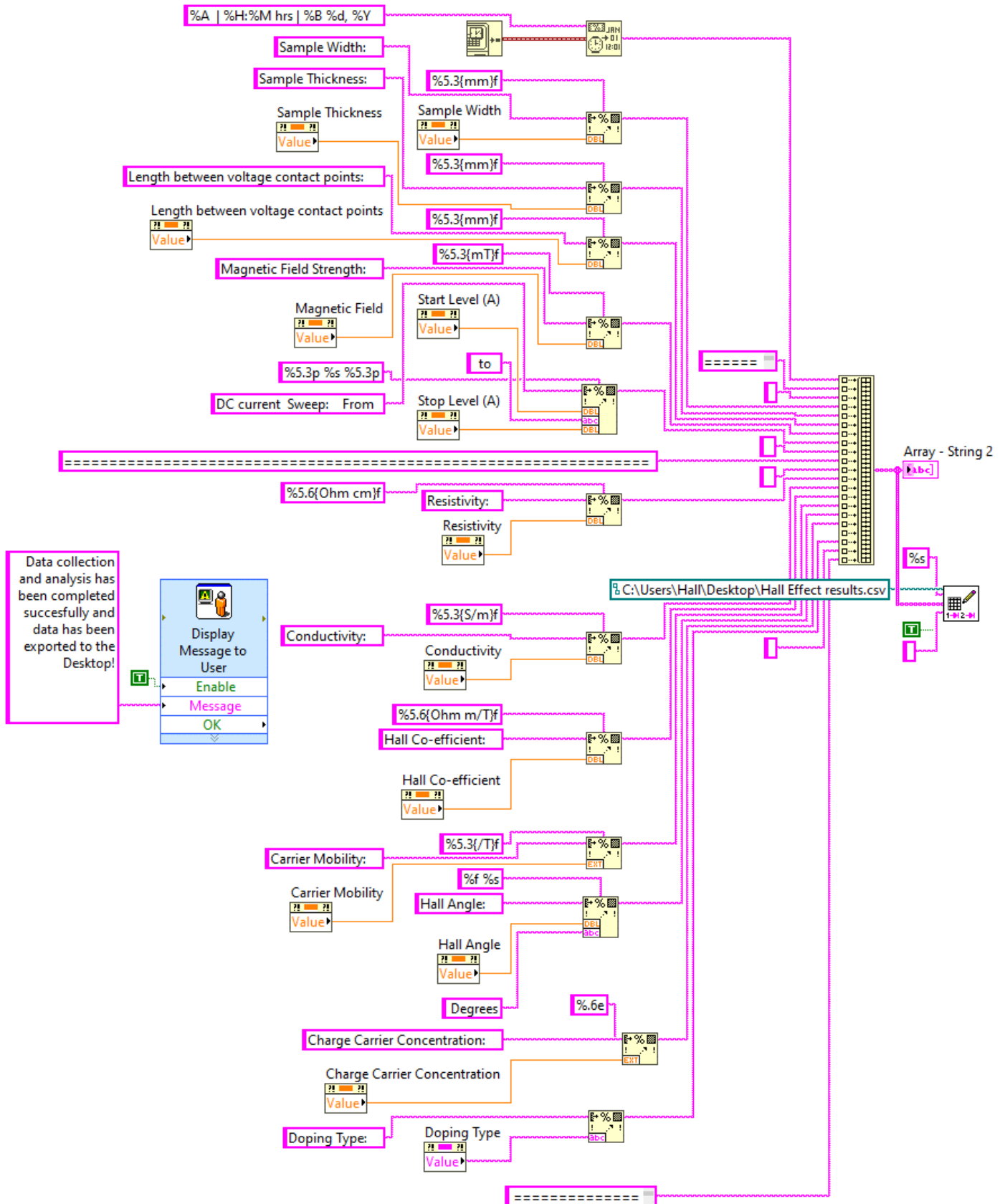


Figure 89.

Block diagram for exporting input and output parameters



The DC linear current Sweep was done with the following settings in Table 7

Table 7.

Sweep Settings

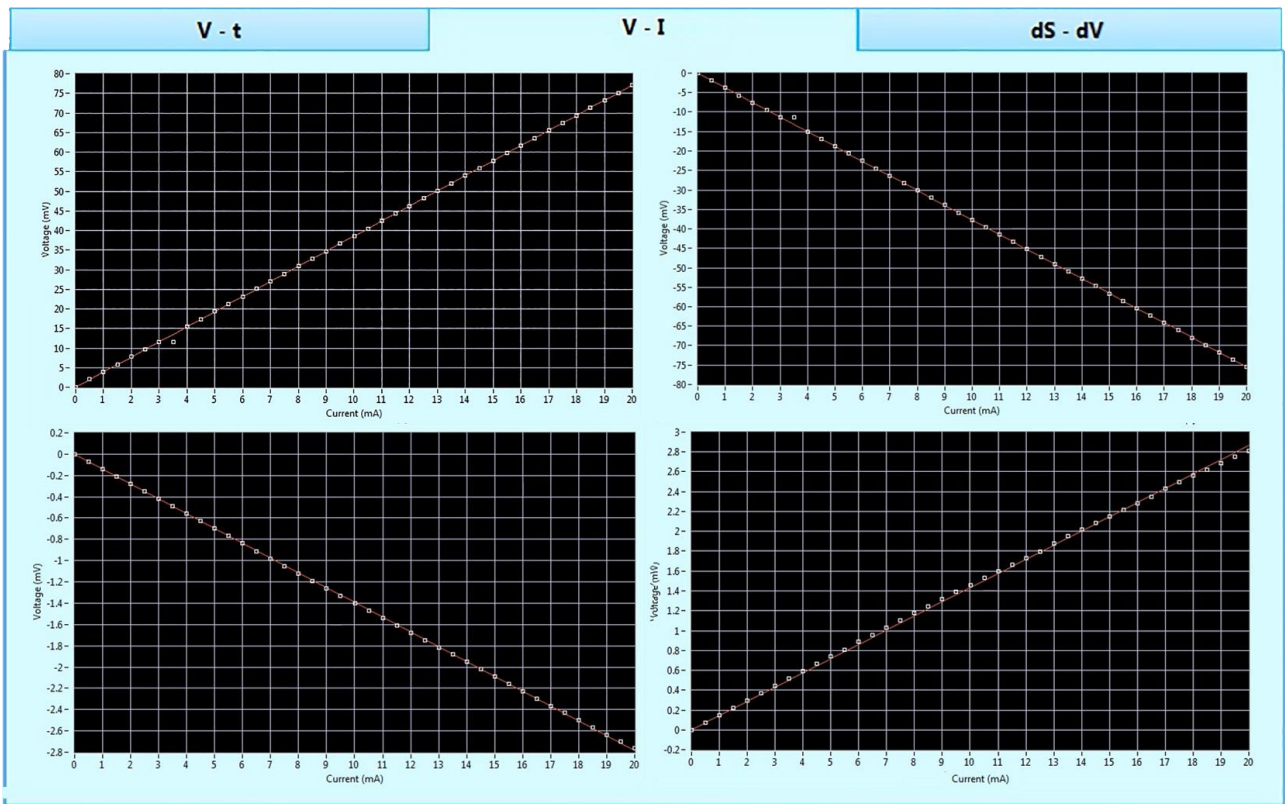
Sweep	Setting
type	Linear
Range	Fixed
Start Value	0 A
Step	0.5 μ A
Delay	1 S
Stop Value	20 mA
Number of Points	41

4.2.3.5 Hall Effect Characterization

The measured Hall voltage recorded was plotted as a function of current as presented in Table 6. The first piece of data to be found was the proportionality factor which relates current and voltage. The graphs obtained are presented in Figure 90

Figure 90.

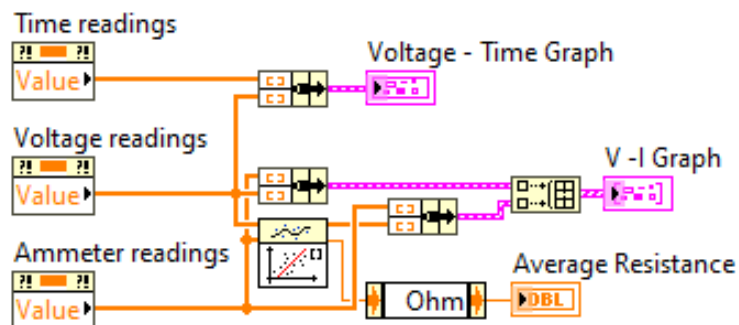
Front panel Showing $V - I$ graphs



The proportionality factor R , the slope of the graph of Hall voltage versus the current in Figure 90 presented the average resistance. The line of best fit was drawn using the least square method with a tolerance of 0.0001 and the Y-intercept fixed at the origin. The VI used to draw the $V - I$ and $V - t$ graphs are illustrated in Figure 91

Figure 91.

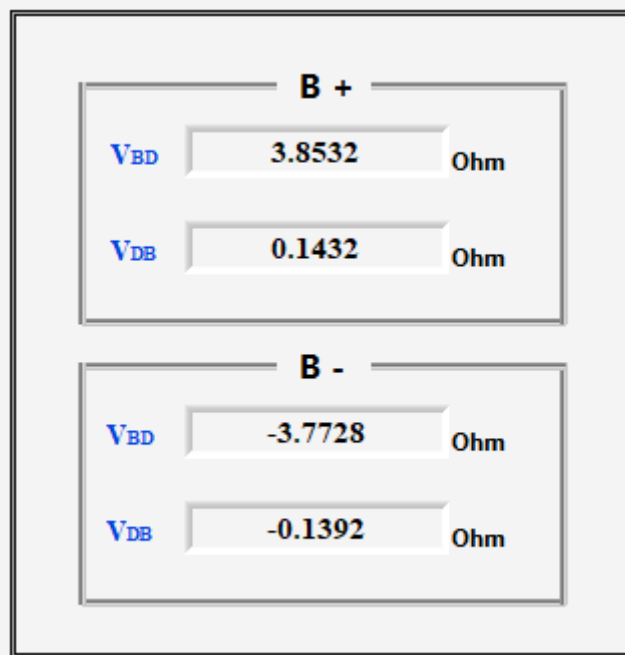
Block diagram for plotting $V - I$ and $V - t$ graph



V – I graphs plotted from Table 6 were used to obtain the average resistance of the semiconductor sample. The resistance from all the switched permutations was taken as absolute and then averaged. The front panel diagram in Figure 92 shows the obtained resistance values.

Figure 92.

Front panel Showing average resistance for different permutations



The average resistance, the fitted model's weighted mean square error and the elapsed time for data collection and analysis were presented on the front panel shown in Figure 93.

Figure 93.

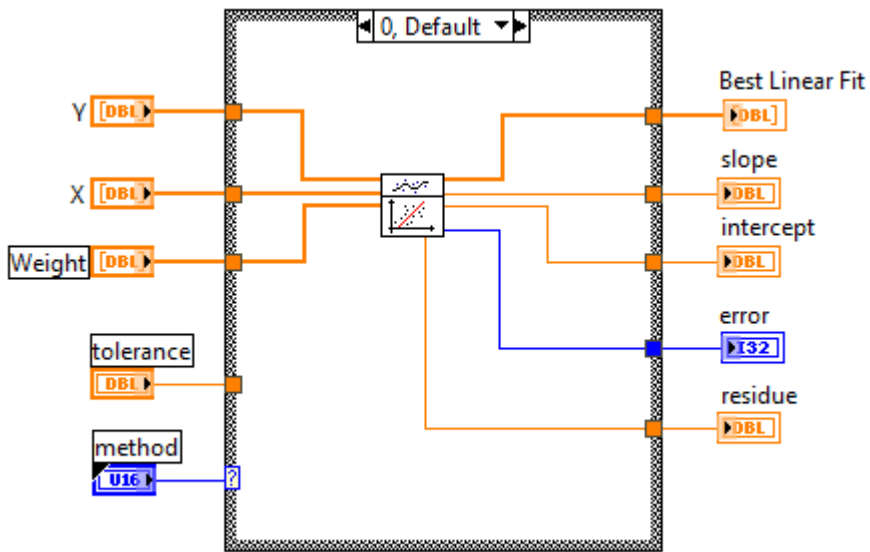


Front panel Showing average resistance and elapsed time

The gradient of the line of best fit represented the resistance of the sample. This was derived from the linear fit VI presented in Figure 94

Figure 94.

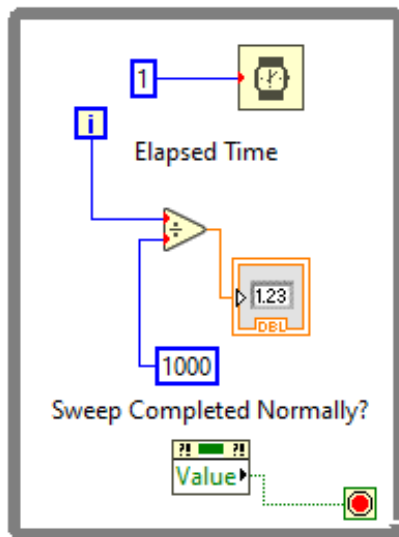
Block diagram for constrained linear fit VI



The VI in Figure 95 was used to generate the elapsed time.

Figure 95.

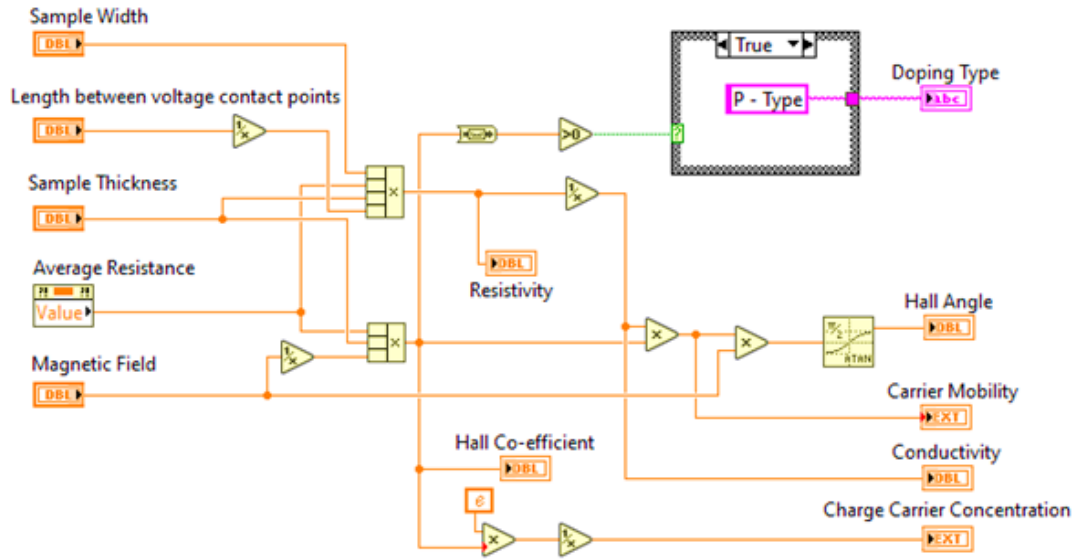
Block diagram for generating the Elapsed time



The average resistance alongside formulas presented in section 2.2.4 was used to calculate the Hall Effect parameters using a VI as illustrated in Figure 96. This was after the graphs were drawn. The doping type was also determined from the Hall coefficient.

Figure 96.

Block diagram for calculating the Hall parameters



The results obtained from the calculations were presented on the front panel as shown in Figure 98 whereas Figure 97 shows the photo of the PC used together with the Keithley Instruments

Figure 97.

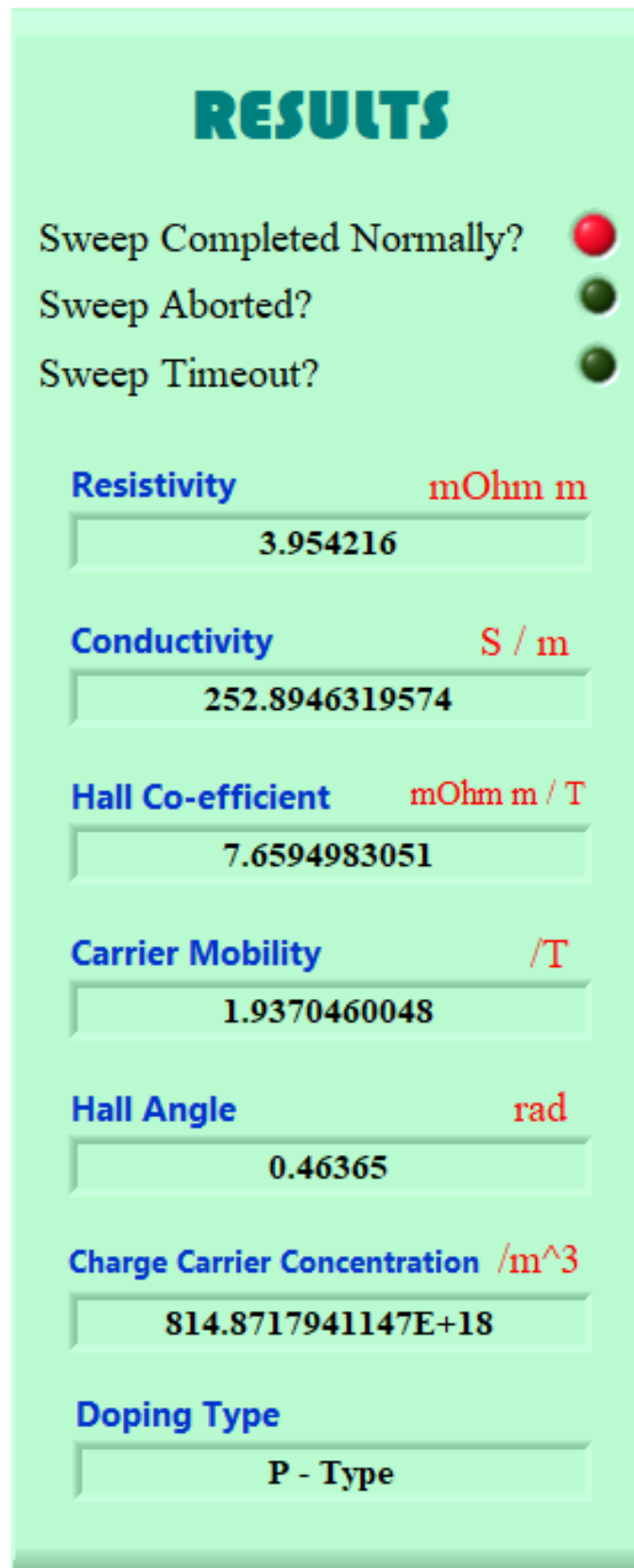
Photo of the PC and Keithley Instruments



Note. Photograph taken by the author.

Figure 98.

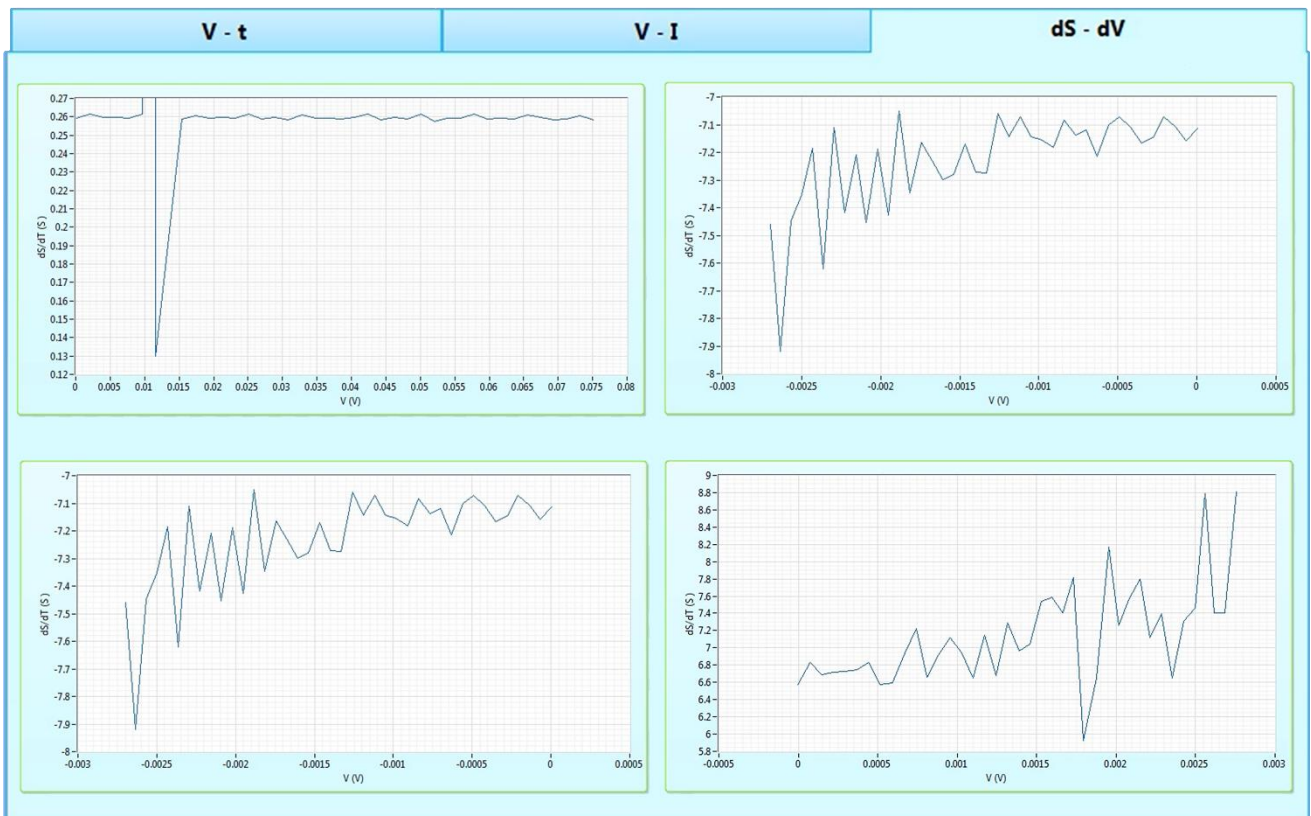
Front panel Showing Hall Effect experiment results



A graph of dI/dV against t was also drawn to cater to non-ohmic scenarios. Ohm's definition of resistance is no longer applicable at the nanoscale because the slope of the I-V curve is no longer a fundamental constant of the substance. Figure 99 shows a front panel of the $dS - t$ graph.

Figure 99.

The front panel of $dS - t$ graphs



4.2.4 Data Validation

Since the data were fitted to a linear model and resistance was obtained from the least square regression line, the resistance was used to validate by checking the percentage errors amongst data collected at different intervals. The difference between an observed value and a true, or accepted value, is measured in percentages. In empirical values, the outcome of data measurement frequently deviates from the true value. Table 8 shows the values obtained at different trials and percentage errors.

Table 8.*Trials and Percentage Errors*

Trial	Resistance (Ω)	Percentage Error
1	1.97711	0.00000%
2	1.98643	0.47140%
3	1.97238	0.07757%
4	1.97405	0.15477%

The Experiment was conducted manually using Keithley models 2182A and 6220 and the obtained data was tabulated as presented in table 9 below.

Table 9.*Manually collected IV data*

I (A)	VBD B+ (V)	VDB B- (V)	VBD B- (V)	VDB B+ (V)
0.0000	0.000000	0.000000	0.000000	0.000000
0.0005	0.002070	-0.000069	-0.001997	0.000071
0.0010	0.003823	-0.000141	-0.003768	0.000143
0.0015	0.005943	-0.000210	-0.005511	0.000220
0.0020	0.007984	-0.000271	-0.007785	0.000286
0.0025	0.009390	-0.000339	-0.009150	0.000369
0.0030	0.011707	-0.000435	-0.010970	0.000456
0.0035	0.011707	-0.000489	-0.012310	0.000537
0.0040	0.015595	-0.000570	-0.014461	0.000598
0.0045	0.018069	-0.000630	-0.016949	0.000695
0.0050	0.018521	-0.000671	-0.018060	0.000733

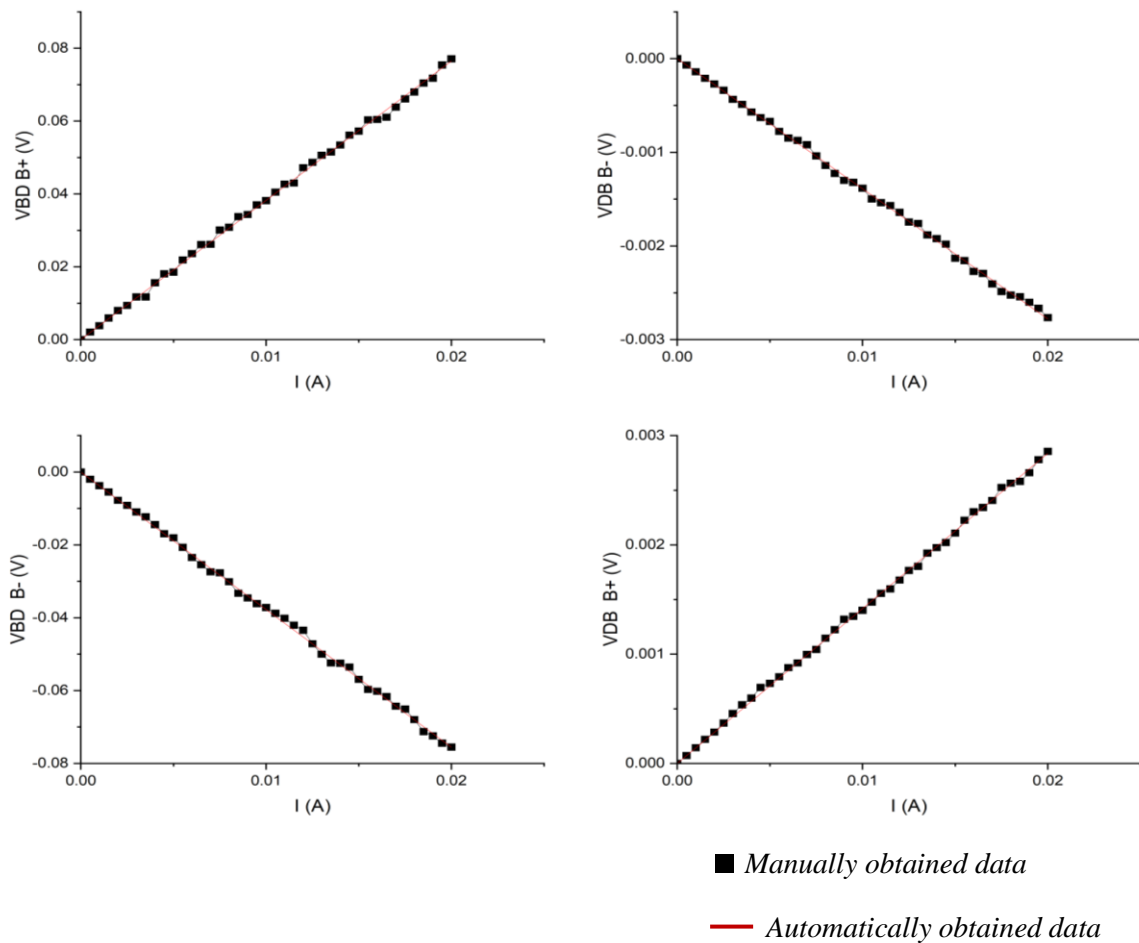
I (A)	VBD B+ (V)	VDB B- (V)	VBD B- (V)	VDB B+ (V)
0.0055	0.021857	-0.000777	-0.020693	0.000793
0.0060	0.023608	-0.000847	-0.023477	0.000876
0.0065	0.026076	-0.000874	-0.025437	0.000919
0.0070	0.026176	-0.000919	-0.027423	0.000996
0.0075	0.030075	-0.001039	-0.027682	0.001043
0.0080	0.030843	-0.001141	-0.030132	0.001146
0.0085	0.033760	-0.001226	-0.033307	0.001224
0.0090	0.034344	-0.001300	-0.034572	0.001319
0.0095	0.036985	-0.001321	-0.036137	0.001346
0.0100	0.038163	-0.001384	-0.037217	0.001401
0.0105	0.040481	-0.001498	-0.038802	0.001476
0.0110	0.042678	-0.001538	-0.040144	0.001556
0.0115	0.042987	-0.001569	-0.042068	0.001596
0.0120	0.047178	-0.001642	-0.043444	0.001678
0.0125	0.048660	-0.001745	-0.047151	0.001766
0.0130	0.050614	-0.001760	-0.050019	0.001803
0.0135	0.051502	-0.001882	-0.052437	0.001924
0.0140	0.053424	-0.001922	-0.052516	0.001975
0.0145	0.056128	-0.001980	-0.053547	0.002021
0.0150	0.057241	-0.002132	-0.056927	0.002107
0.0155	0.060327	-0.002157	-0.059687	0.002225
0.0160	0.060427	-0.002272	-0.060210	0.002303
0.0165	0.061044	-0.002294	-0.061673	0.002341
0.0170	0.063831	-0.002405	-0.064295	0.002406

I (A)	VBD B+ (V)	VDB B- (V)	VBD B- (V)	VDB B+ (V)
0.0175	0.066088	-0.002487	-0.065092	0.002525
0.0180	0.067977	-0.002525	-0.067982	0.002564
0.0185	0.070439	-0.002542	-0.071267	0.002580
0.0190	0.071767	-0.002601	-0.072451	0.002660
0.0195	0.075405	-0.002666	-0.074460	0.002779
0.0200	0.077086	-0.002765	-0.075533	0.002855

VI graphs for the above data were drawn alongside the data obtained automatically by the LabVIEW application and analyzed using the OriginPro application package. The graphs are collated in Figure 100 below.

Figure 100.

Manually obtained vs automatically obtained VI Data Graphs



The line of best fit was drawn using the least square method. The analysis was derived aftermath and is presented in Table 10 below.

Table 10.

Manually obtained VI data analysis

Plot	Weight	Intercept	Slope	Residual Sum of Squares	Pearson's r	R-Square (COD)	Adj. R-Square
VDB B+	No Weighting	$0 \pm --$	3.82505 ± 0.01106	2.71×10^{-5}	0.99983	0.99967	0.99966
VDB B-	No Weighting	$0 \pm --$	$-0.13896 \pm 5.04965 \times 10^{-4}$	5.645×10^{-8}	-0.9997	0.99947	0.99946
VDB B-	No Weighting	$0 \pm --$	-3.7776 ± 0.0108	2.584×10^{-5}	-0.9998	0.99967	0.99966
VDB B+	No Weighting	$0 \pm --$	$0.1418 \pm 6.56255 \times 10^{-4}$	9.54×10^{-8}	0.99957	0.99914	0.99912

When the experiment is conducted manually and contrast drawn between the variables, the following data presented in Table 11 were obtained.

Table 11.

Comparison between automated and manually obtained values

Quantity	Automated	Manual	Error (%)
Resistivity ($m\Omega m$)	3.954216	3.941706	0.32
Conductivity (S/m)	252.894632	253.697257	0.32
Hall Co-efficient ($\times 10^{-3} m^3/C$)	7.659498305	7.63526586	0.32
Carrier Mobility ($m^2(vs)^{-1}$)	1.937046005	1.937046005	0.00
Hall Angle (rad)	0.46365	0.46364	0.00
Charge Carrier Concentration ($/m^3$)	8.14872×10^{20}	8.17458×10^{20}	0.32
Resistance (Ω)	1.97711	1.97085	0.32

4.3 Discussions of the Findings

The instruments were able to be configured in readiness for the electrical characterization of Germanium semiconductor film using the Hall Effect method data acquisition, collation, manipulation analysis, and presentation were also achieved. Data input and acquisition were first done then plotting a $V - I$, $V - t$, and $dS - V$. A line of best fit fitted with least square regression was introduced to the $V - I$ graph and its gradient was used to find the resistance of the Germanium sample when placed in between a magnetic field of 258.125mT. The data in Table 6 was then used to calculate the parameters discussed in section 2.2.4. The data was exported in CSV format after computation.

From the number of trials in Table 8, which presents the average resistance from the four permutations, the percentage error in each trial was less than 2% upholding the validity and repeatability of the data obtained (Yousif, 2018).

Very low current values were sourced to minimize temperature changes within the Germanium semiconductor sample. As the temperature rises in different magnetic fields, the Hall coefficient decreases, carrier concentration rises, and Hall mobility drops. (Schroder, 2015; Shiraguppe *et al.*, 2018). A graph of change in conductivity with voltage (differential conductance) was drawn to present the “non-Ohmic” relationship of the $V - I$ graph. This was useful in studying conductance at atomic levels.

At a room temperature of 292.45 K, the Coefficient was measured to be $7.6595 \times 10^{-3} \Omega \text{ m/T}$, and the carrier concentration was measured to be $814.8718 \times 10^{18} \text{ m}^{-3}$, while V_{BD} at B+ was positive indicating that the sample was P -Type. The comparison between the values obtained automatically and manually had an error of 0.32% implying that the automated system is efficient.

CHAPTER FIVE

SUMMARY, CONCLUSIONS, AND RECOMMENDATION

5.1 Introduction

The objective of this thesis was to design LabVIEW-based automated Hall Effect test equipment using a PC, four-point probe, Keithley 6220 Current precision sources, Keithley 7001 switching system, and 2182A Nanovoltmeter for electrical characterization of thin films. The obtained data was to be validated by comparing it with other experimental values and checking the repeatability.

5.2 Summary of Major Findings

Accurate Hall Effect measurements become more crucial as the requirement to characterize thin film semiconductor materials becomes more demanding. A simple, portable computer-aided Hall Effect measurement system for Hall Effect measurements has been designed and made.

5.2.1 Configuration of Interfaces for Keithley Instruments

The configuration system was able to control Keithley models 2182A, 6220, and 7001. Developing the system's data-collecting method required integrating Keithley measurement equipment. It made data collection and analysis more accurate and productive. Keithley instruments are renowned for their precision and dependability, and they can enable users to collect vital information and make defensible decisions when correctly interfaced with the right hardware or software. To guarantee smooth communication and data handling, LabVIEW software and a thoughtful selection of GPIB interfaces were essential and successful.

5.2.2 LabVIEW Virtual Instruments (VIs) and Sub-VIs

A LabVIEW-based VI and SubVIs were coded and compiled to create a simple program to collect, collate and analyze the electrical and electronic characterization of semiconductor samples using the Hall Effect method. The analysis was then exported as a report.

5.2.3 Integration of LabVIEW VIs and Sub-VIs with the Keithley Instruments

An effective combination of data collection and instrument control was created by integrating LabVIEW Virtual Instruments (VIs) and Sub-VIs with Keithley Instruments. Custom measurement and automation systems could be easily created with the help of LabVIEW, a popular graphical programming environment. The complete potential of these instruments for accurate and automatic data gathering and analysis was realized by smoothly integrating LabVIEW VIs and Sub-VIs with Keithley Instruments. Complex measuring procedures could be streamlined because of this interface, which enabled real-time monitoring, control, and data presentation.

5.2.4 Validation of the Automated Hall Effect Apparatus

A Germanium semiconductor thin film sample was fixed at a fabricated four-point probe and then put perpendicularly across two fixed magnets. The data obtained was validated by checking the consistency and repeatability which was affirmative.

5.3 Conclusion

The LabVIEW graphical software IDE provided a platform for creating an application package able to interface with Keithley models 2182A, 6220, and 7100 via the GPIB port. These devices were able to be set up and configured to enable them to communicate with the PC via the LabVIEW IDE.

Additionally, LabVIEW VIs and SubVIs were coded for data analysis and PC presentation as well as data gathering from peripherals. A thin-film sample's resistance, resistivity, conductivity, Hall Coefficient, carrier mobility, Hall Angle, charge carrier concentration, and the type of doping have all been measured using a software-based approach.

At room temperature of 292.45 K, the resistance of a Germanium sample of length 1.00cm, a width of 2.00cm, and 1.00mm thick was found to be 1.97711 Ω when placed perpendicularly across a magnetic field of 258.125mT. It yielded a conductivity of 252.8946 Sm^{-1} , a resistivity of 3.9542m Ωm , A Hall Co-efficient of $7.6595 \times 10^{-3} \text{ m}^3/\text{C}$, a carrier concentration of $8.1487 \times 10^{22} \text{ m}^{-3}$, a Hall angle of 0.4637 rad, a carrier mobility of $1.9370 \text{ m}^2(\text{vs})^{-1}$ and a doping type of P-type.

The concentration of the charge carriers in the sample was 8.1487×10^{22} electrons per cubic meter and an R_H of 7.6595 m Ω m/T. The experimental values obtained and provided in section 2.2.5.3 have been determined to be consistent with the behaviour of the measured carrier concentration. As reported by Nash (2018), since the carrier capacity is connected to sample manufacturing and is dependent on the material used to make the germanium, there is no board to compare this to. However, the comparison between the automated generated data and the manually done experimental data had insignificant differences which strongly implies that the developed system is operating properly.

From these measurements, it is concluded that an automated system offering a simple, effective, and reliable method for thin film Hall Effect electrical characterization can be developed, assembled and built.

5.4 Recommendation

5.4.1 Recommendation for Policy and Practice

One of the most important steps toward improving product quality, guaranteeing safety, and expediting testing processes is the recommendation of automated test equipment (ATE) for policy and practice in numerous industries. Unmatched benefits from ATE include improved efficacy, reliability, and precision in the testing and assessment of electronic parts, apparatus, and systems. To preserve compliance with safety and performance laws, minimize production faults, and enforce quality control, legislators should support the incorporation of ATE into industry standards and regulatory frameworks. Moreover, adopting ATE can help practitioners in a variety of industries, such as electronics, automotive, aerospace, and healthcare, enhance testing methods, save time, and reduce human error. Organizations can raise their standards for product quality, cost-effectiveness, and, eventually, customer happiness by putting ATE into practice.

5.4.2 Recommendations for Further Research

To improve the outlook, output, and efficiency of the measuring developed system, the following propositions are recommended.

- i. Concentrating more on the Internet of Things (IoT)-based instrument control and fault diagnosis, prophetic and prescriptive examination, and database management system-based report production for query-based observation.
- ii. As the thin film resistance is measured, the sample should be interfaced with a computer for thermocouple temperature measurements and control. This would enhance the outcomes and further automate the system by monitoring and analyzing temperature changes in situ.

- iii. The Keithley Instruments and an electromagnet should be controlled by the same computer that was used for the Hall Effect measurement so that the computer and all the peripherals function as a single, unified system. A sweep of magnetic field strength would be achieved by this.

REFERENCES

- Agarwal, T. (2020). Hall Effect : Principle, Derivation, and Its Applications. *EIProCus - Electronic Projects for Engineering Students*. <https://www.elprocus.com/hall-effect-theory-and-its-applications>.
- Agumba, J., Karimi, P., Okumu, J., & Njoroge, W. (2011). Design and Fabrication of a simple four-point probe system for electrical characterization of thin films. *International Journal Of Current Research*.
- Alomari, S. A., Sumari, P., & Taghizadeh, A. (2011). A comprehensive study of wireless communication technology for the future mobile devices. *European Journal of Scientific Research*, 60(4), pg 583-591.
- Angrisani, L., Bonavolonta, F., D'Arco, M., & Liccardo, A. (2020). A flexible remote laboratory with programmable device under test. *Measurement*, 156.
- Anjum, S., Shaheen, S., Awan, M., & Zia, R. (2019). Effect of various surfactants on optical and electrical properties of Cu⁺ 2-doped ZnS semiconductor nanoparticles. *Applied Physics A*, 125(4), pg 1-10.
- Anwar, U., Khan, S. A., & Ali, A. (2015). Digital speedo meter.
- Averna. (2023). Automated Test Equipment | Averna Technologies. <https://www.averna.com/en/solutions/automated-test-solutions/automated-test-equipment>.
- Balaji, B. A., Sasikumar, S., & Ramesh, K. (2021). SCPI-based integrated test and measurement environment using LabVIEW. *IOP Conference Series: Materials Science and Engineering*,
- Bestwick, A., Fox, E., Kou, X., Pan, L., Wang, K. L., & Goldhaber-Gordon, D. (2015). Precise quantization of the anomalous Hall effect near zero magnetic field. *Physical review letters*, 114(18), 187201.
- Bhavsar, T. (2014). Hall Effect – Principle, Theory, Formula, Applications & FAQs. <https://easyelectronics.co.in/hall-effect>.
- Bishop, R. H. (2015). *Learning with LabVIEW*. Pearson.
- Bitter, R., Mohiuddin, T., & Nawrocki, M. (2017). *LabVIEW™ Advanced Programming Techniques*. CRC press.
- Boubaker, O. (2011). National Instruments® LabVIEW (TM): Ultimate Software for Engineering Education. Proceedings of the International Conference on Frontiers in Education: Computer Science and Computer Engineering (FECS),

- Bress, T., & Hamilton, B. A. (2013). *Effective LabVIEW Programming*.
https://www.researchgate.net/publication/331408353_Effective_LabVIEW_Programming.
- Britannica. (n.d). germanium | Properties, Uses, & Facts.
https://www.britannica.com/science/germanium?utm_source=pj-affiliate&utm_medium=pj&utm_campaign=kids-pj&clickId=4094462271.
- Cai, W., Wang, B., & Zhang, S. (2017). Remote Control and Data Acquisition of Multiple Oscilloscopes Using LabVIEW. In *2017 International Conference on Computer Technology, Electronics and Communication (ICCTEC)* (pp. pg 920–924). IEEE.
<https://doi.org/10.1109/icctec.2017.00203>
- Cervantes, A. d. J. R., Gonzalez, E. R., & Alvarez, J. C. (2018). Development and automation of a thermoelectric characterization system. 2018 International Conference on Mechatronics, Electronics and Automotive Engineering (ICMEAE),
- Chen, K.-Y., Shah, R. C., Huang, J., & Nachman, L. (2017). Mago: Mode of transport inference using the hall-effect magnetic sensor and accelerometer. *Proceedings of the ACM on Interactive, Mobile, Wearable and Ubiquitous Technologies*, 1(2), 1-23.
- Chen, N. (2021). Semiconductor Thin Films for Information Technology. *Inorganic and Organic Thin Films: Fundamentals, Fabrication and Applications*, 1, pg 257-284.
- Choi, H. H., Paterson, A. F., Fusella, M. A., Panidi, J., Solomeshch, O., Tessler, N., Heeney, M., Cho, K., Anthopoulos, T. D., & Rand, B. P. (2020). Hall effect in polycrystalline organic semiconductors: The effect of grain boundaries. *Advanced Functional Materials*, 30(20), 1903617.
- Choudhary, S. K., Jadoun, R. S., Kumar, A., & Rao, D. K. (2018). Role Of Automation In Manufacturing Industries *International Journal of Creative Research Thoughts (IJCRT)*(April 6-7).
- Cigoy, D. (2010). Troubleshoot low-voltage measurement problems - EDN. *EDN*.
<https://www.edn.com/troubleshoot-low-voltage-measurement-problems>.
- Coito, F. P., Luís Brito. (2008). A remote laboratory environment for blended learning. Proceedings of the 1st international conference on Pervasive Technologies Related to Assistive Environments,
- Cunningham, A. (2014). A brief history of USB, what it replaced, and what has failed to replace it. <https://arstechnica.com/gadgets/2014/08/a-brief-history-of-usb-what-it-replaced-and-what-has-failed-to-replace-it>.

- Curtolo, D. C., Friedrich, S., & Friedrich, B. (2017). High purity germanium, a review on principle theories and technical production methodologies. *Journal of Crystallization Process and Technology*, 7(4), pg 65-84.
- Dashveenjit, K. (2021). The semiconductor chips conundrum - from chip draught to chip glut. <https://techwireasia.com/2021/08/semiconductor-chips-conundrum-from-a-chip-draught-to-chip-glut>.
- Deen, M. J., & Pascal, F. (2017). Electrical characterization of semiconductor materials and devices. In *Springer Handbook of Electronic and Photonic Materials* (Vol. 20). Springer.
- Desjardin, L. (2013). SCPI programming: Strengths and weaknesses - EDN. *EDN*. <https://www.edn.com/scpi-programming-strengths-and-weaknesses>.
- Du, J., Li, W., & Guo, J. (2017). Design of LabVIEW based general data acquisition system. 2017 IEEE 2nd Information Technology, Networking, Electronic and Automation Control Conference (ITNEC),
- Gaj, J. A. (2011). Hall Effect - an overview | ScienceDirect Topics. <https://doi.org/10.1016/b978-1-4377-7867-0.00005-2>
- Garnica, B. S. A., Marius, K., & Sergej, F. (2019). Automatic Micro-Robotic Identification and Electrical Characterization of Graphene. *Micromachines*, 10(12), pg 870.
- Germanium | Encyclopedia (2018). <https://www.encyclopedia.com/science-and-technology/chemistry/compounds-and-elements/germanium>.
- Germanium Windows for Thermal Imaging and Night Vision. (2021). *Knight Optical Ltd*. <https://optics.org/products/P000023291>.
- GPIB Messages. (2020). <https://www.ni.com/en-za/support/documentation/supplemental/06/gpib-messages.html>.
- Green, R. (2011). Hall Effect Measurements in Materials Characterization | Tektronix. <https://www.tek.com/en/documents/whitepaper/hall-effect-measurements-materials-characterization>.
- Groover, M. P. (2014). *Fundamentals of modern manufacturing: materials, processes, and systems* (4th Edition ed.). John Wiley & Sons.
- H, F. (n.d). The Hall Effect. *Electronic Materials*. https://www.tf.uni-kiel.de/matwis/amat/elmat_en/kap_1/backbone/r1_3_4.html.
- Hachman, M. (2019, March 4, 2019). The new USB4 spec promises a lot: Thunderbolt 3 support, 40Gbps bandwidth, and less confusion. *PCWorld*.

- Hadley, P. (n.d). Computer supported measurement techniques. <http://lampx.tugraz.at/~hadley/semi/ch9/9.php>.
- Hat, R. (2019). What is an IDE? <https://www.redhat.com/en/topics/middleware/what-is-ide>.
- Hauer, F. (2020). Labforward & SpreadJS. <https://www.grapecity.com/case-studies/20200113-LabFolder-case-study>.
- Herrera, A. (2022). Robotic Process Automation Optimizes Test Instrumentation - EE Times Asia. <https://www.eetasia.com/robotic-process-automation-optimizes-test-instrumentation>.
- Hishiyama, Y., & Inagaki, M. (2013). Magnetoresistance - an overview | ScienceDirect Topics. <https://doi.org/10.1533/9780857093493.1.51>
- Hookway, B. (2014). *Interface*. MIT Press. https://books.google.co.ke/books?id=BQM_AwAAQBAJ.
- Houlihan, S., & Kalman, A. (2014). Applying Standard Commands for Programmable Instruments (SCPI) to CubeSats.
- HP. (2019). What are Computer Drivers? *HP*. <https://www.hp.com/us-en/shop/tech-takes/what-are-computer-drivers>.
- IEEE-488 GPIB Communications. (2020). https://magna-power.com/assets/docs/html_arx/common-magnadc/operation_computer_programming_gpib.html.
- Jamal, D. F., Pascal. (2017). Electrical Characterization of Semiconductor Materials and Devices. 20(Springer Handbook of Electronic and Photonic Materials). <https://www.springerprofessional.de/en/electrical-characterization-of-semiconductor-materials-and-devic/15108326>.
- Karsenty, A. (2020). A comprehensive review of integrated Hall effects in macro-, micro-, nanoscales, and quantum devices. *Sensors*, 20(15), 4163.
- Keithley. (2004). Model 6220 DC Current Source Model 6221 AC and DC Current Source User's Manual. <https://www.tek.com/en/product-series/ultra-sensitive-current-sources-series-6200-manual/model-6220-dc-current-source-model>.
- Keithley. (2020). Model 2107-4 and Model 2107-30 Low-Thermal Input Cables with Spade Lugs. <https://www.tek.com/en/keithley-accessories/cables-manual/model-2107-4-and-model-2107-30-low-thermal-input-cables-spade>.
- Keithley. (2022a). Keithley 7001 80-Channel 2-Slot Switch. <https://www.testequipmentdepot.com/keithley/switching-control-daq-systems/80-channel-switch-system-control-mainframe-7001.htm>.

- Keithley. (2022b). Keithley Nanovoltmeter Model 2182A. <https://www.tek.com/en/products/keithley/low-level-sensitive-and-specialty-instruments/nanovoltmeter-model-2182a>.
- Kelley, K. (2023). Five test automation challenges and how to overcome them - Testlio. *Testlio*. <https://testlio.com/blog/test-automation-challenges>.
- Khalifa, M., Amhedb, A. H., & Al Sharqawi, M. (2021). Position Control of Real Time DC Motor Using LabVIEW. *Journal of Robotics and Control (JRC)*, 2(5), pg 342-348.
- Leadley, D. (2011). Hall Effect Measurements. <https://warwick.ac.uk/fac/sci/physics/current/postgraduate/regs/mpagswarwick/ex5/techniques/electronic/hall-effect>.
- Lekdim, A., Sixdenier, F., Scorretti, R., & Grihe, A. (2022). Reluctance network model of open-loop Hall-effect current sensor for circuit-type simulation software analyses. *IEEE Sensors Journal*, 22(11), 10246-10255.
- Li, J., Wang, Y., & Ba, D. (2012). Characterization of semiconductor surface conductivity by using microscopic four-point probe technique. *Physics Procedia*, 32, pg 347-355.
- Libretexts. (2021a). Electrical Conductivity and Resistivity. *Chemistry LibreTexts*. [https://chem.libretexts.org/Bookshelves/Inorganic_Chemistry/Map%3A_Inorganic_Chemistry_\(Housecroft\)/06%3A_Structures_and_energetics_of_metallic_and_ionic_solids/6.08%3A_Bonding_in_Metals_and_Semiconductors/6.8A%3A_Electrical_Conductivity_and_Resistivity](https://chem.libretexts.org/Bookshelves/Inorganic_Chemistry/Map%3A_Inorganic_Chemistry_(Housecroft)/06%3A_Structures_and_energetics_of_metallic_and_ionic_solids/6.08%3A_Bonding_in_Metals_and_Semiconductors/6.8A%3A_Electrical_Conductivity_and_Resistivity).
- Libretexts. (2021b). I. P-Type, N-Type Semiconductors. *Engineering LibreTexts*. [https://eng.libretexts.org/Bookshelves/Materials_Science/Supplemental_Modules_\(Materials_Science\)/Solar_Basics/D._P-N_Junction_Diodes/I._P-Type%2C_N-Type_Semiconductors](https://eng.libretexts.org/Bookshelves/Materials_Science/Supplemental_Modules_(Materials_Science)/Solar_Basics/D._P-N_Junction_Diodes/I._P-Type%2C_N-Type_Semiconductors).
- Liscouski, J. (2015). *Computerized Systems in the Modern Laboratory: A Practical Guide*. https://www.researchgate.net/publication/275351757_Computerized_Systems_in_the_Modern_Laboratory_A_Practical_Guide.
- Liu, J., & Dai, X. (2020). Anomalous Hall effect, magneto-optical properties, and nonlinear optical properties of twisted graphene systems. *npj Computational Materials*, 6(1), 57.
- Lott, C. (2022). Save Money And Have Fun Using IEEE-488. <https://hackaday.com/2022/01/31/save-money-and-have-fun-using-ieee-488>.
- Lughi, V. (2012). Optical and Electronic Properties. In *Encyclopedia of Nanotechnology* (pp. pg 1924–1932). Springer. https://doi.org/10.1007/978-90-481-9751-4_275

- Manojkumar, P., Suresh, M., Ayub Ahmed, A. A., Panchal, H., Rajan, C. A., Dheepanchakkravarthy, A., Geetha, A., Gunapriya, B., Mann, S., & Sadasivuni, K. K. (2022). A novel home automation distributed server management system using Internet of Things. *International Journal of Ambient Energy*, 43(1), 5478-5483.
- Mary, M. (2022). What Is an Instrument Driver? <https://www.wise-geek.com/what-is-an-instrument-driver.htm>.
- McCain, A. (2022). How Fast Is Technology Advancing? [2022]: Growing, Evolving, And Accelerating At Exponential Rates – Zippia. <https://www.zippia.com/advice/how-fast-is-technology-advancing>.
- Melcher, F., & Buchholz, P. (2014). Germanium. *Critical metals handbook*, pg 177-203.
- Miccoli, I., Edler, F., Pfnür, H., & Tegenkamp, C. (2015). The 100th anniversary of the four-point probe technique: the role of probe geometries in isotropic and anisotropic systems. *Journal of Physics: Condensed Matter*, 27(22).
- Munro, D. (2019). DIY MEMS.
- Nash, S. (2018). Characterizing Germanium with the Hall Effect. *Department of Physics*(The College of Wooster, Wooster, Ohio 44691, USA). https://physics-archive.wooster.edu/JrIS/Files/Web_Article_Nash.pdf.
- Nelson, J. (2015). 5 Ways Automation Improves Quality. <https://info.panelshop.com/blog/5-ways-automation-improves-quality>.
- NI-VISA. (2015). NI-VISA .NET Library - National Instruments. <https://www.ni.com/en-za/support/documentation/supplemental/15/national-instruments-visa--net-library.html>.
- Onwujiariri, T. (2020). Significance of the Hall Effect On SemiConductors. *GulpMatrix*. <https://gulpmatrix.com/significance-hall-effect-semiconductors>.
- PHYWE. (n.d). Hall effect in n- and p-germanium. https://www.phywe.com/experiments-sets/university-experiments/hall-effect-in-n-and-p-germanium_11052_12085.
- Portolan, M. (2019). Automated testing flow: The present and the future. *IEEE Transactions on Computer-Aided Design of Integrated Circuits and Systems*, 39(10), pg 2952-2963.
- PyVISA. (2022). PyVISA: Control your instruments with Python. <https://pyvisa.readthedocs.io/en/latest>.
- Ray, P. P. (2017). A survey on visual programming languages in internet of things. *Scientific Programming*, 2017.
- Research, Z. M. (2022). Global Automated Test Equipment Market Projected To Surpass Around US\$ 4.82 Billion By The End Of 2025. <https://www.zionmarketresearch.com/news/automated-test-equipment-industry>.

- Rohde, GmbH, S., & KG, C. (2022). 1. Basics of Instrument Remote Control. https://www.rohde-schwarz.com/us/driver-pages/remote-control/automation-by-remote-control-step-by-step_231238.html.
- Romanchik, D. (2015). Interfaces for Computer-Controlled Test Systems. *All About Circuits*. <https://www.allaboutcircuits.com/technical-articles/interfaces-for-computer-controlled-test-systems>.
- Ross, R. (2016). Facts About Germanium. *Livescience*. <https://www.livescience.com/29520-germanium.html>.
- Royce, B. S. H., Niculin, A., & Batke, P. (2002). Germanium. *The Structure and Properties of Engineering Materials*. <https://www.princeton.edu/~maelabs/mae324/glos324/germanium.htm>.
- Sahana. (2021). Types of Computer Buses | Meaning, Components, Functions, Structure. *Classmate4u*. <https://www.classmate4u.com/types-of-computer-buses>.
- Saputra, M. I., Sulistiyanti, S. R., Purwiyanti, S., & Murdika, U. (2020). Design of Prototype Measuring Motor Vehicles Velocity Using Hall Effect Sensor Series A-1302 based On Arduino Mega2560. 2020 2nd International Conference on Industrial Electrical and Electronics (ICIEE),
- Sarah, R. (2022, Feb 14,). *Semiconductor Industry Association*. Retrieved Apr 4 from <https://www.semiconductors.org/global-semiconductor-sales-units-shipped-reach-all-time-highs-in-2021-as-industry-ramps-up-production-amid-shortage/>
- Schilling, R., & Steinmetz, F. (2016). *USB devices phoning home*. BoD—Books on Demand.
- Schindler, L. A., Burkholder, G. J., Morad, O. A., & Marsh, C. (2017). Computer-based technology and student engagement: a critical review of the literature. *International journal of educational technology in higher education*, 14(1), pg 1-28.
- Schroder, D. K. (2015). *Semiconductor material and device characterization*. John Wiley & Sons.
- Shalf, J. (2020). The future of computing beyond Moore's Law. *Philosophical Transactions of the Royal Society A*, 378(2166), 20190061.
- Shiraguppe, R., shiraguppe, K., & Shiraguppe, i. (2018). TEMPERATURE DEPENDENCE OF HALL EFFECT [Journal Article]. *International Journal of Advance Research in Science and Engineering*, 07(Special Issue No.01,), pg 652 - 656.
- Sivaranjith. (2018). IEEE 488 - Introduction | Instrumentation and Control Engineering. <https://automationforum.co/ieee-488-introduction>.

- Staron, M., Meding, W., Karlsson, G., & Nilsson, C. (2011). Developing measurement systems: An industrial case study. *Journal of Software Maintenance*, 23(2), 89–107. <https://doi.org/10.1002/smr.470>
- Sui, K., Feng, X., Hou, Y., Zhang, Q., Qi, S., Wang, Y., & Wang, P. (2017). Glass-clad semiconductor germanium fiber for high-speed photo detecting applications. *Opt. Mater. Express, OME*, 7(4), pg 1211–1219. <https://doi.org/10.1364/ome.7.001211>
- Survey, U. S. G. (2020). Mineral commodity summaries 2020. *Mineral Commodity Summaries*. <https://doi.org/10.3133/mcs2020>
- Technologies, A. (2009). Simplified PC Connections for GPIB Instruments. pg 9.
- Technologies, K. (2014). Simplified PC Connections for GPIB Instruments. *Application Note*. <https://www.keysight.com/zz/en/assets/7018-01098/application-notes/5988-5897.pdf>.
- Techopedia. (2020). Universal Serial Bus (USB). *Techopedia*. <https://www.techopedia.com/definition/2320/universal-serial-bus-usb>.
- Teja, R. (2021). 16 Types of Computer Ports and Their Functions. *Electronics Hub*. <https://www.electronicshub.org/types-of-computer-ports>.
- Tektronix. (2023). What Are The Differences Between Device Drivers And Instrument Drivers? <https://www.tek.com/en/support/faqs/what-are-differences-between-device-drivers-and-instrument-drivers>.
- Thin Film Material Market. (2022). *Global Overview and Forecast (2022-2029) by Deposition Process, Types, Applications, and Region*. <https://www.maximizemarketresearch.com/market-report/global-thin-film-material-market/72328>.
- Tian, J., Scaife, N., Kumar, D., Bailey, M., Bates, A., & Butler, K. (2018). SoK:" Plug & Pray" today—understanding USB insecurity in versions 1 through C. 2018 IEEE Symposium on Security and Privacy (SP),
- Tunyagi, A., Kandrai, K., Fülöp, Z., Kapusi, Z., & Simon, A. (2018). Friction coefficient determination by electrical resistance measurements. *Physics Education*, 53(3), 035028.
- Using VISA in LabVIEW - NI. (2022). https://www.ni.com/docs/en-US/bundle/labview/page/lvmeasconcepts/visa_in_labview.html.
- Valladares, S., Tasiguano, C., Narváez, F., Acurio, E., & Lascano, L. (2019). Design and Implementation of an Automatic System for Dielectric Characterization of Ceramic Materials. *LACCEI, Inc*.

- Villarreal, R., & Ivón, A. (2022). NI-VISA Write: basic exercises. *Virtual Instrumentation. Session 6. VISA R/W*.
- Wang, C.-R., Tung, J.-C., Sankar, R., Hsieh, C.-T., Chien, Y.-Y., Guo, G.-Y., Chou, F., & Lee, W.-L. (2013). Magnetotransport in copper-doped noncentrosymmetric BiTeI. *Physical Review B*, 88(8).
- WatElectronics. (2022). IEEE 488 Bus : Basics, Architecture, Advantages and Applications. *WatElectronics*. <https://www.watelectronics.com/ieee-488-bus>.
- What is Hall Effect? (2020). <https://electronicscoach.com/hall-effect.html>.
- Wittmann, R. (2011). Miniaturization Problems in CMOS Technology: Investigation of Doping Profiles and Reliability. *Semiconductor Doping Technology*. <https://www.iue.tuwien.ac.at/phd/wittmann/node7.html>.
- Yousif, H. (2018). How to validate experimental data? <https://www.researchgate.net/post/How-to-validate-experimental-data/5af424c68272c9a8e44f41b8/citation/download>.
- Zhang, F., Wang, G., Ye, J., & Zeng, Q. (2013). Remote Control Techniques to the Digital Storage Oscilloscope by GPIB and VISA. *Telkomnika Indonesian Journal of Electrical Engineering*, 11(4), pg 1835-1840.

APPENDIX I: IPGS INTRODUCTORY LETTER



**KABARAK UNIVERSITY
INSTITUTE OF POSTGRADUATE STUDIES
OFFICE OF THE DIRECTOR**

Private Bag - 20157
KABARAK, KENYA
<http://kabarak.ac.ke/institute-postgraduate-studies/>

Tel: 0773265999
E-mail: directorpostgraduate@kabarak.ac.ke

26th September 2022

The Chairman
Research and Ethics Committee (KUREC)
Kabarak University

Dear Sir,

RE: OREGA K. OWINO - GMP/M/0286/04/18

The above named is a candidate at Kabarak University pursuing Masters in Physics. He is carrying out a research entitled "*Development of an Automated Hall Effect Experimentation Method for Electrical Characterization of Thin Films*".

The student has defended his proposal and has been authorised to proceed with field research.

Kindly provide the KUREC clearance to enable the student obtain NACOSTI research permit.

Thank you

DR. WILSON O. SHITANDI
DIRECTOR, POSTGRADUATE STUDIES



Kabarak University Moral Code

*As members of Kabarak University family, we purpose at all times and in all places, to set apart in one's heart,
Jesus as Lord. (1 Peter 3:15)*



Kabarak University is ISO 9001:2015 Certified

APPENDIX II: KUREC LETTER



KABARAK UNIVERSITY RESEARCH ETHICS COMMITTEE

Private Bag - 20157
KABARAK, KENYA
Email: kurec@kabarak.ac.ke

Tel: 254-51-343234/5
Fax: 254-051-343529
www.kabarak.ac.ke

OUR REF: KABU01/KUREC/001/52/11/22

Date: 12-11-2022

OREGA KIPLAGAT OWINO,
GMP/M/0286/04/18
Kabarak University,

Dear Orega,

**RE: DEVELOPMENT OF AN AUTOMATED HALL EFFECT EXPERIMENTATION
METHOD FOR ELECTRICAL CHARACTERIZATION OF THIN FILMS.**

This is to inform you that **KUREC** has reviewed and approved your above research proposal. Your application approval number is **KUREC-521122**. The approval period is **12/11/2022 – 12/11/2023**.

This approval is subject to compliance with the following requirements:

- i. All researchers shall obtain an introduction letter to NACOSTI from the relevant head of institutions (Institute of postgraduate, School dean or Directorate of research)
- ii. The researcher shall further obtain a RESEARCH PERMIT from NACOSTI before commencement of data collection & submit a copy of the permit to **KUREC**.
- iii. Only approved documents including (informed consents, study instruments, MTA Material Transfer Agreement) will be used
- iv. All changes including (amendments, deviations, and violations) are submitted for review and approval by **KUREC**;
- v. Death and life-threatening problems and serious adverse events or unexpected adverse events whether related or unrelated to the study must be reported to **KUREC** within 72 hours of notification;
- vi. Any changes, anticipated or otherwise that may increase the risk(s) or affected safety or welfare of study participants and others or affect the integrity of the research must be reported to **KUREC** within 72 hours;
- vii. Clearance for export of biological specimens must be obtained from relevant institutions and submit a copy of the permit to **KUREC**;
- viii. Submission of a request for renewal of approval at least 60 days prior to expiry of the approval period. Attach a comprehensive progress report to support the renewal and;
- ix. Submission of an executive summary report within 90 days upon completion of the study to **KUREC**

Sincerely,


KABARAK UNIVERSITY
INSTITUTIONAL RESEARCH ETHICS COMMITTEE
14 NOV 2022
APPROVED
P.O. PRIVATE BAG - 20157, KABARAK

Prof. Jackson Kitetu PhD.
KUREC-Chairman

Cc Vice Chancellor
DVC-Academic & Research
Registrar-Academic & Research
Director-Research Innovation & Outreach
Institute of Post Graduate Studies

*As members of Kabarak University family, we purpose at all times and in all places, to set apart in one's heart, Jesus as Lord.
(1 Peter 3:15)*



Kabarak University is ISO 9001:2015 Certified

APPENDIX III: NACOSTI PERMIT


REPUBLIC OF KENYA
 Ref No: **373323**
RESEARCH LICENSE

This is to Certify that Mr., Orega K Owino of Kabarak University, has been licensed to conduct research as per the provision of the Science, Technology and Innovation Act, 2013 (Rev.2014) in Uasin-Gishu on the topic: Development of an automated Hall Effect Experimentation method for electrical characterization of thin films for the period ending : 06/December/2023.
License No: NACOSTI/P/22/22391
373323
Applicant Identification Number

Director General
NATIONAL COMMISSION FOR SCIENCE, TECHNOLOGY & INNOVATION
Verification QR Code

NOTE: This is a computer generated License. To verify the authenticity of this document, Scan the QR Code using QR scanner application.
See overleaf for conditions

THE SCIENCE, TECHNOLOGY AND INNOVATION ACT, 2013 (Rev. 2014)
Legal Notice No. 108: The Science, Technology and Innovation (Research Licensing) Regulations, 2014

The National Commission for Science, Technology and Innovation, hereafter referred to as the Commission, was established under the Science, Technology and Innovation Act 2013 (Revised 2014) herein after referred to as the Act. The objective of the Commission shall be to regulate and assure quality in the science, technology and innovation sector and advise the Government in matters related thereto.

CONDITIONS OF THE RESEARCH LICENSE

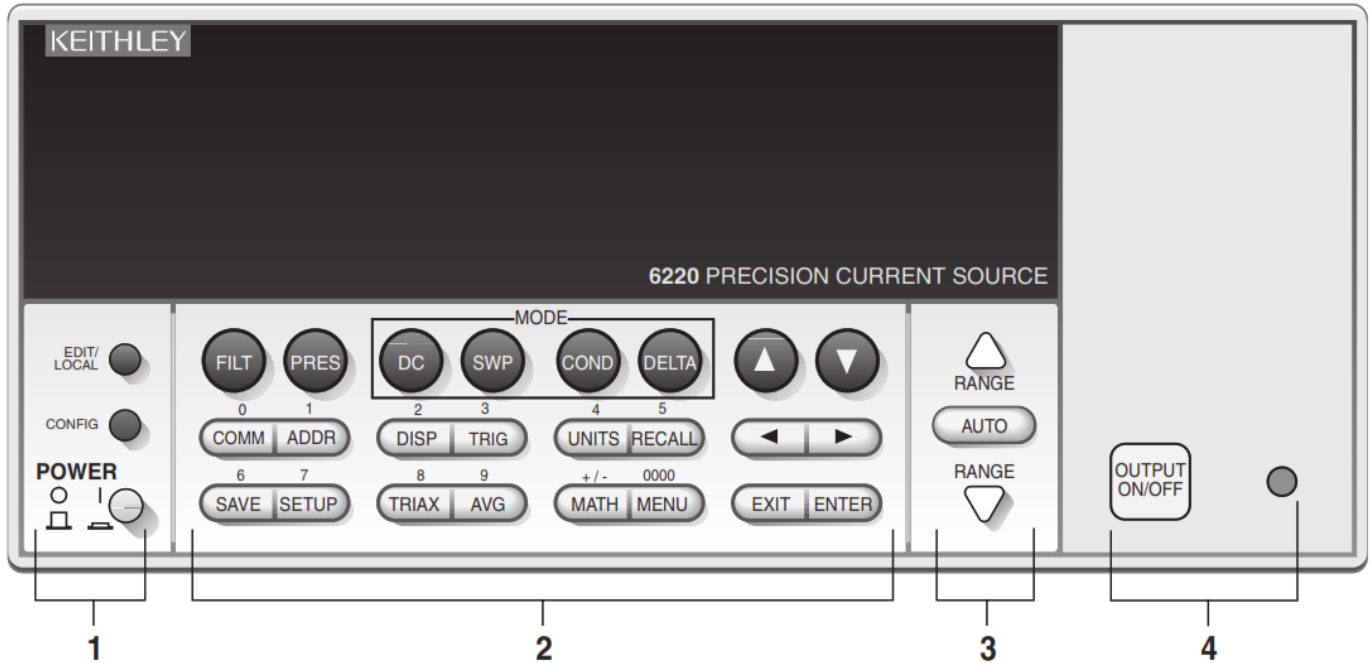
1. The License is granted subject to provisions of the Constitution of Kenya, the Science, Technology and Innovation Act, and other relevant laws, policies and regulations. Accordingly, the licensee shall adhere to such procedures, standards, code of ethics and guidelines as may be prescribed by regulations made under the Act, or prescribed by provisions of International treaties of which Kenya is a signatory to
2. The research and its related activities as well as outcomes shall be beneficial to the country and shall not in any way;
 - i. Endanger national security
 - ii. Adversely affect the lives of Kenyans
 - iii. Be in contravention of Kenya's international obligations including Biological Weapons Convention (BWC), Comprehensive Nuclear-Test-Ban Treaty Organization (CTBTO), Chemical, Biological, Radiological and Nuclear (CBRN).
 - iv. Result in exploitation of intellectual property rights of communities in Kenya
 - v. Adversely affect the environment
 - vi. Adversely affect the rights of communities
 - vii. Endanger public safety and national cohesion
 - viii. Plagiarize someone else's work
3. The License is valid for the proposed research, location and specified period.
4. The license any rights thereunder are non-transferable
5. The Commission reserves the right to cancel the research at any time during the research period if in the opinion of the Commission the research is not implemented in conformity with the provisions of the Act or any other written law.
6. The Licensee shall inform the relevant County Director of Education, County Commissioner and County Governor before commencement of the research.
7. Excavation, filming, movement, and collection of specimens are subject to further necessary clearance from relevant Government Agencies.
8. The License does not give authority to transfer research materials.
9. The Commission may monitor and evaluate the licensed research project for the purpose of assessing and evaluating compliance with the conditions of the License.
10. The Licensee shall submit one hard copy, and upload a soft copy of their final report (thesis) onto a platform designated by the Commission within one year of completion of the research.
11. The Commission reserves the right to modify the conditions of the License including cancellation without prior notice.
12. Research, findings and information regarding research systems shall be stored or disseminated, utilized or applied in such a manner as may be prescribed by the Commission from time to time.
13. The Licensee shall disclose to the Commission, the relevant Institutional Scientific and Ethical Review Committee, and the relevant national agencies any inventions and discoveries that are of National strategic importance.
14. The Commission shall have powers to acquire from any person the right in, or to, any scientific innovation, invention or patent of strategic importance to the country.
15. Relevant Institutional Scientific and Ethical Review Committee shall monitor and evaluate the research periodically, and make a report of its findings to the Commission for necessary action.

National Commission for Science, Technology and
Innovation(NACOSTI),
Off Waiyaki Way, Upper Kabete,
P. O. Box 30623 - 00100 Nairobi, KENYA
Telephone: 020 4007000, 0713788787, 0735404245
E-mail: dg@nacosti.go.ke
Website: www.nacosti.go.ke

APPENDIX IV: KEITHLEY INSTRUMENTS

I. MODEL 6220

a) Front Panel Summary



1. Special keys and power switch:

EDIT/LOCAL Dual function — while in local, EDIT selects the source editing mode.

While in remote, LOCAL cancel the remote mode.

CONFIG Use to configure a function or operation.

POWER Power switch — In position turns 6220 on (I), out position turns it off (O).

2. Function and operation keys:

Top Row

FILT Enables/disables analog filters.

PRES Enables/disables the pre-set source value. Press CONFIG > PRES to set the source value for PRES.

DC	Selects DC source function.
SWP	Arms the sweep function. Press CONFIG > SWP to configure the sweep.
COND	Arms Differential Conductance. Press CONFIG > COND to configure Differential Conductance.
DELTA	Arms Delta. Press CONFIG > DELTA to configure Delta.
△	Increments value.
▽	Decrements value.

Middle Row

COMM	ConFIGures communications: GPIB, RS-232, or Ethernet (6221). Can also press CONFIG > COMM to configure communications.
ADDR	Sets GPIB address.
DISP	Turns off the display. Press LOCAL or DISP to turn the display back on.
TRIG	Starts a sweep, delta, or wave (6221) test, or causes a manual trigger event. Press CONFIG > TRIG to configure triggers.
UNITS	Use to select measurement units for a delta function. Can also press CONFIG > UNITS to select measurement units.
RECALL	Displays buffer readings and statistics. Press CONFIG > RECALL to access the menu to clear the buffer.
◀	Moves cursor (blinking digit or menu item) to the left.
▶	Moves cursor (blinking digit or menu item) to the right.

Bottom Row

SAVE	Saves up to five instrument setups for future recall and selects power-on setup.
SETUP	Restores a default setup (Preset or *RST) or a user-saved setup.

- TRIAX** Configures Triax connector: inner shield and output Low. Can also press CONFIG > TRIAX to configure the Triax connector.
- AVG** Enables/disables the averaging filter. Press CONFIG > AVG to configure the averaging filter.
- MATH** Enables/disables math. Press CONFIG > MATH to configure math.
- MENU** Accesses the main menu for calibration, self-tests, serial numbers, and beeper control.
- EXIT** Cancels selection, backs out of menu structure.
- ENTER** Accepts selection, moves to next choice or exits the menu.

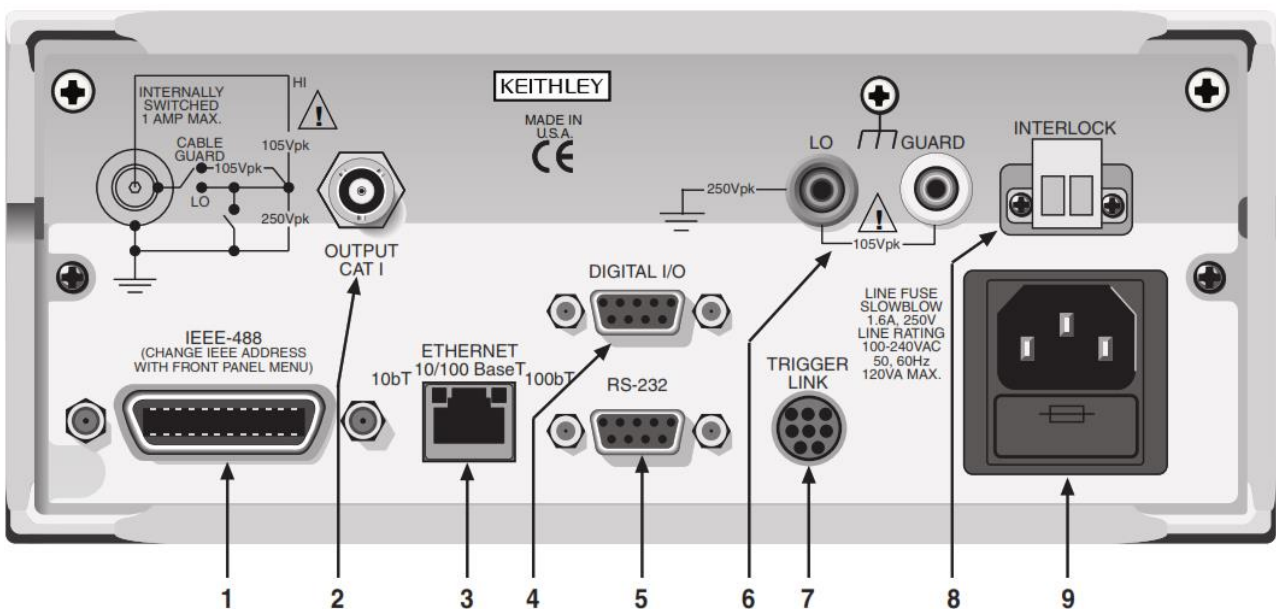
3. Range keys:

- △ and ▽ Dual function — Selects the next higher or lower source range. When in a menu, these keys increment or decrement values.
- AUTO** Enables or disables source autorange.

4. Output control and LED status indicator:

- OUTPUT ON/OFF** Turns source output on or off.
- LED indicator** Turns on when output is on. Blinks if the source goes into compliance.

b) Rear panel Summary



- 1. IEEE-488** Connector for IEEE-488 (GPIB) operation. Use a shielded cable, such as the Model 7006, 7007, or 7008.
- 2. OUTPUT** 3-lug female Triax connector for current source output. Mates to the supplied Triax cable (237-ALG-2). Will also mate to any Triax cable terminated with a 3-slot male Triax connector.
- 3. ETHERNET (6221 only)** RJ45 female connector for Ethernet operation. Use an RJ45 male/male cable for connection. Two status LEDs are located at the top of the connector. These LEDs indicate the status of the Ethernet
- 4. DIGITAL I/O** Male DB-9 connector. Four pins for digital output, one pin for the Start of Test (SOT) trigger, and one for external voltage (VEXT) input.
- 5. RS-232** Female DB-9 connector:
 - For RS-232 operation, use a straight-through (not null modem) DB-9 shielded cable for connection to the PC.
 - For Delta, Pulse Delta, and Differential Conductance, use the supplied serial cable (CA-351) for connections between the Model 622x and the Model 2182/2182A.
- 6. LO and GUARD** Banana safety jacks for output low and banana jack Guard.
- 7. TRIGGER LINK** Eight-pin micro-DIN connector for sending and receiving trigger pulses among connected instruments. Use a trigger link cable (Model 8501) for connections.

8. INTERLOCK

Interlock connector — Provides two screw terminals for connection to an interlock switch. When the interlock switch is closed, the OUTPUT of the 622x is enabled, allowing it to be turned on. When the interlock switch is opened, the OUTPUT is disabled (OUTPUT cannot be turned on and will turn off if it is on).

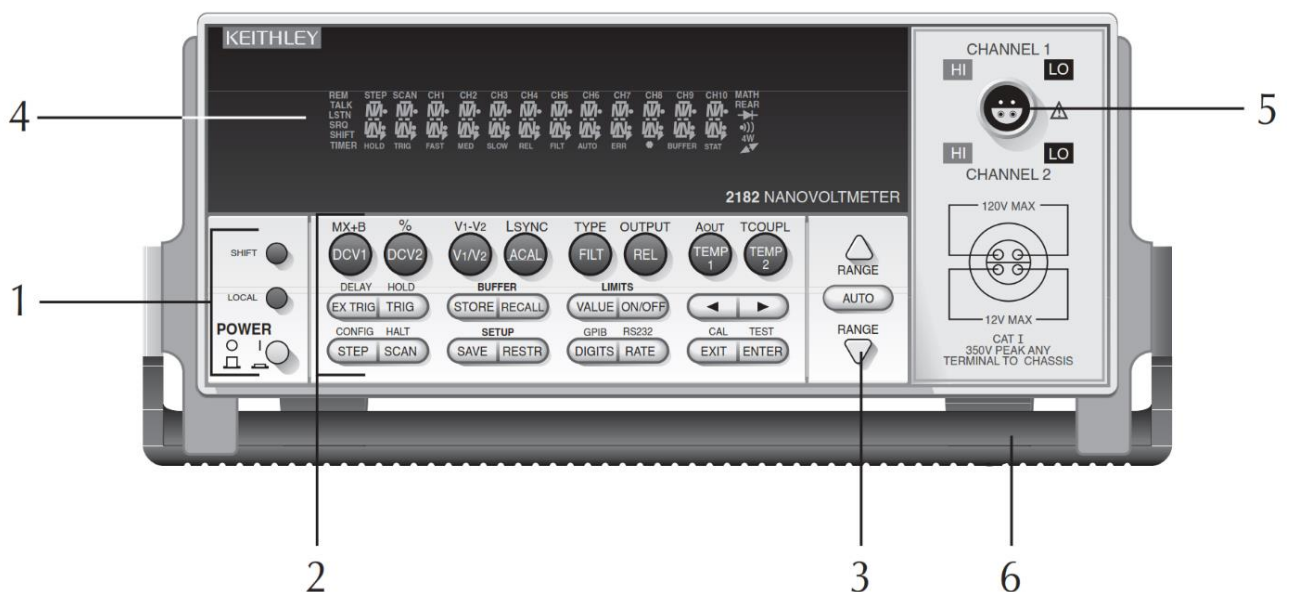
9. Power module

Contains the AC line receptacle and power line fuse. The instrument can operate on line voltages of 100V to 240VAC at line frequencies of 50 or 60Hz.

II. MODEL 2182A

a) Front panel summary

The majority of keys provide two distinct actions or functions. The designation on a key indicates the key's unshifted function or operation when the key is pushed. A shifted function can be selected by pressing the function or operation key, then the SHIFT key.



1. Special keys and power switch

SHIFT	Use to select a shifted function or operation.
LOCAL	Cancel GPIB remote mode.
POWER	Power switch. In position turns 2182A on (1), out position turns it off (0).

2. Function and operation keys

Top Row

Un-shifted

DCV1	Selects Channel 1 voltage measurement function.
DCV2	Selects Channel 2 voltage measurement function.
V1/V2	Selects Ratio (Channel 1 voltage reading / Channel 2 voltage reading).
ACAL	Selects automatic gain calibration.
FILT	Enables/disables filter for selected measurement function.
REL	Enables/disables relative for selected measurement function.
TEMP1	Selects Channel 1 temperature measurement function.
TEMP2	Selects Channel 2 temperature measurement function.

Shifted

MX+B	Multiplies a scale factor (M) to the reading (X) and then adds an offset (B).
%	Calculates percent deviation from a specified reference.
V1-V2	Selects Delta; $(V1t1 - V1t2)/2$.
LSYNC	Enables/disables line cycle synchronization. When enabled, noise induced by the power line is reduced at the expense of speed.

TYPE	Select filter (analogue and/or digital) and configure digital filter (window, count, and type).
OUTPUT	Enables/disables relative for Analog Output.
AOUT	Enables/disables Analog Output.
TCOUP	Configure temperature measurement (units, junction type, thermocouple type, sensor type).

Middle Row

Un-shifted

EX-TRIG	Selects external triggering (front panel, bus, or trigger link) as the trigger source.
TRIG	Triggers a measurement from the front panel.
STORE	Sets reading count for buffer and enables buffer.
RECALL	Displays stored readings (including maximum, minimum, peak-to-peak, average, and standard deviation). The ▲ and ▼ range keys scroll through the buffer, and the ◀ and ▶ key toggles between reading number and reading.
VALUE	Set the upper and lower limits for limit testing.
ON/OFF	Enables/disables limit testing, and selects beeper mode for limit testing.
◀ and ▶	Controls cursor position for making selections or editing values.

Shifted

DELAY	Sets user delay between trigger and measurement.
HOLD	Holds reading when the specified number of samples is within the selected tolerance.

Bottom Row

Un-shifted

STEP	Steps through channels; sends a trigger after each channel.
SCAN	Scans through channels; sends a trigger after the last channel. SAVE Saves presents configuration for power-on user default.
RESTR	Restores factory or user default configuration.
DIGITS	Changes the number of digits of reading resolution.
RATE	Changes reading rate; the number of power line cycles (PLC).
EXIT	Cancels selection, moves back to the measurement display.
ENTER	Accepts selection, moves to next choice or back to measurement display.

Shifted

CONFIG	ConFIGures a scan (type, timer, channel count, and reading count).
HALT	Turns off step/scan operation.
GPIB	Enables/disables GPIB, sets the address, and selects the language.
R8232	Enables/disables RS-232 interface, selects baud rate, flow control, and terminator.
CAL	Accesses calibration.
TEST	Tests display annunciators and front panel keys.

3. Range keys

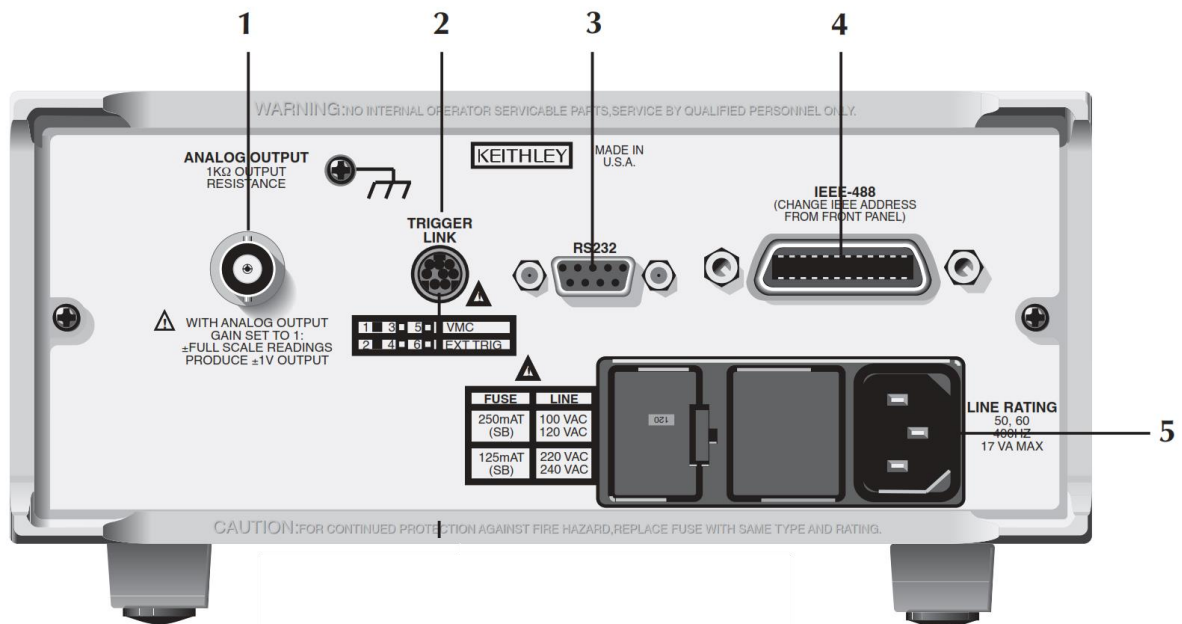
▲	Selects the next higher voltage measurement range.
▼	Selects the next lower voltage measurement range.
AUTO	Enables/disables autorange.

4 Display annunciators

* (asterisk)	Readings being stored in the buffer.
↔ (more)	Indicates additional selections are available.
))) (speaker)	Beeper on for limit testing.
AUTO	Autorange enabled.
BUFFER	Recalling readings stored in the buffer.
CH1	Channel 1 input displayed.
CH2	Channel 2 input displayed.
CH1 and CH2	Ratio (V1 /V 2) reading displayed.
ERR	Questionable reading, or invalid cal step.
FAST	Fast (0.1 PLC) reading rate selected.
FILT	Filter enabled.
HOLD	Instrument in hold mode.
LSTN	Instrument addressed to listen over GPIB.
MATH	mX+b or Percent (%) calculation enabled.
MED	Medium (1 PLC) reading rate selected.
REAR	Indicates that Analog Output is on.
REL	Relative enabled for present measurement function.
REM	Instrument in GPIB remote mode.
SCAN	Scan mode selected.
SHIFT	Accessing a shifted key.
SLOW	Slow (5 PLC) reading rate selected.
SRQ	Service request over GPIB.
STAT	Displaying buffer statistics.
STEP	Step mode selected.
TALK	Instrument addressed to talk over GPIB bus.

- TIMER Timer-controlled scans in use.
- TRIG External triggering (front panel, bus or trigger link) selected.
- 5 Input connector**
- CHANNEL 1 Measure voltage or temperature. Volts Ranges: IOmV, 100mV, 1V, 10V, and 100V.
- CHANNEL 2 Measure voltage or temperature. Volts Ranges: 100mV, 1V, and 10V.
- 6 Handle** Pulls out and rotate to the desired position.

b) Rear panel summary

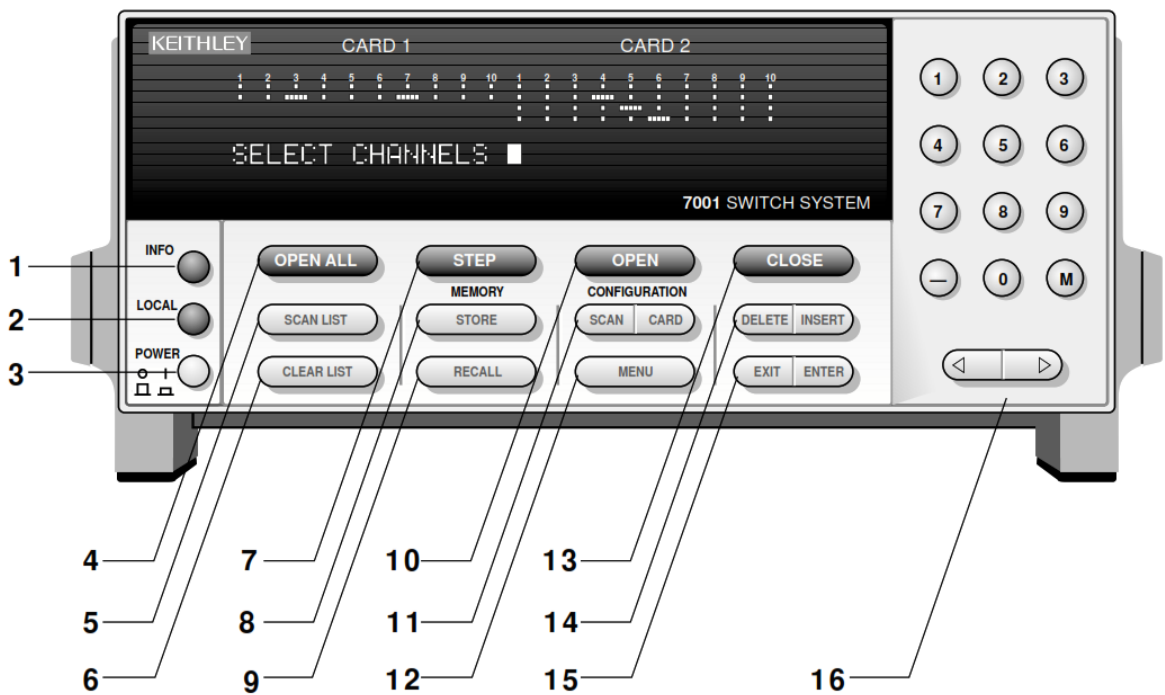


- 1. ANALOG OUTPUT : Provides a scaled non-inverting DC voltage. With analogue output gain set to one, a full range input will result in a 1V analogue output.
- 2. TRIGGER LINK : Eight-pin micro-DIN connector for sending and receiving trigger pulses among connected instruments. Use a trigger link cable or adapter, such as Models 8501-1, 8501-2, 8502, and 8503.

- 3. RS-232 : Connector for RS-232 operation. Use a straight-through (not null modem) DB-9 shielded cable.
- 4. IEEE-488 :Connector for IEEE-488 (GPIB) operation. Use a shielded cable, such as the Models 7007-1 and 7007-2.
- 5. Power Module : Contains the AC line receptacle, power line fuse, and line voltage setting. The instrument can be configured for line voltages of 100V/120V/220V/240VAC at line frequencies of 45Hz to 66Hz or 360Hz to 440Hz.

MODEL 7001

a) Front panel summary



- 1. INFO :Displays on-line help information. Press again (or EXIT) to cancel message.
- 2. LOCAL :Cancels remote, restores front panel control.
- 3. POWER 0 = off
1 = on

- 4 OPEN ALL :Opens all channels of both slots. Also, aborts a scan that is in progress and places 7001 in idle state.
- 5. SCAN LIST :Toggles between Scan List and Channel List
- 6. CLEAR LIST :Clears the displayed Channel List or Scan List.
- 7. STEP :Takes 7001 out of idle state and steps through Scan List
- 8. STORE :Stores channel pattern at a specified memory location.
- 9. RECALL :Restores 7001 to a channel pattern stored at a specified memory location.
- 10. OPEN :Opens the specified (displayed) channels in Channel List.
- 11. SCAN CONFIGURATION :Enables CONFIGURE SCAN

MENU :

CHAN-CONTROL SCAN-CONTROL ARM-CONTROL

CHAN-RESTRICTIONS

CARD CONFIGURATION

Enables CARD CONFIG MENU : TYPE

#-OF-POLES

CARD-PAIR

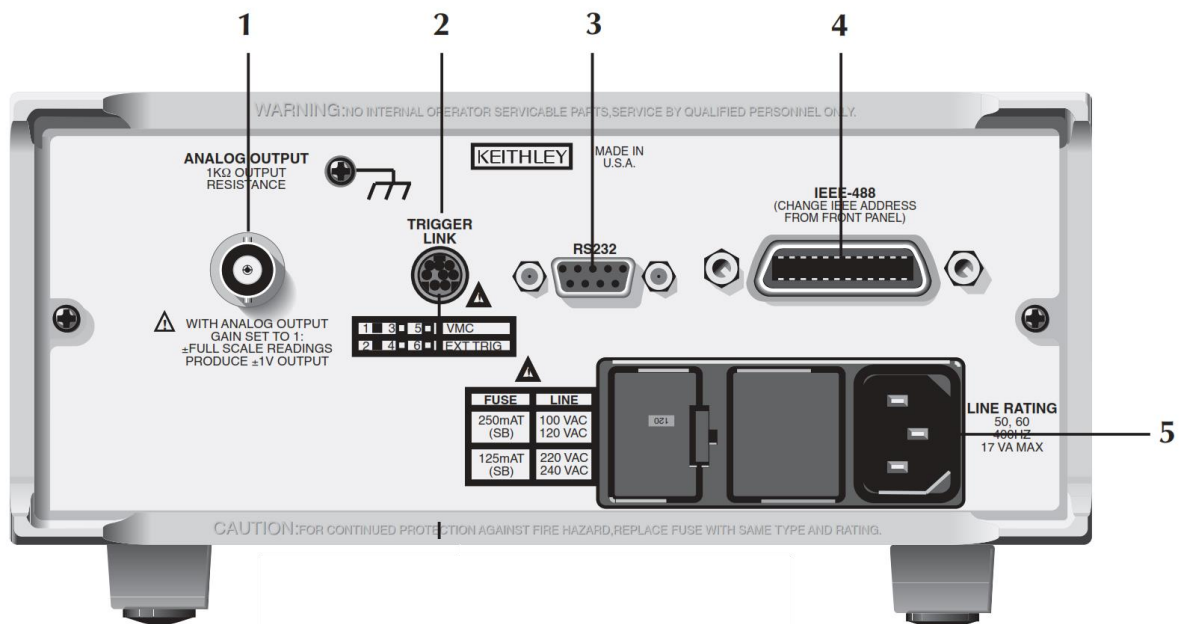
DELAY

READ-I/O-CARD

- 12. MENU :Enables MAIN MENU: SAVESETUP
:GPIB
:DIGITAL-I/O
:TEST LANGUAGE GENERAL
- 13. CLOSE :Closes the specified (displayed) channels in Channel List.
- 14. DELETE :Delete selected entry from Channel List or Scan List.
- INSERT :Insert next entry at selected location in the Channel List or Scan List.

15. EXIT :Back up to previous menu selection, o exit from the menu.
- ENTER :Execute the pending operation. Also, separate channels and terminate a Channel List or Scan List.
16. KEYPAD 0 - 9; use to enter numbers.
- ; use to specify a range of channels (i.e. 1!1 - 1!40).
- M ; use to precede a specified memory location number.
- ◁ ; use to move cursor left or
- ▷ ; use to move cursor right. Also, use to separate channels and terminate a Channel List on Scan List.

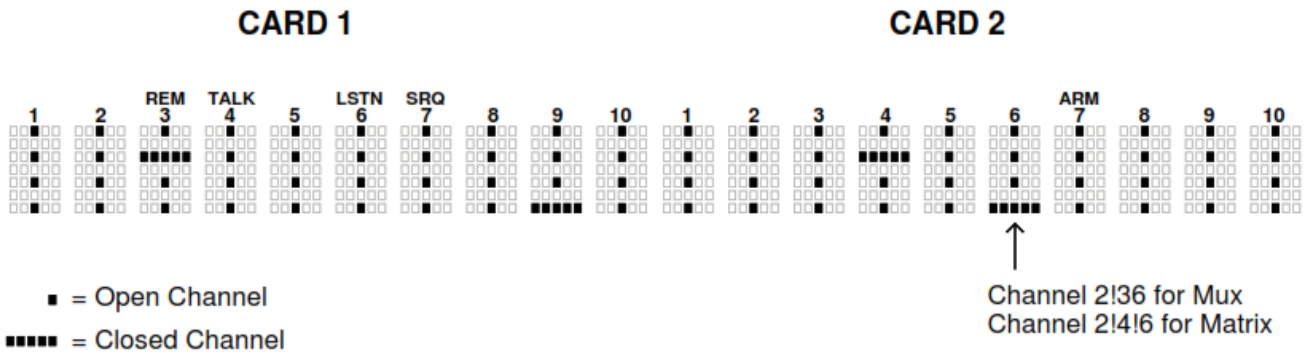
b) rear panel summary



1. CARD 1 :Slot 1 for switch card. Corresponds to Card 1 channel status display.
2. CARD 2 :Slot 2 for switch card. Corresponds to Card 2 channel status display.
3. IEEE-488 CONNECTOR :Use standard IEEE-488 cables.
- 4 DIGITAL I/O :Micro 8-pin DIN connector. Port consists of four TTL output lines and one TTL input line (one common line).
5. TRIGGER LINK IN AND OUT :Two micro 8-pin DIN connectors.

- 6. CHANNEL READY :Female BNC connector for TTL output trigger pulse.
- 7. EXTERNAL TRIGGER :Female BNC connector for TTL input trigger pulse.
- 8 LINE POWER INPUT *WARNING: Connect to grounded outlet using three-wire power cord.*

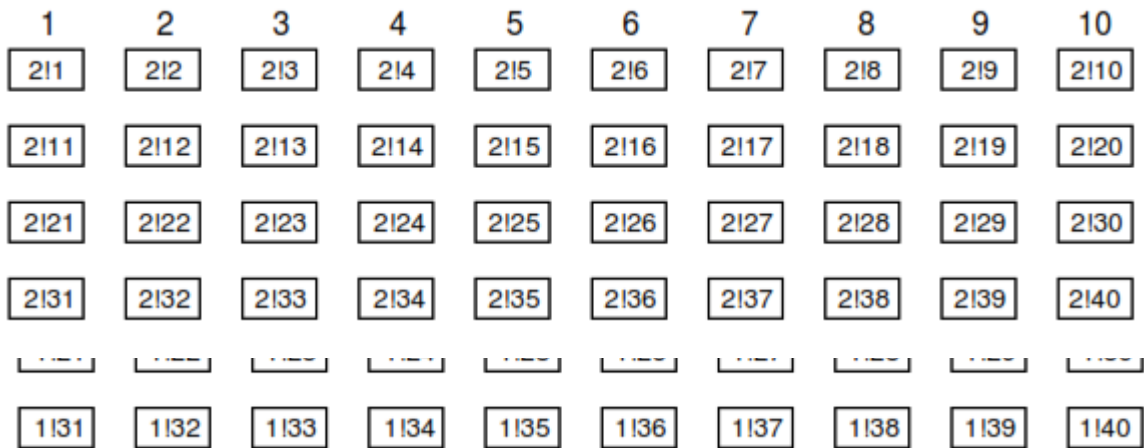
c) Channel status display



d) Channel assignments (matrix cards)

A. Slot 1 (Card 1)

B. Slot 2 (Card 2)

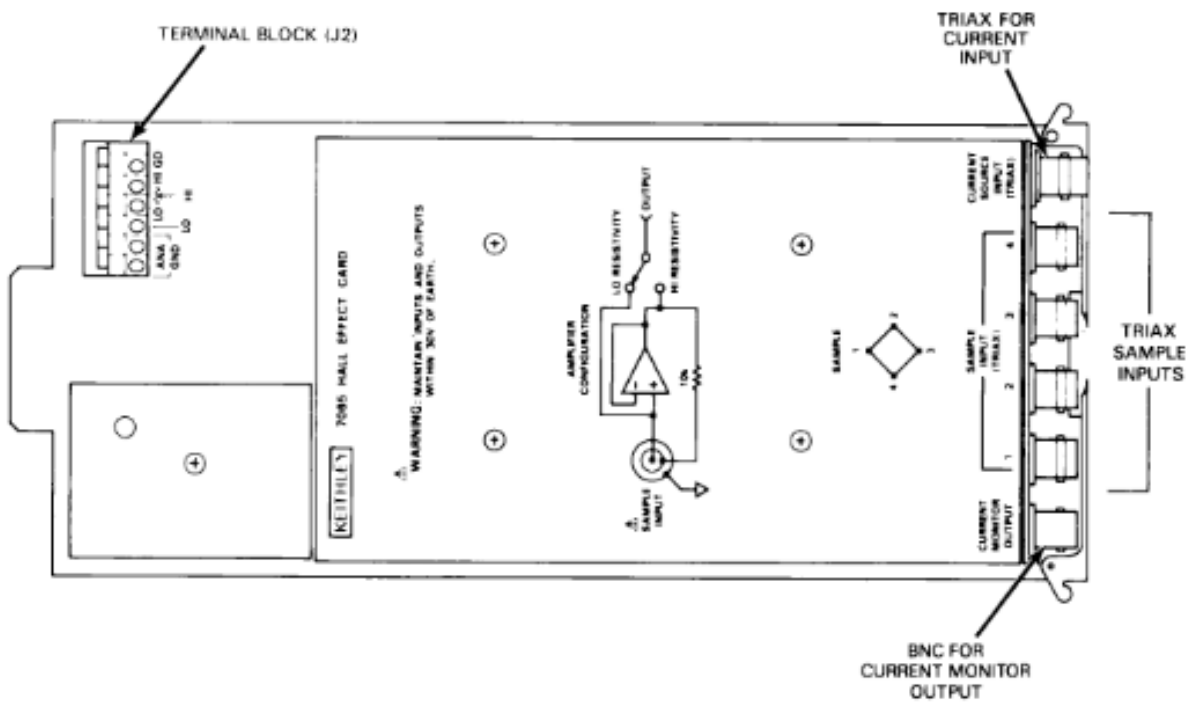


Examples : 1!18 = Slot 1, Channel 18

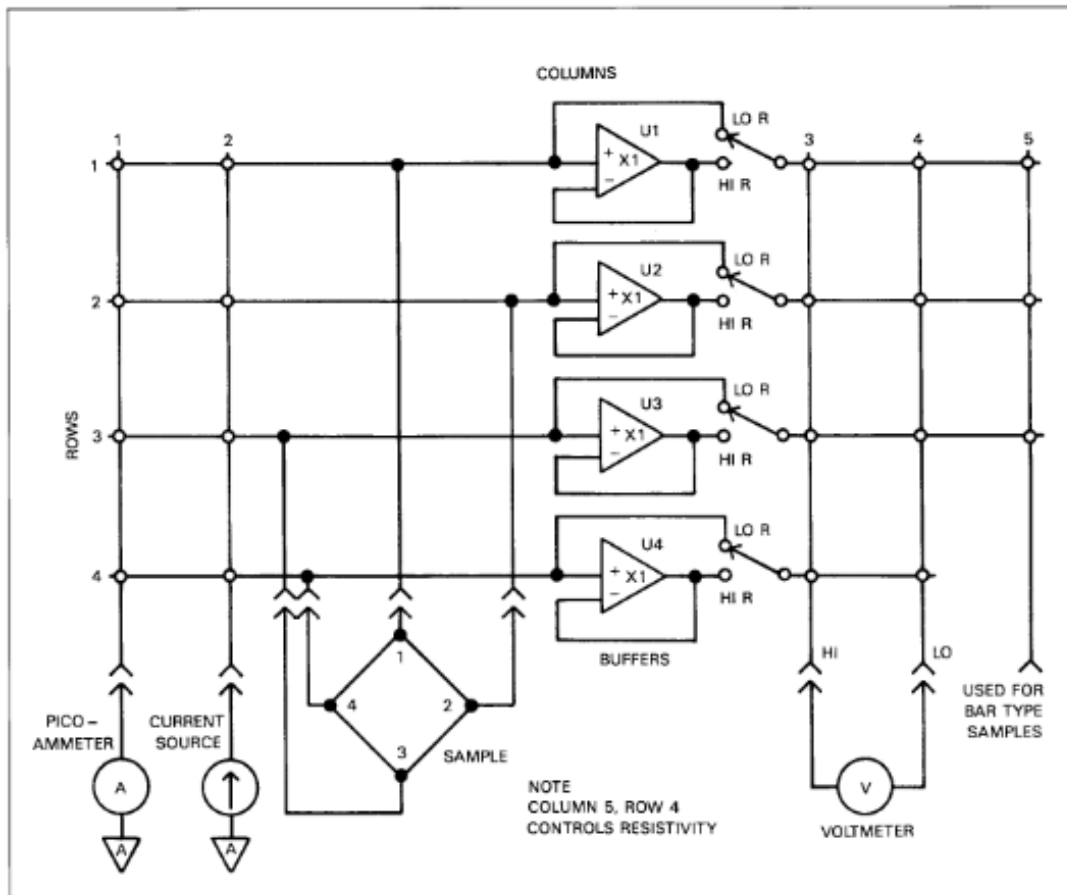
2!36 = Slot 2, Channel 36

III. Model 7065

a) Connectors



b) Matrix configuration



c) Channel configurations

Voltage designation	Flux	Model 7001 channel list*	Current applied between	Voltage measured between
V ₁	+B	1!1!2, 1!3!1, 1!4!3, 1!2!4	1-3	4-2
V ₂	+B	1!3!2, 1!1!1, 1!4!3, 1!2!4	3-1	4-2
V ₃	+B	1!2!2, 1!4!1, 1!1!3, 1!3!4	2-4	1-3
V ₄	+B	1!4!2, 1!2!1, 1!1!3, 1!3!4	4-2	1-3
V ₅	-B	1!1!2, 1!3!1, 1!4!3, 1!2!4	1-3	4-2
V ₆	-B	1!3!2, 1!1!1, 1!4!3, 1!2!4	3-1	4-2
V ₇	-B	1!2!2, 1!4!1, 1!1!3, 1!3!4	2-4	1-3
V ₈	-B	1!4!2, 1!2!1, 1!1!3, 1!3!4	4-2	1-3

* Assumes Model 7065 card is in Slot 1 of Model 7001. For Slot 2, change first digit of each item in every list to 2.

APPENDIX V: NATIONAL INSTRUMENTS' SOFTWARE

Name	Maintainer	Category	Version
NI Web Server Development Support for LabVIEW 2020 32-bit	NI	Add-Ons	20.51
LabVIEW Report Generation Toolkit (32-bit)	NI	Add-Ons	2020
LabVIEW DataFinder Connectivity Vis (32-bit)	NI	Add-Ons	2020
LabVIEW Database Connectivity Toolkit (32-bit)	NI	Add-Ons	2020
NI LabVIEW Command-line Interface	NI	Add-Ons	310
JO VI Package Manager	JIG	Add-Ons	2020
NI System Configuration support for LabVIEW 2020 (32-bit)	NI	Add-Ons	2050
TDM Excel Add-In	NI	Add-Ons	19
NI DataPugin AOPS	NI	Add-Ons	19.5
NI Web-Based Configuration and Monitoring 20.5	NI	Application Software	2051
MG1 Solution Explorer	More Good Ideas Inc	Application Software	240-23
IV! Compliance Package Documentation	NI	Documentation	17
IVI Class Simulation Drivers	NI	Drivers	17
IVI Compliance Package	NI	Drivers	17
NI-VISA .NET Runtime 17.5	NI	Drivers	17.5
NI-VISA Runtime	NI	Drivers	17.5
IVI Class Simulation Drivers Source	NI	Drivers	17
GPIB-488 version 9.2	GPIB-488	Other Software	2.304915
LabVIEW (32-bit) English	NI	Programming Environments	202OSP 1
LabVIEW Runtime (32-bit)	NI	Programming Environments	2019 SP1 f3
LabVIEW Runtime (32-bit)	NI	Programming Environments	202OSP 1
LabWindows/CVI Shared Runtime	NI	Runtime	2019
NI System Configuration .NET Runtime	NI	Runtime	2050
LabWindows/CVI Shared Runtime Base	NI	Runtime	2019
NI Distributed System Manager 2020	NI	Runtime	20
LabVIEW DataFinder Connectivity Runtime (32-bit)	NI	Runtime	2020

Name	Maintainer	Category	Version
LabWindows/CVI TDM Streaming Library Runtime	NI	Runtime	2019
NI System Configuration Runtime	NI	Runtime	2050
NI System Web Server 2020 SP1	NI	Runtime	2051
Variable Engine	NI	Runtime	20
LabWindows/CVI Network Variable library Runtime	NI	Runtime	2019
LabWindows/CVI Network Streams library Runtime	NI	Runtime	2019
NIUSICorc	NI	Runtime	19.6
LabWindows/CVI .NET Library Runtime	NI	Runtime	2019
NI Web Server Deployment Support for LabVIEW 2020 32-bit	NI	Runtime	205.1
LabWindows/CVI Analysis Library Runtime	NI	Runtime	2019
NI System Configuration Runtime	NI	Runtime	20.5
NI System Web Server 2020 SP1	NI	Runtime	20.5.1
Variable Engine	NI	Runtime	20
LabWindows/CVI Network Variable library Runtime	NI	Runtime	2019
LabWindows/CVI Network Streams library Runtime	NI	Runtime	2019
NIUSICore	NI	Runtime	19.6
LabWindows/CVI .NET Library Runtime	NI	Runtime	2019
NI Web Server Deployment Support for LabVIEW 2020 32-bit	NI	Runtime	20.5.1
LabWindows/CVI Analysis Library Runtime	NI	Runtime	2019
DataSocket	NI	Runtime	20
NI Update Service	NI	Utilities	19
NI License Manager	NI	Utilities	4.7
NI Measurement & Automation Explorer	NI	Utilities	20.5
NI Certificates Installer	NI	Utilities	202
NI Package Manager	NI	Utilities	20.6

APPENDIX VI: CONFERENCE CERTIFICATE



KABARAK UNIVERSITY

Certificate of Participation

Awarded to

Alfred Orega

for successfully participating in the 13th Annual Kabarak University International Research Conference held from 10th – 11th July 2023, and presented a paper entitled *“Development of an automated hall effect experimentation method for the electrical characterization of thin films”*.

Conference Theme

Bridging the research gap through basic and applied sciences

Dr. Peter Rugiri
Dean, School of Science
Engineering & Technology

Dr. Moses Thiga
Director - Research, Innovation
and Outreach

Kabarak University Moral Code

As members of Kabarak University family, we purpose at all times and in all places, to set apart in one's heart, Jesus as Lord.

(1 Peter 3:15)



Kabarak University is ISO-9001:2015 Certified

APPENDIX VII: PUBLICATION



**Development of an Automated Hall Effect Experimentation Method for
the Electrical Characterization of Thin Films**

A. Orega, M. Mwamburi & C. Maghanga

ISSN: 2617-3573

Development of an Automated Hall Effect Experimentation Method for the Electrical Characterization of Thin Films

¹A.Orega

Kabarak University, Kenya, Department of Physical Sciences and Biological Sciences

*Email of corresponding authors: al.for@live.com

²M. Mwamburi

University of Eldoret, Department of Physics

³C. Maghanga

Kabarak University, Kenya, Department of Physics and Biological Sciences

How to cite this article: Orega, A., Mwamburi, M. & Maghanga, C. (2023). Development of an Automated Hall Effect Experimentation Method for the Electrical Characterization of Thin Films. *Journal of Information and Technology*, 7(1), 58-68. <https://doi.org/10.53819/81018102t4208>

Abstract

There has been drastic growth in the microelectronics industry in the recent past. The performance of these materials is influenced by their structural, electrical, and optical properties among others, depending on their applications. Therefore, the need to conduct measurements of the semiconductor characteristics precisely, quickly, and conveniently cannot be overstated. Some of the desirable features of measurements include usability, accuracy, resolution, repeatability, and consistency which cannot be assured with manually operated systems. This study strived to design and interface an automated computer-aided four-point probe test equipment that characterizes materials to determine their electrical properties. A four-point probe head, an electromagnet, NI Keithley model 6220 Precision current source, model 7001 switch, model 2182A Nanovoltmeter, and model 7065 Hall Effect card instruments were interfaced with the NI LabVIEW program running in a computer through a GPIB hub to a PC USB for its full control. The four-probe head was utilized to probe the samples with a square symmetry that was adopted for the measurement of the semiconductor properties. Reliability tests were conducted on a standard P-type Germanium sample. The collected data was within 0.32% of the expected results. This work forms a basis for automating similar systems that were inherently designed to be operated manually.

Keywords: *Automated Hall Effect, manually operated systems, Hall angle, thin films, string manipulation routines.*

<https://doi.org/10.53819/81018102t4208>